Partial Tip60 Loss Slows Cerebellar Degeneration in a Spinocerebellar Ataxia Type 1 (SCA1) Mouse Model

A DISSERTATION
SUBMITTED TO THE FACULTY OF THE GRADUATE SCHOOL
OF THE UNIVERSITY OF MINNESOTA
BY

Kristin Marie Gehrking

IN PARTIAL FULFILLMENT OF THE REQUIREMENTS
FOR THE DEGREE OF
DOCTOR OF PHILOSOPHY

Harry T. Orr

July 2009

Acknowledgements

This project was made possible with the generous help and support of many people. My advisor, Dr. Harry Orr, provided invaluable guidance and leadership throughout my research. My committee members, Dr. Vivian Bardwell, Dr. Brent Clark, Dr. Deb Ferrington, Dr. Dennis Livingston, and Dr. Howard Towle, provided helpful feedback throughout my graduate training.

The mouse colony was maintained and DigiGait experiments were run by Robert Ehlenfeldt and Orion Rainwater. Lisa Duvick provided FVB molecular layer thickness data.

Thanks to Dr. John Lough at the Medical College of Wisconsin for providing *Tip60*$^{+/-}$ mice and the Tip60 construct. Thanks also to Dr. Beverly Davidson at the University of Iowa, in which I performed all of the Tip60 RNAi experiments.

Past and present lab members, especially Lisa Duvick, were of great help in teaching lab techniques, providing reagents, and participating in helpful discussions.

Thanks to the faculty, fellow students, and administrative support of the Biochemistry, Molecular Biology, and Biophysics Department and the Medical Scientist Training Program at the University of Minnesota. Final thanks to the National Institutes of Neurological Disorders and Stroke for funding this research.

Abstract

Spinocerebellar Ataxia Type 1 (SCA1) is one of nine dominantly inherited neurodegenerative diseases caused by polyglutamine tract expansion. In SCA1, the expanded polyglutamine tract is in the ataxin-1 (ATXN1) protein. Increased polyglutamine tract length results in earlier onset and greater disease severity. Pathology is mainly cerebellar Purkinje cell degeneration. ATXN1 is part of an in vivo complex with the nuclear receptor (retinoid acid receptor-related orphan receptor alpha [RORα]) and acetyltransferase (tat-interactive protein 60 kD [Tip60]). ATXN1 and Tip60 interact directly; however, the significance of this interaction is unclear. To test the effect of partial Tip60 loss on disease progression, I developed a mutant *ATXN1*[82Q]/+:*Tip60*$^{+/-}$ mouse model. Partial *Tip60* loss increased expression of Rora and RORα-mediated genes and delayed *ATXN1*[82]-mediated cerebellar degeneration during midstage disease progression. Finally I discovered an ATXN1 polyglutamine length effect on Tip60 acetyltransferase activity. My research suggests a specific temporal role for Tip60 during disease progression and a potential role for Tip60 acetylation in SCA1 pathologic mechanisms.

Table of Contents

List of Tables v

List of Figures vi

Abbreviations ix

Chapter 1

Introduction 1

Chapter 2

Genetic Background Strain Effect on SCA1 Disease 16

Chapter 3

ATXN1[82Q]/+:*Tip60*$^{+/-}$ Mouse Model. 21

Chapter 4

ATXN1 Modulates Tip60 Histone Acetylation. 72

Chapter 5

Tip60 miRNA. 79

Chapter 6

Conclusions and Future Directions 90

Chapter 7

Methods 98

List of Tables

1 Statistical significance of DigiGait data 56

2 Gene expression summary in *ATXN1*[82Q]/+:*Tip60*$^{+/-}$ mice 71

List of Figures

1 ATXN1 protein diagram 13

2 Model for RORα-dependent gene expression in Purkinje cells 14

3 Acetylation is a regulatory mechanism directed at a variety of cellular proteins 15

4 Molecular layer thickness of wt mice on mixed and FVB genetic backgrounds 20

5 Q-RT-PCR of Tip60, in cerebella of C57BL/6 mice comparing *Tip60*$^{+/+}$ and *Tip60*$^{+/-}$ expression 43

6 Breeding strategy for *ATXN1*[82Q]/+:*Tip60*$^{+/-}$ mice 44

7 Q-RT-PCR of *ATXN1* in *ATXN1*[82Q]/+:*Tip60*$^{+/-}$ mice and *ATXN1*[82Q]/+ littermate cerebella 45

8 Immunofluorescence of wt mouse cerebellum at 9, 12, 16, and 20 weeks, probed with anti-calbindin antibody 46

9 Molecular layer thickness of wt, *Tip60*$^{+/-}$, *ATXN1*[82Q]/+, and ATXN1[82Q]/+:*Tip60*+/- mice at 9, 12, 16, and 20 weeks 47

10 CF-PC terminals at 9 weeks in wt, *Tip60*$^{+/-}$, *ATXN1*[82Q]/+, and ATXN1[82Q]/+:*Tip60*+/- mice 48

11 CF-PC terminals at 9 weeks in wt, *Tip60*$^{+/-}$, *ATXN1*[82Q]/+, and ATXN1[82Q]/+:*Tip60*+/- mice. 49

12 CF-PC terminals at 9 weeks in wt, *Tip60*$^{+/-}$, *ATXN1*[82Q]/+, and ATXN1[82Q]/+:*Tip60*+/- mice. 50

13 CF-PC terminals at 9 weeks in wt, *Tip60*$^{+/-}$, *ATXN1*[82Q]/+, and *ATXN1*[82Q]/+:*Tip60*+/- mice. 51

14 CF-PC terminals quantification at 9, 12, 16, and 20 weeks in wt, Tip60$^{+/-}$, *ATXN1*[82Q]/+, and *ATXN1*[82Q]/+:*Tip60*+/- mice . . 52

15 DigiGait analysis of rear stride time of wt, *Tip60*$^{+/-}$, *ATXN1*[82Q], and ATXN1[82Q]/+:*Tip60*$^{+/-}$ mice 53

16 DigiGait analysis of rear stance width of wt, *Tip60*$^{+/-}$, *ATXN1*[82Q], and *ATXN1*[82Q]/+:*Tip60*$^{+/-}$ mice 54

17 DigiGait analysis of rear step angle of wt, Tip60$^{+/-}$, *ATXN1*[82Q], and *ATXN1*[82Q]/+:*Tip60*$^{+/-}$ mice 55

18 DigiGait analysis of rear stride time of FVB and B05/+ mice 57

19 DigiGait analysis of rear stance width of FVB and B05/+ mice 58

20 DigiGait analysis of rear step angle of FVB and B05/+ mice 59

21 Rota-Rod performance of wt, *Tip60*$^{+/-}$, *ATXN1*[82Q], and *ATXN1*[82Q]/+:*Tip60*+/- mice at 9 weeks 60

22 Rota-Rod performance of wt, *Tip60*$^{+/-}$, *ATXN1*[82Q], and *ATXN1*[82Q]/+:*Tip60*+/- mice at 12 weeks 61

23 Rota-Rod performance of wt, *Tip60*$^{+/-}$, *ATXN1*[82Q], and *ATXN1*[82Q]/+:*Tip60*+/- mice at 16 weeks 62

24 Rota-Rod performance of wt, *Tip60*$^{+/-}$, *ATXN1*[82Q], and *ATXN1*[82Q]/+:*Tip60*+/- mice at 20 weeks 63

25 Rota-Rod performance of wt, *Tip60*$^{+/-}$, *ATXN1*[82Q], and *ATXN1*[82Q]/+:*Tip60*+/- mice at 30 weeks 64

26 Rota-Rod performance of FVB and B05/+ mice at 12 weeks 65

27 Western blot of 12 week old cerebellar lysates, probed with anti-RORα antibody 66

28 qRT-PCR of RORα isoforms 1 and 4 in cerebella of wt, *ATXN1*[82Q], and *ATXN1*[82Q]/+:*Tip60*$^{+/-}$ mice 68

29 qRT-PCR of RORα-mediated genes in cerebella of wt, *ATXN1*[82Q], and *ATXN1*[82Q]/+:*Tip60*$^{+/-}$ mice 70

30 Western blot with quantification: CHO cells transfected without *ATXN1*, with *ATXN1*[30Q], or with *ATXN1*[82Q], (all +/-Tip60), probed with anti-acetyl-histone H3 antibody 78

31 Tip60β cDNA sequence 84

32 Tip60 protein sequence with target miRNAs and schematic 86

33 qRT-PCR of *Tip60* knockdown efficiency 87

34 Western blot of Tip60 knockdown efficiency, probed with Anti-Flag antibody 89

35 Model of hypothesized effects of Tip60 on mechanisms of SCA1 pathogenesis 98

36 Model of SCA1 disease stages 99

Abbreviations

+/-	heterozygous
+/+	homozygous
[30Q]	30 CAG (encoding glutamine) repeat units
[82Q]	82 CAG (encoding glutamine) repeat units
ALS	amyotrophic lateral sclerosis (Lou Gehrig's Disease)
ANOVA	analysis of variance
ATM	Ataxia Telangiectasia Mutated
ATXN1	human ataxin-1 gene
ATXN1	human ataxin-1 protein
Atxn1	mouse attains-1 gene
AXH	ataxin-1 and HMG-box protein 1
CBP	CREB binding protein
CHO	Chinese Hampster Ovary
CIC	capicua
CMV	cytomegalovirus
DRPLA	dentatorubral pallidoluysian atrophy
EDTA	ethylene-diamine-tetra-acetic acid
EtOH	ethyl alcohol/ethanol

ES cells	embryonic stem cells
EST	expressed sequence tag
FAT	factor acetyltransferase
FBS	fetal bovine serum
g	the force of gravity
GAPDH	glyceraldehyde phosphate dehydrogenase
Gfi-1	growth factor-independent 1
GFP	green fluorescent protein
HAT	histone acetyltransferase
HD	Huntington's disease
HDACi	histone deacetylase inhibitor
HBP1	high mobility group box transcription factor-binding protein 1
HIV-1	human immunodeficiency virus type 1
Htt	Huntingtin protein
Itpr1	Inositol 1,4,5-triphosphate receptor, type 1
MEM	minimum essential medium
miRNA	micro RNA
n	sample size
NLS	nuclear localization signal
OB	oligonucleotide binding
P#	postnatal day #

p53	tumor protein 53
PBS	phosphate buffered saline
PC	Purkinje cell
P/CAF	p300/CBP associated factor
Pcp2	Purkinje cell protein 2
Pcp4	Purkinje cell protein 4
PQBP1	poly-Q binding protein 1
RORα	retinoic acid receptor-related orphan receptor alpha
RORE	RORα response element
RMB17	RNA binding motif protein 17
SAR	self-association region
SBMA	spinobulbar muscular atrophy
SCA1	spinocerebellar ataxia type 1
SCA1[82Q]/+	heterozygous murine mutant SCA1
SEM	standard error of the mean
sg/sg	homozygous null *staggerer* mouse
shRNA	short hairpin RNA
Slc1A6	solute carrier family 1 (high affinity aspartate/glutamate transporter), member 6
SMRT	silencing mediator of retinoid and thyroid hormone
SDS	sodium dodecyl sulfate
RT	room temperature

Tip60	tat-interactive protein, 60 kD
VGluT	vesicular glutamate transporter, Slc17a6
wt	wild-type

Chapter 1

Introduction

Part I: Spinocerebellar Ataxia Type I and Polyglutamine Diseases

Ataxia, from the Greek meaning “lack of order”, describes a neurological condition characterized by a lack of coordination. Ataxia is a broad term which implies dysfunction within the nervous system, often arising from the cerebellum; cerebellar ataxias are the most common subgroup of ataxias. Spinocerebellar ataxia describes a specific variant in which the cerebellar cortex or its inputs are dysfunctional. There are 28 versions of spinocerebellar ataxia; all have changes at different genetic loci (Carlson and Andresen, 2009).

Spinocerebellar ataxia type 1 (SCA1) is one of nine inherited polyglutamine diseases that cause neurodegeneration: Huntington's disease (HD), spinobulbar muscular atrophy (SBMA, Kennedy Disease), dentatorubropallidoluysian atrophy (DRPLA), and six autosomal-dominant spinocerebellar ataxias (Zoghbi and Orr, 2000; Taylor et al., 2002; Orr and Zoghbi, 2007). Each of these diseases is dominantly inherited except SBMA, which has an X-linked inheritance pattern. In these diseases the mutant gene encodes an expanded CAG tract, which results in a polyglutamine expansion within the protein. In SCA1, the mutant *ATXN1* gene encodes the protein ataxin-1 (ATXN1), which is widely expressed (Servadio

et al., 1995; Banfi et al., 1996); however, neurodegeneration is limited to cerebellar Purkinje cells (PCs), brainstem, and spinal cord (Clark and Orr, 2000). As with most autosomal dominant ataxias, symptoms are characterized by a progressive loss of motor coordination, neuropathies, slurred speech, cognitive impairment, and loss of other functional abilities arising from deep cerebellar nuclei (Zoghbi, 1995). Most spinocerebellar ataxias result from PC loss in the cerebellar cortex, PCs are the only efferent pathway from the cerebellar cortex. SCA1 can include other brain region degeneration, including the dentate nucleus, the inferior olive, the pons, and the red nuclei. Cranial nerve nuclei III, X, and XII can also be affected (Voogd and Glickstein, 1998).

CAG mutations are not stably transmitted from one generation to the next, but instead are dynamic, resulting in increasing tract length with paternal transmission to successive generations. Unaffected SCA1 alleles have between 6 to 42 CAG repeats. Unaffected individuals with repeat tracts longer than 21 CAGs have CAT (encoding histidine) interruptions within the repeat. Mutant SCA1 alleles have pure polyglutamine expansions ranging from 39 to 82 repeats (Chung et al., 1993; Orr et al., 1993). This increase in repeat size, as the mutant gene is passed from parent to offspring, is called anticipation, and it results in an earlier onset and more rapid disease progression. For example, affected individuals with 40 to 50 repeat tracts usually begin to have symptoms during the 4^{th} or 5^{th} decade, whereas those with more than 70 repeats experience juvenile onset. Dynamic mutations that result from germ line instability are also seen in Huntington's disease, inherited ataxias, many types of mental retardation, and

myotonic dystrophies (Fu et al., 1991; Spada et al., 1991; Nance, 1997; Machuca-Tzili et al., 2005).

ATXN1 functional domains. The SCA1 phenotype likely involves a gain-of-function mechanism, as evidenced by the lack of an SCA1 phenotype in knockout mice (Matilla et al., 1998). Several regions are important for ATXN1's endogenous function, including the N-terminal polyglutamine tract, an ATXN1 and HMG-box protein 1 (AXH) domain, a C-terminal nuclear localization sequence (NLS), and serine 776 (S776), the last NLS residue (Figure 1). The self-association region (SAR) seems to be important for forming nuclear inclusions that contain several chaperone and proteasome-related proteins, but not necessarily for disease pathogenesis (Chung et al., 1993; Cummings et al., 1998; Klement et al., 1998). Discovering protein domains outside the polyglutamine (polyQ) tract that impact disease mechanisms suggests the polyQ tract may exert a toxic effect in concert with other domains. The AXH domain is a 120 amino acid stretch named for ATXN1 and the domain's high homology to part of high mobility group box transcription factor-binding protein 1 (HBP1) (de Chiara et al., 2003; Chen et al., 2004). The crystal structure has been solved for the ATXN1 AXH domain and reveals an oligonucleotide binding (OB) fold (Chen et al., 2004) with a proposed RNA binding function similar to full-length ATXN1 (Yue et al., 2001). The AXH domain is required for the ATXN1 interaction with many other proteins including ATXN1-like (ATXN1L/BOAT [brother of ataxin-1]) (Mizutani et al., 2005), silencing mediator of retinoid and thyroid hormone receptors (SMRT) (Mizutani et al., 2005), *Drosophila* Senseless (SENS) and its

mammalian homolog growth factor-independent 1 (Gfi) (Tsuda et al., 2005), the human homolog of *Drosophila* Capicua (CIC) (Lam et al., 2006), transcription factor Sp1 (Sp1) (Goold et al., 2007), and Tip60 (Serra et al., 2006). Most proteins that interact with ATXN1 via its AXH domain have a role in transcription. For example, SMRT is a co-repressor of HDAC3 activity. While ATXN1 and HDAC3 do not interact directly, they co-localize with SMRT in nuclear foci (Mizutani et al., 2005). Capicua also is a transcriptional repressor (Jimenez et al., 2000), as is Gfi (Karsunky et al., 2002). Sp1 is a transcription factor (Dynan and Tjian, 1983), and Tip60 is a transcriptional coactivator for retinoid acid receptor-related orphan receptor alpha (RORα). RORα does not directly bind ATXN1, but is in an endogenous complex with ATXN1 and Tip60 (Serra et al., 2006). Interestingly ATXN1 can be SUMOylated on at least five residues (Riley et al., 2005), consistent with the idea that SUMOylation is a common post-translational modification in proteins with a role in transcription (Muller et al., 2004). In the case of ATXN1, SUMOylation is dependent on a functional NLS and decreases with increasing polyglutamine tract length (Riley et al., 2005).

RORα. Atrophy and loss of cerebellar PCs are characteristic of SCA1 pathology. This restricted degeneration is not explained by mutant ATXN1 expression, since ATXN1 is widely expressed in the brain (Servadio et al., 1995). However RORα is highly expressed in the cerebellum (especially PCs) (Matsui et al., 1995) and is part of an *in vivo* complex with ATXN1, suggesting that the selective vulnerability of PCs is linked to RORα-Tip60's interaction with ATXN1 (Ino, 2004; Serra et al., 2004).

RORα is a member of the steroid hormone receptor superfamily (Giguere et al., 1994). It functions as a ligand-dependent transcription factor and regulates key biological processes during embryonic development and adulthood. RORα (Becker-Andre et al., 1993; Giguere et al., 1994), RORβ (Carlberg et al., 1994; André et al., 1998), and RORγ (He et al., 1998) (Hirose et al., 1994; Jetten et al., 2001; Jetten, 2004) comprise a nuclear receptor subfamily. Among RORs the DNA binding domain is highly conserved, and the ligand binding domain is moderately conserved (Jetten et al., 2001). Each subfamily member has several isoforms (with variable amino termini) that arise from alternate promoter usage and exon splicing (Giguere et al., 1994). Like other hormone receptors RORs bind ligand, translocate to the nucleus, and subsequently regulate transcription of target genes. However unlike other nuclear receptors, RORs bind as monomers to specific ROR response elements (ROREs). The consensus RORE contains an AGGTCA preceded by an A/T-rich region. Cell-type ROR specificity may be achieved through distinct interactions with cofactors, both activators and repressors, allowing for RORE-dependent regulation (Jetten et al., 2001). This characteristic may also be related to receptor stability, posttranslational modifications, agonists, and antagonists.

ROR is an orphan receptor most similar to retinoic acid receptor (RAR) but has no identified ligand. It is suggested, based on structural crystallographic studies, that cholesterol or a cholesterol derivative is the putative ligand. In functional studies, higher binding of cholesterol sulfate results in increased RORα transcriptional activity (Kallen et al., 2004).

Of the three ROR subfamily isoforms, RORγ is most highly expressed in the thymus; it functions in thymopoesis, lymph node organogenesis, and immune system regulation. RORβ expression is restricted to the neurophotoendocrine system, the pineal gland, the retina, and suprachiasmatic nuclei; mouse studies suggest that RORβ likely regulates circadian rhythms. While studies in the mouse show that RORα is widely expressed throughout the body, its expression in the cerebellum is limited to PCs. In addition to key roles in cerebellar development, RORα may also function in bone development, angiogenesis, and atherosclerosis (Mamontova et al., 1998; Meyer et al., 2000; Jarvis et al., 2002).

Staggerer mice have a naturally occurring deletion that disrupts the RORα ligand-binding homology domain (Hamilton et al., 1996). The homozygous *staggerer* mutation ($RORα^{sg/sg}$) results in a cell-autonomous cerebellar PC defect, which stunts development (Hatten and Messer, 1978; Landis and Sidman, 1978) and results in cerebellar hypoplasia and severe, nonprogressive ataxia (Sidman et al., 1962). Heterozygous *staggerer* mice ($RORα^{sg/+}$) display a mild and progressive, age-dependent phenotype similar to SCA1 mice. They have increased PC atrophy and cell loss, suggesting an RORα role in the mature PC (Zanjani et al., 1992; Hadj-Sahraoui et al., 2001).

Unlike ATXN1, which is widely expressed, RORα's cellular expression pattern is limited. RORα is not expressed in most areas of the brain; however, RORα is highly expressed in cerebellar PCs, a major site of SCA1 pathology (Ino, 2004). Thus the key to increased PCs susceptibility to SCA1 pathology may stem from

interactions of ATXN1 with RORα-Tip60. Previous studies suggest PCs are particularly susceptible to neurodegeneration when mutant ATXN1 is expressed during postnatal cerebellar development (Serra et al., 2006). Mutant *ATXN1* expression enhances the RORα degradation, but RORα expression is restored when conditional mutant *ATXN1* expression is turned off. Delaying *ATXN1*[82Q] expression until after cerebellar development reduces disease severity in adult mice compared to mice expressing *ATXN1*[82Q] during the early postnatal period. *ATXN1* mutant toxicity is partially or wholly due to its ability to reduce RORα in cerebellar PC nuclei and subsequently decrease the expression of RORα-mediated genes, which are important for proper PC maturation (Serra et al., 2006). These genes, which are linked by their roles in calcium and glutamate signaling, are downregulated before symptom onset in a mutant *ATXN1* mouse model (Lin et al., 2000; Serra et al., 2004).

Comparative studies show that many genes that are downregulated in SCA1 mice are also decreased in *staggerer* mice. These genes include calbindin-28K, Ca^{2+} binding protein (*Calb*), inositol 1, 4, 5-triphosphate receptor 1 (*Itpr1*), solute carrier family 1 (high affinity aspartate/glutamate transporter), member 6 (*Slc1A6*, EAAT4), Purkinje cell protein 2 (*Pcp2*/*L7*), RAR-related orphan receptor alpha (*Rora*), kit ligand (*Kit1*), Purkinje cell protein 4/calmodulin inhibitor (*Pcp4*), brain-specific beta-spectrin III (*Spnb3*), inhibitor of DNA binding 2 (*Idb2*), mGluR1 glutamate receptor subunit (*Grm1*), SERCA2, Ca^{2+}-transporting ATPase (*Atp2a2*), CARP, an Itpr1 binding protein (*Cals1*), and *Homer2* (Serra et al., 2006). *In vivo staggerer* mouse studies show that RORα is present at calcium

and glutamate signaling gene promoters (including *Itpr, Slc1A6, Pcp2*, and *Pcp4*) and regulates their transcription *in vivo* (Figure 2) (Gold et al., 2003).

Four isoforms arise from alternate human RORα locus splicing. These isoforms (RORα 1-4) are identical from the DNA-binding domain to the carboxyl terminus (including putative ligand-binding domains), but have distinct amino-terminal domains. The variations in RORα amino termini dictate DNA binding properties of these RORα splice variants (Becker-Andre et al., 1993; Giguere et al., 1994). Of the four isoforms, only RORα1 and RORα4 are present in the murine cerebellum, and *Rora4* RNA expression is higher (Matysiak-Scholze and Nehls, 1997).

SCA1 mouse models. To study SCA1 pathologic mechanisms, many mouse lines have been generated. These lines include *Atxn1* null mice, transgenic mice expressing the normal or expanded form of human ATXN1, a conditional transgenic line, and mice containing various amino acid substitutions at key residues. While the SCA1 null mice have subtle defects, they do not have pathologic cerebellar changes, suggesting a toxic gain-of-effect mutation in ATXN1 (Matilla et al., 1998). Two SCA1 transgenic models express either a normal human ATXN1 with 30 CAG (encoding glutamine) repeats or a mutant, expanded form with 82 repeats. Transgene expression is driven by the PC-specific promoter Pcp2/L7. The *ATXN1*[82Q] transgenic line most commonly used is the B05 line, which has an early onset ataxia and high transgene levels. Northern blots detected transgene RNA in heterozygotes (*ATXN1*[82Q]/+) by day P10. By 5-6 weeks mild changes in both PC morphology (perikarya vacuolation

and a subtle decrease in proximal dendritic arborization) are visible, and mice exhibit significant deficits in motor coordination, as assessed by Rota-Rod performance. By 12 weeks the pathology has progressed to obvious molecular layer (ML) thinning. At 24 weeks the cerebellar degeneration includes significant cerebellar PC death and progressively severe ataxia. The conditional SCA1 model highlights the hypothesis that cellular dysfunction, rather than cell death, is primarily responsible for PC pathology and gait ataxia (Clark et al., 1997).

The conditional SCA1 transgenic mice express a PC-specific, tetracycline/doxycyclin-suppressible *ATXN1*[82Q]. In early stage disease (mutant *ATXN1* expression for 6 weeks), SCA1 behavioral phenotypes (Rota-Rod performance and home cage behavior), as well as pathological changes, (specifically ML thickness, cytoplasmic vacuoles, dendritic pruning, and nuclear inclusions) are almost completely reversed after turning off mutant *ATXN1* expression. Mice with midstage disease (mutant ATXN1 expression for more than 12 weeks) clear mutant ATXN1 from their PC neurons within days after *ATXN1*[82Q] expression is turned off. After 12 weeks gene-on—4 weeks gene-off, mice show home cage behavior improvements and stalled dendritic atrophy. After 12 weeks gene-on—8/12 weeks gene-off, mice improve in Rota-Rod performance to a level intermediate between 19 week wild-type (wt) and 20-24 week gene-on. Twelve week gene-on—8-12 week gene-off mice also have some ML thickness and dendritic tree arborization restoration. Late stage disease (after 32 weeks) is only mildly reversible after 8-12 weeks without mutant gene

expression. Generally disease process is not reversible, because recovery is more difficult with prolonged *ATXN1*[82Q] expression (Zu et al., 2004).

Tip60. Efforts to characterize the pathologic mechanisms of SCA1 include identifying ATXN1 interacting proteins. Interestingly several of these binding partners include transcriptional regulators and modulators of gene expression, such as Capicua (CIC), RNA-binding motif protein 17 (RBM17), silencing mediator of retinoid and thyroid hormone receptors (SMRT), polyglutamine binding protein 1 (PQBP1), and growth factor independent (Gfi-1) (Fernandez-Funez et al., 2000; Okazawa et al., 2002; Tsai et al., 2004; Tsuda et al., 2005; Lam et al., 2006; Lim et al., 2008). Particularly relevant for my experiments are two additional transcriptional regulators in this group: RORα and Tat interactive protein 60kDa (Tip60, HTATIP) (Kamine et al., 1996b; Serra et al., 2006). I utilized a genetic approach to examine whether the ATXN1/Tip60 interaction is relevant for disease.

Tip60 was initially identified as an interacting protein of the HIV-1 Tat transactivator (Kamine et al., 1996a). Tip60 is an acetyltransferase; it catalyzes the reversible addition of acetyl groups to lysine residues. Acetylation can affect a wide variety of target protein activities and is targeted to histone and nonhistone proteins, including nuclear acetylases, transcription factors, nuclear import factors, and tubulin. Acetylation can impact DNA binding, protein stability, and protein-protein interactions (Kouzarides, 2000).

Tip60 has been shown to transactivate class I nuclear hormone receptors, including RORα, (Yamamoto and Horikoshi, 1997; Brady et al., 1999; Gaughan et al., 2001; Gold et al., 2003) and is recruited by RORα, along with other transcriptional coactivators, to the target gene promoter regions. (Brady et al., 1999); Gaughan et al., 2001; Gold et al., 2003; Yamamoto and Horikoshi, 1997). *Tip60* expression during mouse embryogenesis peaks at day E11 and is expressed widely in adult tissues including, but not limited to, the following: testis > heart > whole brain > kidney > liver > lung > spleen and skeletal muscle (McAllister et al., 2002). *Tip60* expressed sequence tag (ESTs) dot blots in over 30 tissue types suggest that *Tip60* expression is highest in the adult brain, followed by bone and lymph nodes; *Tip60* expression is somewhat higher in the zygote, post implantation, and late gestational stages, when compared to other developmental periods (www.ncbi.nil.nih.gov).

Previous studies using murine cerebella show that ATXN1, RORα, and Tip60 are part of an *in vivo* complex. However *in vitro* GST pull-down assays suggest that only ATXN1 and Tip60 interact directly; *in vivo* data suggests this interaction is polyglutamine tract length independent (Serra et al., 2006). Given that mutant ATXN1 depletes RORα from the cerebellum and early postnatal RORα expression is necessary for proper PC development, I hypothesize that ATXN1 and Tip60 interaction in the ATXN1/Tip60/RORα-containing complex has important relevance for SCA1 disease pathogenesis.

To investigate the effects of Tip60 on disease, I crossed *ATXN1*[82Q]/+ transgenic with *Tip60*$^{+/-}$ mice. F_1 littermates allowed the direct comparison of *ATXN1*[82Q] disease with full expression of *Tip60* versus a partial loss of *Tip60*, along with wt littermates that expressed only endogenous, 2Q *Atxn1*. If my hypothesis is correct, then I expect partial *Tip60* loss to change SCA1 disease course. Due to different parental mouse strains, all offspring were on the mixed genetic background of FVB, SV-129, and C57BL/6. I used the multiple mouse model genotypes to compare pathologic neurodegeneration markers, changes in mRNA and protein expression, and behavioral phenotypes. Because ATXN1 has a toxic gain-of-function effect, and Tip60 interacts directly with ATXN1, partial *Tip60* loss could be predicted to block neurodegeneration by destabilizing or similarly silencing ATXN1. Conversely if Tip60 promotes ATXN1 degradation or positively regulates RORα, partial *Tip60* loss would worsen neurodegeneration. I also explored whether Tip60 acetyltransferase activity was affected by ATXN1 polyglutamine repeat length. Finally I identified interfering RNA (RNAi) targets with potential therapeutic applications for SCA1.

Figure 1. ATXN1 protein diagram. N-terminal region of Boat and Ataxin-1 (NBA) region, Polyglutamine tract (QQQ), self-association region (SAR), and ATXN1 and HMG-box protein 1 (AXH) domain. The AXH domain is the only domain with a known biochemical function (oligonucleotide binding), and it mediates interactions with several transcriptional co-activators and co-repressors.

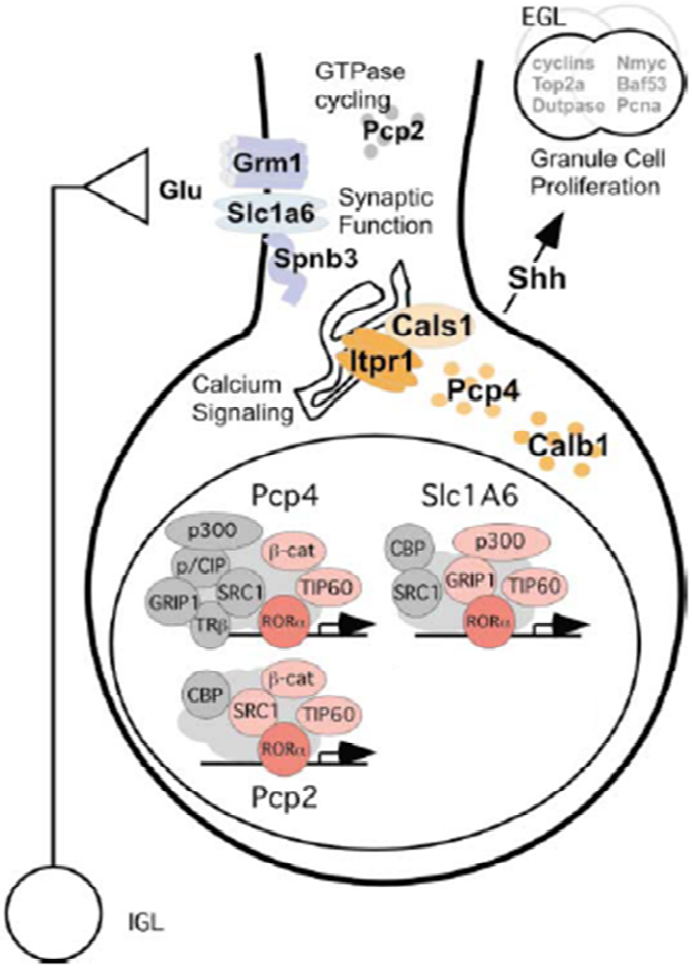

Figure 2. Model for RORα-dependent gene expression in Purkinje cells. Gene products of RORα-mediated targets are involved in PC calcium and glutamate signaling pathways. RORα recruits promoter-specific sets of co-activators to target gene promoters, shown in the nucleus. At day P0, Tip60 is present at Pcp4, Slc1A6, and Pcp2 promoter complexes (modified from Gold et al., 2003.)

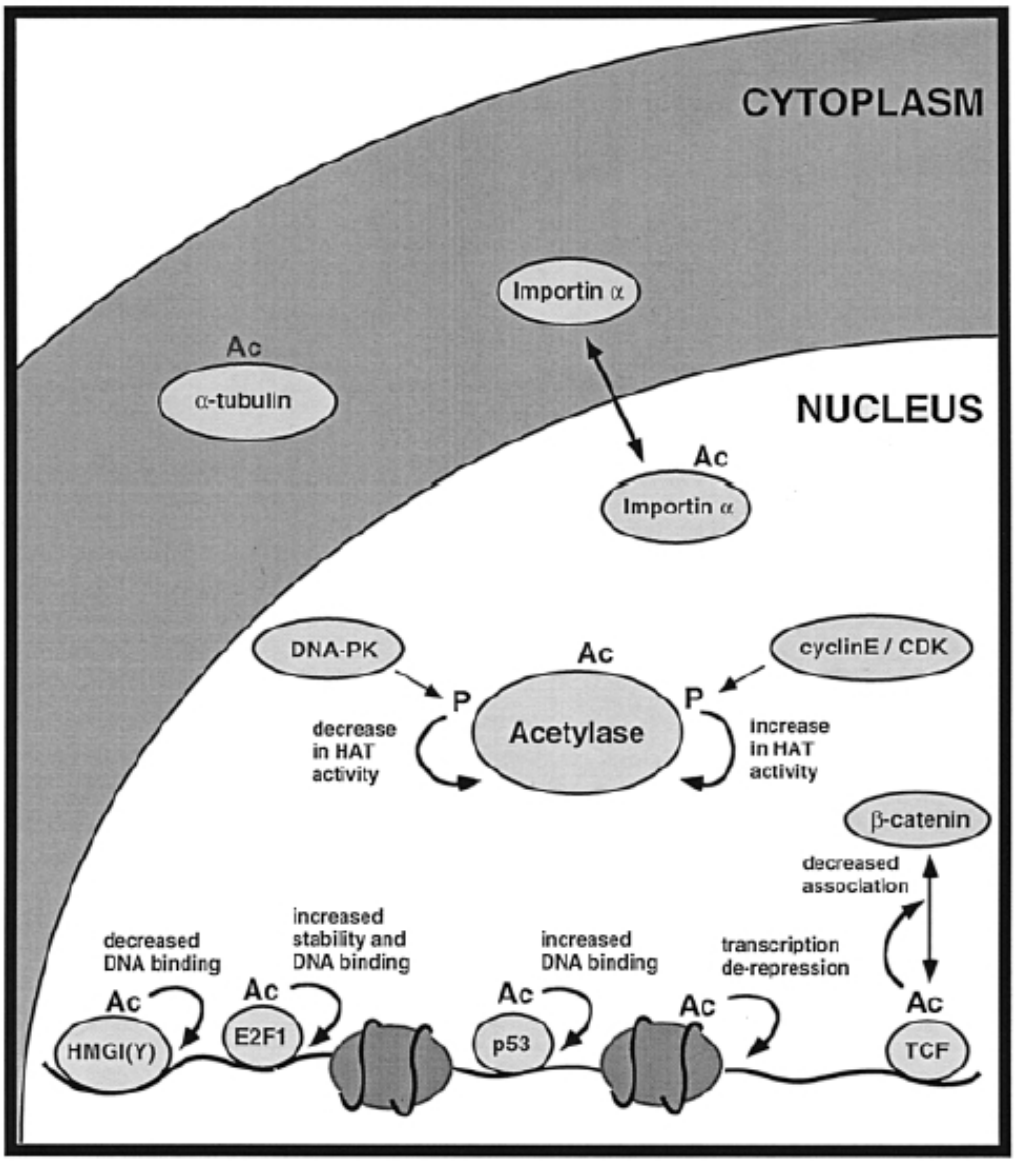

Figure 3. Acetylation is a regulatory mechanism directed at a variety of cellular proteins. Substrates include histones, nuclear acetylases, transcription factors, and nuclear import factors. Acetylation can impact protein stability, DNA binding, and protein-protein interactions (Kouzarides, 2000).

Chapter 2

Mouse Genetic Background Strain Effect on SCA1 Disease

Part I: Genetic Background Strains

A variety of inbred genetic mouse strains and substrains are available to create experimental mouse models. Genetic background variation exists among the strains, which can result in phenotypic differences, especially when mice are engineered with genetic insertions or deletions. To interrogate the genetic background effect on *ATXN1*[82Q]/+ mediated disease, I compared mice with an FVB background to mice with an FVB;SV-129;C57BL/6 mixed genetic background. The mixed genetic background mice are further described and characterized in Chapter 3. All mice expressed the same mutant *ATXN1*[82Q]/+ transgene.

Part II: Results and Discussion: Genetic Background Strain Effect on Neurodegeneration by Molecular Layer Thickness

Genetic background strain: effect on wt (FVB) and wt (FVB;SV-129;C57BL/6) ML thickness. Wt mice on the FVB genetic background have a relatively stable ML thickness. At 5, 12, and 20 weeks, the PC dendrites average 178 µM, 188 µM, and 185 µM, respectively (Orr lab, unpublished data; Serra et al., 2006). The mixed genetic background (FVB;SV-129;C57BL/6) wt mice had slightly declining

MLs measuring 162 µM (9 weeks), 158 µM (12 weeks), 148 µM (16 weeks), and 147 µM (20 weeks) (Figure 4A). When ML thicknesses were compared at 9, 12, 16, and 20 weeks, no two consecutive time points had significantly different ML thicknesses. However at 20 weeks the wt (FVB;SV-129;C57BL/6) mice had a significantly thinner ML than wt mice on the same genetic background at 9 weeks.

The wt (FVB;SV-129;C57BL/6) mice showed a greater decline in ML thickness than wt (FVB) mice. The wt (FVB;SV-129;C57BL/6) MLs were on average 30 µM less than wt (FVB) counterparts (average of 154 µM versus 184 µM). In nontransgenic mice, the mixed genetic background lowered the baseline molecular layer thickness and predisposed the mice to greater ML decline over time.

Genetic background strain: effect on B05 (*ATXN1*[82Q]/+ on FVB background) and *ATXN1*[82Q]/+ (FVB;SV-129;C57BL/6) ML thickness. A*TXN1*[82Q]/+ (FVB) mice demonstrate slow, progressive PC degeneration between 5 and 20 weeks (Clark et al., 1997). At 5 weeks the *ATXN1*[82Q]/+ (FVB) ML thickness is 172 µM; at 12 weeks the ML thickness is 157 µM, a decrease of 15 µM. At 20 weeks the *ATXN1*[82Q]/+ (FVB) ML is 149 µM, an additional thinning of 8 µM (Orr lab, unpublished data; Serra et al., 2006). The *ATXN1*[82Q]/+ (FVB;SV-129;C57BL/6) experienced a more rapid loss of ML thickness (Figure 4B). At 9 weeks the average ML thickness of *ATXN1*[82Q]/+ (FVB;SV-129;C57BL/6) mice was 138 µM. At 12 weeks the ML thickness decreased to 115 µM and remained at 115

μM from 16 to 20 weeks. The mutant *ATXN1*[82Q]/+ transgene on the mixed genetic background (FVB;SV-129;C57BL/6) resulted in a more rapid, progressive neurodegeneration than the FVB background alone.

Part III: Discussion

PC degeneration rate is more rapid when *ATXN1*[82Q]/+ is expressed on the mixed genetic background versus the FVB background. Both groups of mice express the same mutant transgene, which is driven by the same PC-specific promoter. However FVB mice experience a more constant, slowly progressive disease course, and the FVB;SV-129;C57BL/6 mice have early, rapidly progressive cerebellar degeneration followed by a statically thin (23% less than FVB counterparts at 20 weeks) ML over time. Characterizing the genetic background modifying effect provides insight into a similar phenomenon observed in SCA1 patients. Polyglutamine repeat length is strongly and inversely correlated (r=0.9) with age of onset. Patients with the same *ATXN1* repeat length have a variable symptom onset age (up to 20 years) (Netravathi et al., 2009). Another way to analyze disease course in SCA1 patients is the correlation between CAG repeat length and age-adjusted disease severity, as measured by the International Cooperative Ataxia Rating Scale (IARS). As expected, there is a significant, positive correlation between disease severity measures and CAG repeat length (r=0.6). More variation exists within ataxia symptom severity for a given CAG repeat length than the variation inherent to symptom onset age (Netravathi et al., 2009). The neurodegenerative rate variation among mouse

genetic background strains suggests that human genetic modifiers may contribute to SCA1 disease course variation. Identifying SCA1 genetic modifiers may illuminate additional pathways that influence neurodegeneration. Since I observed faster degenerative rates in both wt and *ATXN1*[82Q] mice on the mixed genetic background, my findings have important implications for both SCA1 patients and the unaffected population at large.

A.

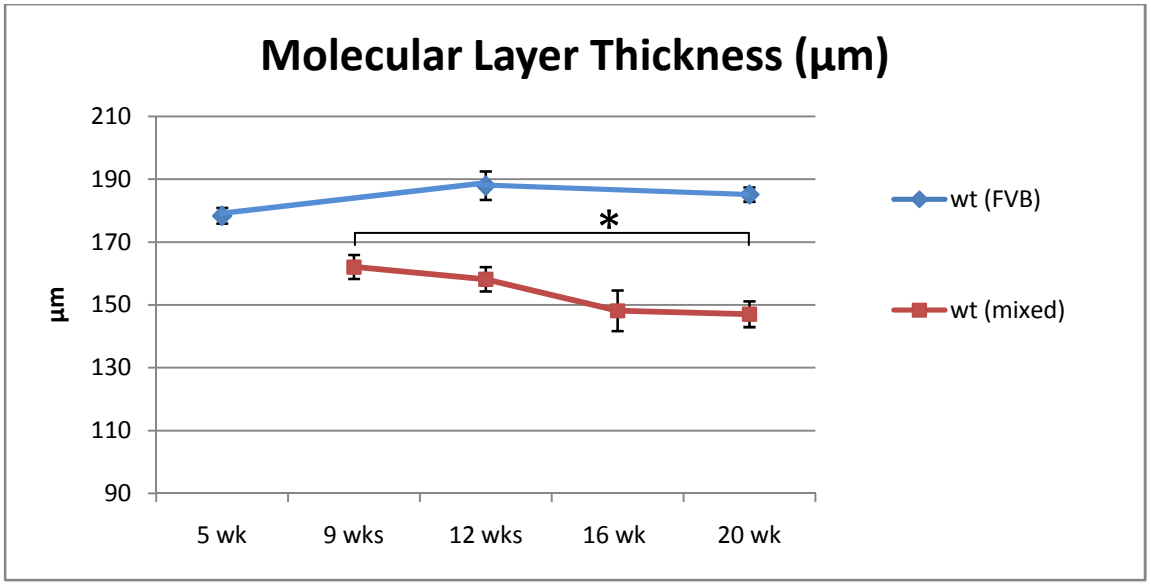

B.

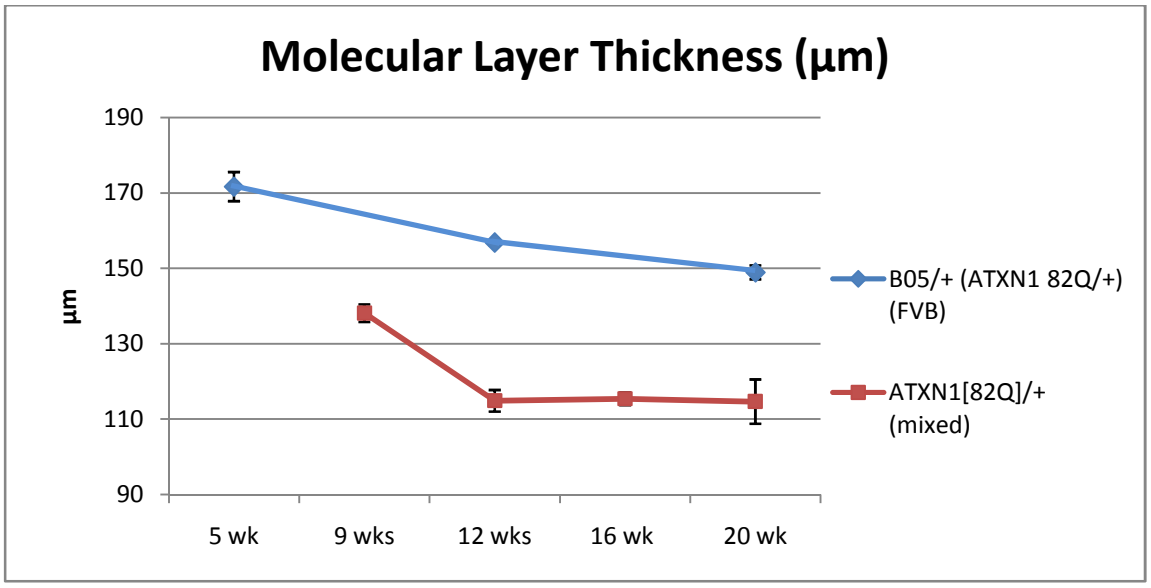

Figure 4. Molecular layer thickness of A) wt (FVB) and wt (FVB;SV-129; C57BL/6) mice and B) B05 mice (*ATXN1*[82Q]/+ on FVB background) and *ATXN1*[82Q]/+ (FVB;SV-129;C57BL/6) mice at various ages, measured with calbindin immunostaining and confocal microscopy. Error bars represent SEM. [p-values: A) 9 wks vs. 20 wks: p=0.015 B) 9 wks vs. 12 wks: p=0.0008; 9 wks vs. 16 wks: p=0.0006; 9 wks vs. 20 wks: p=0.0049]. Wt (FVB) and B05 data measured by Lisa Duvick (Orr lab).

Chapter 3

ATXN1[82Q]/+:*Tip60*$^{+/-}$ Mouse Model

Part I: Generation of *ATXN1*[82Q]/+:*Tip60*$^{+/-}$ Mice

Heterozygous *Tip60* (*Htatip*) knockout mice were generated by the Lough lab (Medical College of Wisconsin) on the SV-129;C57BL/6 background using homologous recombination with a neomycin targeting vector. Heterozygous *Tip60* mice are viable and phenotypically normal; however, homozygous *Tip60* knockouts are embryonically lethal just after the blastocyst developmental stage (Dr. John Lough, personal communication).

Tip60$^{+/-}$ mRNA levels in murine whole brain are approximately half the *Tip60*$^{+/+}$ amount (Gorrini et al., 2007). I observed similar results when analyzing *Tip60* mRNA expression levels in the cerebellum. Heterozygous *Tip60* mice expressed approximately 50% of wt *Tip60* levels (both SV-129;C57BL/6), validating *Tip60*$^{+/-}$ mice for investigating effects of partial *Tip60* expression in a cerebellar disease model (Figure 5).

I crossed *Tip60*$^{+/-}$ and *ATXN1*[82Q]/+ mice to create compound heterozygotes. The *ATXN1*[82Q]/+ mice were from the B05 line, which express human, expanded *ATXN1* on the FVB background. The human *ATXN1*[82Q] transgene is

driven by the PC-specific *Pcp2*/L7 promoter. B05 mice are extensively characterized and exhibit classic SCA1 cerebellar degeneration and gait ataxia (Burright et al., 1995; Clark et al., 1997). The resulting *ATXN1*[82Q]/+:*Tip60*$^{+/-}$ offspring had mixed FVB;SV-129;C57BL/6 backgrounds (Figure 6).

Part II: Results: *ATXN1*[82Q]/+:*Tip60*$^{+/-}$ Transgenic Mice Expressed Decreased *Tip60* Levels and Constant *ATXN1*[82Q] Transgene Levels

To assess whether partial *Tip60* loss had an effect on *ATXN1*[82Q] transgene expression, I compared transgene expression between *ATXN1*[82Q]/+ and *ATXN1*[82Q]/+:*Tip60*$^{+/-}$ mice. Mutant *ATXN1* transgene expression was similar regardless of *Tip60* dosage (Figure 7), confirming that differences between *ATXN1*[82Q]/+:*Tip60*$^{+/-}$ and *ATXN1*[82Q]/+ mice were not due to altered *ATXN1*[82Q] transgene expression. This control is important because the Pcp2 promoter, which drives expression of the PC-specific *ATXN1*[82Q] transgene, is regulated by RORα, and Tip60 is present in the Pcp2 promoter complex (Gold et al., 2003). If partial Tip60 loss decreased Pcp2 expression, a decrease in *ATXN1*[82Q] transgene expression would result in a less severe disease. Since transgene expression was unchanged, any differences between *ATXN1*[82Q]/+:*Tip60*$^{+/-}$ and *ATXN1*[82Q]/+ mice resulted from the partial loss of *Tip60*.

Part III: Results: *ATXN1*[82Q]/+:*Tip60*$^{+/-}$ Mice Have Slowed Cerebellar Degeneration Relative to *ATXN1*[82Q]/+ Littermates

PC degeneration is an SCA1 hallmark (Zoghbi and Orr, 2000). Molecular layer thinning reflects cerebellar degeneration and dendritic tree atrophy of *ATXN1*[82Q] mice (Zu et al., 2004). I assessed ML morphology in the *ATXN1*[82Q]/+:*Tip60*$^{+/-}$ model to quantify degeneration. Cerebellar sections were immunostained with calbindin, a calcium binding and buffering protein highly expressed in PCs (Batini, 1990). Two sagittal sections were analyzed per mouse in at least five mice per genotype. Using confocal laser scanning microscopy, six systematically sampled measurements were taken at the primary fissure and averaged to determine ML thickness.

Tip60 partial loss: effect on *ATXN1*[82Q]/+ ML thickness. Partial *Tip60* loss slowed the neurodegeneration in *ATXN1*[82Q]/+:*Tip60*$^{+/-}$ mice relative to *ATXN1*[82Q]/+ mice (Figure 8). *ATXN1*[82Q]/+:*Tip60*$^{+/-}$ mice had a significantly thicker ML than their *ATXN1*[82Q]/+ littermates at 12 and 16 weeks. At 12 and 16 weeks *ATXN1*[82Q]/+ mice had an average ML thickness of 115 µM. However at 12 and 16 weeks, *ATXN1*[82Q]/+:*Tip60*$^{+/-}$ ML thickness was 134 and 143 µM, respectively. At 20 weeks *ATXN1*[82Q]/+:*Tip60*$^{+/-}$ ML thickness thinned to 114 µM, which was comparable to *ATXN1*[82Q]/+ littermates (115 µM, unchanged from 12 and 16 weeks) (Figure 9). There was a protective window after 9 weeks and before 20 weeks during which ML thinning was slowed in *ATXN1*[82Q]/+:*Tip60*$^{+/-}$ mice. Qualitative observation at 16 weeks revealed that

ATXN1[82Q]/+:*Tip60*$^{+/-}$ mice exhibited MLs similar in size to wt littermates, and the *ATXN1*[82Q]/+:*Tip60*$^{+/-}$ dendritic arbor appeared more highly branched and complex than age-matched controls.

In summary, the amount of *Tip60* did not affect ML thickness at an early age; 9 week *ATXN1*[82Q]/+ mice, whether *Tip60*$^{+/-}$ or *Tip60*$^{+/+}$, had similar ML thicknesses (134 µM vs. 138 µM). Instead *Tip60* partial loss was important during midstage disease (12 and 16 weeks) to slow cerebellar degeneration. At 20 weeks half *Tip60* levels did not protect the *ATXN1*[82Q]/+:*Tip60*$^{+/-}$ ML thickness relative to *ATXN1*[82Q]/+ littermates.

Part III: Results and Discussion: The Partial Loss of *Tip60* Delays Reduction of Climbing Fiber Terminals Along the PC Dendrite

Climbing fiber terminals in the *ATXN1*[82Q]/+:*Tip60*$^{+/-}$ mouse model. PCs receive afferent, stimulatory input from climbing fibers (CFs) expressing VGluT2 (Chan-Palay, 1974; Fremeau et al., 2001). CF input is important for PC circuitry development, coordination, and learning (Crepel, 1982; Ito, 1989; Linden and Connor, 1995). Using calbindin immunofluorescence to visualize PC dendrites and VGluT2 immunofluorescence to visualize CF terminals, I measured the extent of CF terminals along the PC dendrite in the *ATXN1*[82Q]/+:*Tip60*$^{+/-}$ mouse model (Figures 10-13). CF-PC dendrite percent innervation in wt, *ATXN1*[82Q]/+, and *ATXN1*[82Q]/+:*Tip60*$^{+/-}$ mice is expressed as a percentage in Figure 14. CF terminals were characterized at 9, 12, 16, and 20 weeks. At all ages, wt mice had significantly more climbing fiber extension along the dendrite

compared to *ATXN1*[82Q]/+ expressing mice. However at 12 and 16 weeks, the *Tip60* partial loss prevented the full degree of CF terminal regression observed in *ATXN1*[82Q]/+ mice. At 12 and 16 weeks *ATXN1*[82Q]/+:*Tip60*$^{+/-}$ mice had significantly higher CF-PC terminal percentages than their *ATXN1*[82Q]/+ littermates. At 20 weeks *ATXN1*[82Q]/+:*Tip60*$^{+/-}$ and *ATXN1*[82Q]/+ mice had similar (approximately 75%) CF-PC dendrite extension, which was significantly less than wt controls. The slowed CF-PC dendrite regression at 12 and 16 weeks coincides with suspension of ML thinning.

VGluT2 and climbing fiber terminals at Purkinje cells. PCs receive two types of stimulatory inputs: climbing fibers (CFs) and parallel fibers (PFs) (Chan-Palay, 1974). These afferent fibers are important for PC circuitry development, cerebellar motor coordination, and learning (Crepel, 1982; Ito, 1989; Linden and Connor, 1995), all processes which involve postsynaptic glutamate receptors and downstream signal targets (Aiba et al., 1994; Ichise et al., 2000). Glutamate is the major excitatory neurotransmitter in the nervous system. Glutamate molecules are actively trafficked to axon terminals (Maycox et al., 1988; Carlson et al., 1989), where they are released from synaptic vesicles and taken up by dendritic NMDA receptors (Dingledine et al., 1999).

The vesicular glutamate transporter (VGluT) has three subtypes: VGluT1, VGluT2, and VGluT3 (Ni et al., 1994; Yasuo Aihara, 2000; Gras et al., 2002); VGluT1 and VGluT2 are functionally relevant (Bellocchio et al., 2000; Takamori et al., 2000; Fremeau et al., 2001). *VLGuT1* and *VGluT2* mRNA have

nonoverlapping patterns in the adult brain. *VGluT1* mRNA is expressed in cerebral cortex, cerebellar cortex, and hippocampus; *VGluT2* mRNA is expressed in thalamus, brainstem, and deep cerebellar nuclei. Synapses expressing VGluT2 are more likely to release neurotransmitters than synapses expressing VGluT1 (Fremeau et al., 2001; Varoqui et al., 2002).

In the mature brain PF inputs at PC dendrites express VGluT1, while CF inputs onto the same cells express VGluT2 (Fremeau et al., 2001). VGluT1 and VGluT2 expression overlaps during development, but becomes discrete during postnatal weeks 2 and 3 (Miyazaki et al., 2003; Fremeau et al., 2004). VGluT2 is specifically expressed on PFs until the second 10 days of postnatal development (when cells begin switching to the VGluT1 subtype) and on CFs throughout all of mature postnatal life (Fremeau et al., 2001; Miyazaki et al., 2003; Fremeau et al., 2004). It follows that subtype switching (after P10) is a key period in PC maturation. The synaptic organization changes rapidly, PC dendrites actively arborize, and parallel fibers synapse on distal PC dendrites (Altman, 1972a, b; J. Takács, 1994).

Interestingly when RORα is absent, as in the homozygous *staggerer* mouse, there is delayed developmental subtype switching of VGluT1/VGluT2 at synapses (Sonja Janmaat, 2009). Only a small fraction of *Rora*$^{sg/sg}$ PCs survive early postnatal development, and these PCs are reminiscent of an earlier developmental stage; dendrites are simple and spineless, PF synapses are rare, and multiple CF innervations persist (Crepel et al., 1980; Jean Mariani, 1982;

Boukhtouche et al., 2006). RORα, perhaps via mutant ATXN1, impacts PC VGluT2 terminals. I have demonstrated decreased PC-CF VGluT2 terminals in *ATXN1*[82Q]/+ mice on the mixed genetic background and a Tip60 role in *ATXN1*[82Q]/+:*Tip60*$^{+/-}$ PC-CF regression delay (Figure 14).

Part IV: Results: Behavioral Phenotypes of *ATXN1*[82Q]/+:*Tip60*$^{+/-}$ Mice

Gait ataxia is a prominent SCA1 symptom. Ataxia, or lack of motor coordination, can be measured in several ways. I thoroughly characterized the behavioral phenotype by two methods, Rota-Rod and DigiGait apparatus, at five ages. A third measure of ataxia, home cage behavior, was not obvious in *ATXN1*[82Q]/+ transgenic mice on the mixed genetic background, in contrast to *ATXN1*[82Q]/+ (FVB) mice. A blind test by an objective scorer at 16 weeks confirmed the lack of ataxic home cage behavior.

DigiGait. The main components of the DigiGait apparatus (Mouse Specifics, Inc., Boston, MA) are a treadmill with a transparent belt and a camera that captures a series of live images as mice walk on the treadmill. DigiGait software collects and analyzes gait parameters for each paw (Hampton et al., 2004; Kale et al., 2004; Amende et al., 2005). I found the most useful parameters in this mouse model were stride time, rear stance width, and rear step angle, which are gait components affected by ataxia.

At 20 and 34 weeks *ATXN1*[82Q]/+ mice had a significantly longer rear stride time than wt littermates (Figure 15). This increase in stride time is an expected

difference between unaffected and ataxic (B05) mice, so it was surprising that these differences were not observed earlier than 20 weeks. *ATXN1*[82Q]/+:*Tip60*$^{+/-}$ and *ATXN1*[82Q]/+ mice have significantly longer stride times than their wt littermates at 34 weeks. This difference was expected beyond the protective window when the partial *Tip60* loss no longer delayed ML thinning. However partial *Tip60* protection was absent at 20 weeks, and differences in rear stride time were not neutralized until later. Analysis of wt (FVB) and B05/+ (FVB) animals by DigiGait did not reveal significant differences in rear stride time at 6, 9, 12, 16, or 20 weeks (Figure 18), limiting the sensitivity of this measurement and the interpretation of *ATXN1*[82Q]/+:*Tip60*$^{+/-}$ mice.

Rear stance width measurements were also performed (Figure 16). Generally an ataxic mouse has a wider rear stance width than a nonataxic mouse. At 16 weeks, when the *ATXN1*[82Q]/+ mice had more severe pathology than *ATXN1*[82Q]/+:*Tip60*$^{+/-}$, the *ATXN1*[82Q]/+:*Tip60*$^{+/-}$ mice had a surprisingly wider gait than their *ATXN1*[82Q]/+ littermates. At 20 weeks *ATXN1*[82Q]/+:*Tip60*$^{+/-}$ mice had a significantly wider gait than wt mice, which was expected beyond the protective window. Wt (FVB) and B05/+ (FVB) DigiGait analysis revealed significant differences in rear stance width at 9, 12, and 16 weeks (Figure 19). However no significant differences were detected between wt (FVB;SV-129;C57BL/6) and *ATXN1*[82Q]/+ (FVB;SV-129;C57BL/6) mice at the same ages. One important conclusion derived from these experiments is that the mixed genetic background (FVB;SV-129;C57BL/6) dampens the *ATXN1*[82Q]/+ (FVB) ataxic phenotype. This dampening may be a result of hybrid vigor or differences

inherent to each background strain. These observations have important implications for characterizing ataxia in transgenic models.

Rear step angle measurement is the third output of DigiGait analysis (Figure 17); step angle is thought to increase in ataxic mice relative to wt controls. In the *ATXN1*[82Q]/+:*Tip60*$^{+/-}$ model, changes in step angle are seen at 16 and 34 weeks. At 16 weeks, within the protective PC window, *ATXN1*[82Q]/+ mice had a significantly larger rear step angle than their wt and *ATXN1*[82Q]/+:*Tip60*$^{+/-}$ littermates. This observation is consistent with the delay in *ATXN1*[82Q]/+:*Tip60*$^{+/-}$ neurodegeneration that also was seen at 16 weeks. At 34 weeks the protective *Tip60*$^{+/-}$ effect on the ML is lost. At 34 weeks the rear step angle of *ATXN1*[82Q]/+ and *ATXN1*[82Q]/+:*Tip60*$^{+/-}$ mice was significantly higher than their wt littermates, suggesting a more ataxic gait in both *ATXN1*[82Q]/+ transgenic genotypes at this later disease stage. Wt (FVB) and B05/+ (FVB) comparison by DigiGait did not reveal significant differences in rear step angle at 6, 9, 12, 16, or 20 weeks (Figure 20), limiting *ATXN1*[82Q]/+:*Tip60*$^{+/-}$ interpretations by this measurement.

Generally DigiGait analysis demonstrates an important genetic strain effect on *ATXN1*[82Q]/+-induced ataxia. Ataxia could be detected by rear stance width in wt versus B05/+ (FVB) mice, but stance width differences in wt versus *ATXN1*[82Q]/+ (FVB;SV-129;C57BL/6) were undetectable. In summary, rear step angle correlates best with ML thickness in *ATXN1*[82Q]/+:*Tip60*$^{+/-}$ mice at 16 and 34 weeks.

Rota-Rod. The Rota-Rod test is based on a rotating rod suspended over a platform. As the rod accelerates, balance and coordination are tested (Jones and Roberts, 1968). Mice are placed on the Rota-Rod at 4 rpm, and during a 10 minute trial the rod accelerates to 40 rpm. The trial concludes when the mice fall off the Rota-Rod or at the end of the 10 minute testing period. Each mouse performs four trials per day for 4 consecutive days, and each day's average trial result is calculated for each genotype. Results are reported as latency to fall (seconds). A shorter latency to fall indicates more severe ataxia. The Rota-Rod has been used previously to characterize ATXN1[82Q]/+ (FVB) and conditional ATXN1[82Q]/+ (FVB) mouse models (Clark et al., 1997; Zu et al., 2004). I performed Rota-Rod analysis for each of the four *ATXN1*[82Q]/+:*Tip60*$^{+/-}$ genotypes at 9, 12, 16, 20, and 30 weeks (Figures 21-25). The most striking differences were observed at 30 weeks. *ATXN1*[82Q]/+ and *ATXN1*[82Q]/+:*Tip60*$^{+/-}$ mice performed more poorly than wt littermates. Other significant comparisons included wt vs. *ATXN1*[82Q]/+ mice (week 9, day 3), wt vs. *ATXN1*[82Q]/+:*Tip60*$^{+/-}$ mice (week 9, day 3), wt vs. *ATXN1*[82Q]/+ mice (week 12, day 3), wt vs. ATXN1[82Q]/+:Tip60$^{+/-}$ mice (week 12, day 3). Of note, Tip60 heterozygotes perform similarly to wt mice.

At 12 weeks I performed Rota-Rod analysis on FVB and B05/+ mice (Figure 26), because 12 weeks is a well-characterized age for SCA1 mouse models, and ataxia is present (Burright et al., 1995). B05/+ (FVB) had a shorter latency to fall than wt (FVB) mice, but these differences were not significant in my trials. These observations underscore the confounding factors that affect Rota-Rod sensitivity

(environmental conditions, sensorimotor differences among mice, variable attention to the task, and stress) and limit the interpretations of the *ATXN1*[82Q]/+:*Tip60*$^{+/-}$ data.

Part V: Discussion: The Effects of Genetic Background on Behavioral Phenotype

Previous reports show that as early as 5 weeks, and at 12 weeks, a significant difference in Rota-Rod performance is measurable between wt (FVB) and B05 (*ATXN1*[82Q] heterozygotes on the FVB background) mice (Clark et al., 1997). In contrast, there was no significant difference between wt (FVB;SV-129;C57BL/6) mice and *ATXN1*[82Q]/+ mice (FVB;SV-129;C57BL/6). These wt and SCA1 mice expressed the same transgene, but were on different genetic backgrounds, suggesting that strain variation may modify behavioral phenotype. At 12 weeks I did not detect significantly different Rota-Rod phenotypes between FVB and B05 mice. This observation may be a result of different testing locations, environmental conditions, sample size, test administrator, or genetic drift over time.

Gene targeting by homologous recombination in mouse embryonic stem (ES) cells is an important tool for isolating specific gene effects (Lathe and Morris, 1994; Takahashi et al., 1994). ES cell donor strains are often chosen for technical reasons such as ES cell line availability and breeding characteristics. As with the *Tip60* heterozygous line, ES cells are frequently derived from inbred 129 strains (such as 129/Sv, 129/J, or 129/Ola), and successfully targeted chimeras are subsequently combined with C57BL/6 blastocysts (Gerlai, 1996).

In a recent study on prostate tissues comparing 8,300 genes from five commonly studied mouse genotypes (C57BL/6, 129X1/Sv, BALB/c, FVB/N and DBA/2), approximately 13% of the genes (932 genes) showed significantly different expression in any one strain relative to other strains (false discovery rate ≤ 10%) (Bianchi-Frias et al., 2007). Another study compared gene expression in six different brain regions (cortex, hippocampus, amygdale, entorhinal cortex, midbrain, and cerebellum) between two mouse strains (C57BL/6 and SV-129(Ev)) that have diverse behavioral phenotypes and disease susceptibility (Crawley et al., 1997; Ingram and Jucker, 1999). Approximately 1% (73 genes) are significantly different in at least one brain region, and the cerebellum has the most distinct expression profile (Sandberg et al., 2000). When creating a transgenic or knockout model, this becomes important when one or more differentially expressed genes are linked to the targeted gene.

Animals from a mixed genetic background such as those from a cross between C57BL/6 and SV-129 have a variable combination of parental alleles. While it is true that naturally occurring populations are also genetically variable, the confounding effect on experimental variables can be minimized by increasing sample size. Backcrossing does not protect from false-positives that arise when donor strain alleles are linked to the targeted gene (Gerlai, 1996; Lathe, 1996). Furthermore inbred strains can also have considerable variation within individuals, making backcrossing a debatable utility (Lipp et al., 1995; Wolfer et al., 1995). Repeated backcrossing into an inbred background may also result in

inbreeding depression and increased sensitivity to aging, resulting in performance deficits (Lassalle et al., 2008).

Among the strains in my mouse model (FVB, SV-129, and C57BL/6), many phenotypic variations have been described in a wide variety of model systems (Crawley, 1996; Crusio, 1996; Gerlai, 1996; Lathe, 1996). For example, C57BL/6 mice are more susceptible to ketamine, pentobarbital, and N_20 than FVB mice (Sato et al., 2006). Previous studies have used 129/Sv x C57BL/6 crosses to evaluate learning and memory with the Morris water maze (Morris, 1984), Wolfer et al. (1995) show that the hybrid offspring strain performs better than both individual parental strains. Furthermore they predict that creating congenic lines through backcrossing is unlikely to enhance, and may even reduce, the sensitivity of the Morris test. The enhanced hybrid strain performance was not surprising to the authors and may be the result of hybrid vigor (Upchurch et al., 1988; Upchurch and Wehner, 1989; Fordyce and Wehner, 1993). As a caveat, hybrid animal sample size should be large enough to overcome genetic and epigenetic variability, and the control group's performance should be verified. In my behavioral studies sample size ranged from 6 to 14 mice per genotype.

Other researchers have used the Rota-Rod to measure motor coordination in mice with different genetic backgrounds. For example, D_2 dopamine receptor (*Drd2*)-deficient mice in a Parkinson's disease model have a Rota-Rod phenotype. The mice tested were the F_2 generation bred from a 129/Sv x C57BL/6 cross. However the discrepancy in coordination is not attributed to the

Drd2 allele, but rather to an inherent difference in *Drd2* knockout progenitor strains. Hybrid mice have a Rota-Rod deficiency that is corrected in the congenic C57BL/6 background. Interestingly when wt 129/SvEv, wt C57BL/6, and the F2 generations of *Drd2*$^{+/-}$, *Drd2*$^{+/+}$, and *Drd2*$^{-/-}$ hybrid lines are compared, 129/SvEv mice perform poorest on the Rota-Rod, suggesting that alleles linked to the 129 strains are responsible for the reduced performance rather than the *Drd2* knockout. When the lines are compared, C57BL/6 mice perform the best of all (Kelly et al., 1998). These studies in a neurodegenerative model highlight behavioral phenotype variability due to background strains and underscore careful data interpretation. Of particular interest for my studies are 129/SvEv versus C57BL/6 motor coordination differences. The *ATXN1*[82Q]/+:*Tip60*$^{+/-}$ model is further complicated by the additional FVB background strain. These experiments may help to interpret the differences in Rota-Rod performance between the wt (FVB) and wt (129/SV;C57BL/6;FVB) mice, as well as the B05/+ (FVB) and *ATXN1*[82Q]/+ (129/SV;C57BL/6;FVB). Furthermore my research highlighted using littermate controls to minimize strain effects when analyzing wt, transgenic, and transgenic/knockout mice behavioral phenotypes.

To ensure that transgenic and knockout strains do not genetically drift away from wt controls, periodic mutant and control mice interbreeding to produce heterozygotes helps maintain line integrity. Heterozygotes can be interbred with each other to regenerate wt and knockout mice with a more constant genetic background. To be even more meticulous, only heterozygous matings (while

more expensive and labor-intensive than homozygous breeding) further minimize genetic drift and control for maternal effects (Phillips et al., 1999).

Part VI: Results and Discussion: Partial *Tip60* Loss Restores RORα Protein Levels in *ATXN1*[82Q]/+:*Tip60*$^{+/-}$ Mice Relative to *ATXN1*[82Q]/+ During the Period When Cerebellar Degeneration is Slowed

An important observation of the *ATXN1*[82Q]/+ model is that mutant *ATXN1* depletes RORα protein and RNA from cerebellar PCs (Serra et al., 2006). Because *ATXN1*[82Q]/+:*Tip60*$^{+/-}$ mice experience a protective pathology window, I sought to characterize mechanisms that contribute to this protection. Because a key step in SCA1 pathology is a destabilization of RORα protein, I measured RORα protein in *ATXN1*[82Q]/+ relative to *ATXN1*[82Q]/+:*Tip60*$^{+/-}$ mice (Figure 27). Western blot analysis revealed that partial *Tip60* loss increased RORα protein expression relative to *ATXN1*[82Q]/+ littermates (lanes 1 versus 2). RORα isoforms 1 and 4 are present in cerebella (Matysiak-Scholze and Nehls, 1997). Except for unique amino-terminal domains, RORα1 and RORα4 are identical (Giguere et al., 1994). The difference between RORα isoforms results in proteins that are not clearly resolvable by the SDS-PAGE gel shown in Figure 27, suggesting the upper band at the predicted molecular weight of 55 kD (indicated by an asterisk) represents RORα, and the lower band is nonspecific or represents a degradation product. Northern blots by others and my qRT-PCR analysis suggest that absolute Rora4 mRNA levels are approximately two to tenfold higher than Rora1 (Matysiak-Scholze and Nehls, 1997). RORα4 likely

constitutes the majority of the band indicated by the asterisk. Protein lysates from homozygous *staggerer* (Rora$^{sg/sg}$) cerebellum (lane 3) are a negative control and confirm RORα antibody specificity, since *staggerer* mice contain a null mutation in the gene encoding RORα (Hamilton et al., 1996). Cell lysates isolated from COS cells transfected with Rora1 (lane 4) serve as a positive control. Taken together with RORα protein restoration in the conditional *ATXN1*[82Q]/+ mouse model, partial *Tip60* loss may slow cerebellar degeneration by stabilizing RORα protein in the *ATXN1*[82Q]/+:*Tip60*$^{+/-}$ mice.

Part VII: Results and Discussion: Analysis of Gene Expression in the *ATXN1*[82Q]/+:*Tip60*$^{+/-}$ Mouse Model

Tip60 is a transcriptional cofactor for RORα (Yamamoto and Horikoshi, 1997a; Brady et al., 1999; Gaughan et al., 2001). Because ATXN1 and Tip60-RORα are in a complex together (Serra et al., 2006), we characterized the effects of partial *Tip60* loss on *Rora* (isoforms 1 and 4) and RORα-mediated gene (*Pcp2* [Purkinje cell protein 2], *Pcp4* [Purkinje cell protein 4], *Slc1A6* [solute carrier family 1 {high affinity aspartate/glutamate transporter}, member 6], and *Itpr1* [Inositol 1,4,5-triphosphate receptor, type 1]) expression in the *ATXN1*[82Q]/+:*Tip60*$^{+/-}$ mouse model. Based on experiments in postnatal day 0 (P0) mice, Tip60 is present at the *Pcp2*, *Pcp4*, and *Slc1A6* promoters but not the *Itpr1* promoter (Gold et al., 2003). I measured gene expression at three ages: 8 weeks (an early stage with intermediate degeneration in both the *ATXN1*[82Q]/+ and *ATXN1*[82Q]/+:*Tip60*$^{+/}$) mice,12 weeks (a middle stage when *ATXN1*[82Q]/+ mice had reached the most

dramatic level of ML thinnng, and *ATXN1*[82Q]/+:*Tip60*$^{+/-}$ degeneration had slowed), and 20 weeks (a later stage when both *ATXN1*[82Q]/+ and *ATXN1*[82Q]/+:*Tip60*$^{+/-}$ degeneration had reached advanced levels).

In 8-week-old mice there were no significant differences between wt, *ATXN1*[82Q]/+, and *ATXN1*[82Q]/+:*Tip60*$^{+/-}$ expression of *Rora1*, *Rora4*, *Pcp4*, *Slc1A6*, or *Itpr1* (Figures 28A and 29A). At 12 weeks *Rora4*, *Pcp4*, and *Slc1A6* expression was significantly higher in *ATXN1*[82Q]/+:*Tip60*$^{+/-}$ compared to *ATXN1*[82Q]/+ mice (Figures 29A and 29B). At 20 weeks *Rora4*, *Pcp4*, and *Slc1A6* expression remained high in the *ATXN1*[82Q]/+:*Tip60*$^{+/-}$ mice compared to *ATXN1*[82Q]/+, and *ATXN1*[82Q]/+:*Tip60*$^{+/-}$ *Itpr1* expression was also higher than *ATXN1*[82Q]/+ (Figures 30A and 30B). Gene expression levels at 12 and 20 weeks (during and after the protective window) in *ATXN1*[82Q]/+ and *ATXN1*[82Q]/+:*Tip60*$^{+/-}$ mice are summarized in Table 2.

<u>*ATXN1*[82Q]/+ effect on *Rora* and RORα-mediated gene transcription.</u> These gene expression studies revealed that mutant ATXN1 alone (*ATXN1*[82Q]/+ mice) decreased *Rora* and RORα-mediated genes (*Rora4*, *Slc1A6*, *Pcp4*, *Pcp2 and Itpr1*) expression beginning at 12 weeks compared to wt. These genes are implicated in PC calcium and glutamate signaling. Previous microarray experiments using *ATXN1*[82Q]/+ (B05) mice on the FVB background support this data. B05 (FVB) and *ATXN1*[82Q]/+ (mixed genetic background) mice have decreased expression of *Rora* and RORα-mediated genes, as does the

staggerer mouse, supporting the hypothesis of a common pathway for ATXN1 and RORα that mediates calcium and glutamate signaling gene transcription.

Effect of partial *Tip60* loss on *Rora* and RORα-mediated gene transcription.

Partial *Tip60* loss prevented decreased expression of *Rora4*, *Slc1A6*, and *Pcp4* genes in *ATXN1*[82Q]/+:*Tip60*$^{+/-}$ mice at 12 and 20 weeks. Partial *Tip60* loss also was associated with increased *Itpr* expression at 20 weeks in *ATXN1*[82Q]/+:*Tip60*$^{+/-}$ mice (right-side column, Table 2), but because this effect was only seen at a later timepoint and Tip60 may not be present in the adult *Itpr* promoter complex, the significant of this observation is unclear. If *Tip60* loss increased the expression of *Rora4*, *Slc1A6*, and *Pcp4* at 12 weeks through histone acetylation, an increase in target gene expression would be predicted (high expression in *ATXN1*[82Q]/+ mice versus low expression in *ATXN1*[82Q]/+:*Tip60*$^{+/-}$ mice). My research demonstrated the opposite effect; partial *Tip60* loss increased gene expression. Two hypotheses for this observation are: (a) Tip60 stabilizes mutant ATXN1 via their direct interaction *in vivo* (Serra et al., 2006); decreased *Tip60* destabilizes mutant ATXN1 and relieves the inhibitory effects of ATXN1 on gene expression, and (b) Tip60 has a deleterious effect on RORα that decreases downstream RORα-mediated gene transcription. Thus partial *Tip60* expression relieves RORα transcription complex inhibition.

Hypothesis (a) suggests that Tip60 may stabilize ATXN1 through direct interaction or acetylation. Others groups have shown that Tip60 acetylates the

androgen receptor, another polyglutamine protein (LaSpada et al., 1991; Gaughan et al., 2002). Further support for a stabilizing mechanism is that tumor protein 53 (p53) acetylation by Tip60 interferes with p53 degradation, perhaps by preventing nuclear export of p53 (Legube et al., 2004). Alternatively ATXN1 acetylation may be a prerequisite for downstream kinase activity, as previously demonstrated for Tip60 Ataxia Telangiectasia mutated (ATM) acetylation (Sun et al., 2005). S776-phosphorylated ATXN1 does stably interact with 14-3-3, decreasing ATXN1 degradation and mediating neurodegeneration in the Drosophila SCA1 model (Chen et al., 2003).

Possible mechanisms for hypothesis (b) involve Tip60 inhibition of RORα. Tip60 is known to acetylate the androgen receptor, which regulates AR activity (Gaughan et al., 2002). RORα acetylation may decrease RORα-mediated transcription, which would be a novel effect on nuclear receptor activity. However negative regulation of signaling pathways is an established function of Tip60 acetylation. Tip60 interacts with and acetylates the Notch1 signaling receptor, which inhibits the Notch1 signaling pathway (Kim et al., 2007). Whether partial *Tip60* loss enhances RORα-mediated gene expression through a stabilizing interaction with ATXN1, or whether acetylation is required for subsequent posttranslational modifications or signaling pathway inhibition, remains an open question.

Role of RORα-mediated genes during the protective window in *ATXN1*[82Q]/+:*Tip60*$^{+/-}$ mice. Pathologic measures at 12 and 16 weeks (ML

thickness and climbing fiber-PC dendrite innervation) revealed a protective window in the *ATXN1*[82Q]/+:*Tip60*$^{+/-}$ mice during which cerebellar degeneration was slowed relative to *ATXN1*[82Q]/+ littermates (Figure 8). At 12 weeks *Rora4*, *Pcp4*, and *Slc1A6* expression was significantly higher in *ATXN1*[82Q]/+:*Tip60*$^{+/-}$ mice compared to *ATXN1*[82Q]/+ mice. While these genes may be necessary for protective window initiation, they are not sufficient to sustain the protection (compare top and bottom rows, Table 2). At 20 weeks the same genes (*Rora4*, *Pcp4*, and *Slc1A6)* remained highly expressed in *ATXN1*[82Q]/+:*Tip60*$^{+/-}$ mice, but cerebellar degeneration progressed to the *ATXN1*[82Q]/+ level at the same age.

Increased *Rora4*, *Pcp4*, and *Slc1A6* transcription and disease suspension should be looked at as separate events, or considered in combination with other unidentified modifying factors. Mouse age and disease stage, rather than the aforementioned gene subset, have changed between disease suspension (12 weeks) and disease progression (20 weeks) in the *ATXN1*[82Q]/+:*Tip60*$^{+/-}$ mice. Partial *Tip60* loss may upregulate genes that temporarily slow degeneration (perhaps as a compensatory mechanism), but over time toxic ATXN1[82Q] effects may accumulate in the PC, blunting the positive effects of *Rora4*, *Pcp4*, and *Slc1A6*. At 20 weeks any protection afforded by calcium and glutamate signaling upregulation is lost. It is important to remember that *Tip60* is still expressed in this heterozygote model; eventually the remaining Tip60's effects may dampen the initial benefit of partial *Tip60* loss. More dramatic rescue may

be achieved in a PC-specific *Tip60* null model, which may cause a complete loss of ATXN1 function.

Two genes in Table 2, *Rora1* and *Itpr1*, do not follow the strict expression pattern explained by mutant *ATXN1*[82Q] expression or partial *Tip60* loss. *Itpr1* was included in these experiments as a negative control, since previous experiments suggest that *Tip60* is not present at the *Itpr1* promoter complex *in vivo*. *Itpr1* is an RORα-mediated gene; all *ATXN1*[82Q]/+ mice are predicted to have low *Itpr1* expression, regardless of *Tip60* dosage. Unexpectedly *ATXN1*[82Q]/+:*Tip60*$^{+/-}$ mice at 20 weeks had significantly higher *Itpr1* levels compared to *ATXN1*[82Q]/+ mice at 20 weeks. It is interesting to speculate that either the *Itpr1* promoter complex in 20-week-old mice is distinct from that in younger mice (e.g. Tip60 is present) or that another unidentified factor is driving *Itpr* transcription after the protective window in *ATXN1*[82Q]/+:*Tip60*$^{+/-}$ mice.

Rora1 expression did not mirror *Rora4*, *Pcp4*, and *Slc1A6* expression. (*Rora1* expression was unchanged between *ATXN1*[82Q]/+ and *ATXN1*[82Q]/+:*Tip60*$^{+/-}$ mice at 12 weeks.) Four *Rora* isoforms result from alternate RORα splicing and promoter usage (Becker-Andre et al., 1993; Giguere et al., 1994). All isoforms differ in their N-terminal protein domains, which affect DNA-binding properties and target recognition (Giguere et al., 1994). *Rora1* and *Rora4* are differentially expressed, either separately or together, in several mouse tissues but are co-expressed in murine cerebellum. This co-regulation of *Rora1* and *Rora4* suggests that both isoforms are functionally required in the cerebellum and that

RORα1 and RORα4 control distinct, and perhaps overlapping, target gene sets (Matysiak-Scholze and Nehls, 1997). My results indicate that changes in *Rora4*, but not *Rora1*, levels are accompanied by concomitant changes in *Pcp4* and *Slc1A6*, suggesting that RORα isoforms likely do control unique sets of target genes. If so, it follows that *Pcp4* and *Slc1A6* are regulated by RORα4.

A model for pathogenesis. In the conditional mouse, mutant *ATXN1* expression timing dictates differential recovery; early-, mid-, and late-stage disease recovery are unique when the mutant gene is turned off (Zu et al., 2004). Furthermore mutant *ATXN1* expression during postnatal cerebellar development results in a more severe disease, perhaps because the ATXN1 pathway also is linked to cerebellar development pathways (Serra et al., 2006). Not only does SCA1 disease have at least three unique stages, ATXN1 plays a role in the pathology of each stage.

RORα-mediated genes are important for PC development (Gold et al., 2003). Similarly mice null for *calbindin* (Airaksinen et al., 1997) and *Grm1* (Ichise et al., 2000) develop a severe ataxia, and *Itpr1* null mice that survive *in utero* development are born with a severe ataxia (Matsumoto et al., 1996). The *Rora*$^{sg/sg}$ mouse has a partial cerebellar agenesis; in contrast, the *Rora*$^{sg/+}$ mouse has an age-dependent cerebellar degeneration (Zanjani et al., 1992). The s*taggerer* mouse, along with gene expression profiling (Lin et al., 2000; Hadj-Sahraoui et al., 2001; Serra et al., 2004; Serra et al., 2006), suggests that RORα

is important during two SCA1 stages: early (development) and mid (progression) disease.

The observation that *Rora* and RORα-mediated calcium and glutamate genes (*Rora4*, *Slc1A6*, and *Pcp4*) are not sufficient to sustain slowing of cerebellar degeneration in *ATXN1*[82Q]/+:*Tip60*$^{+/-}$ during advanced disease (20 weeks) may lead to the finding that *Rora4*, *Slc1A6* and *Pcp4* are critical for midstage PC function, while other pathways predominate during advanced disease. In either case, it is clear that partial *Tip60* loss plays a specific temporal role in disease, slowing the neurodegenerative rate during disease progression, but not development or advanced disease.

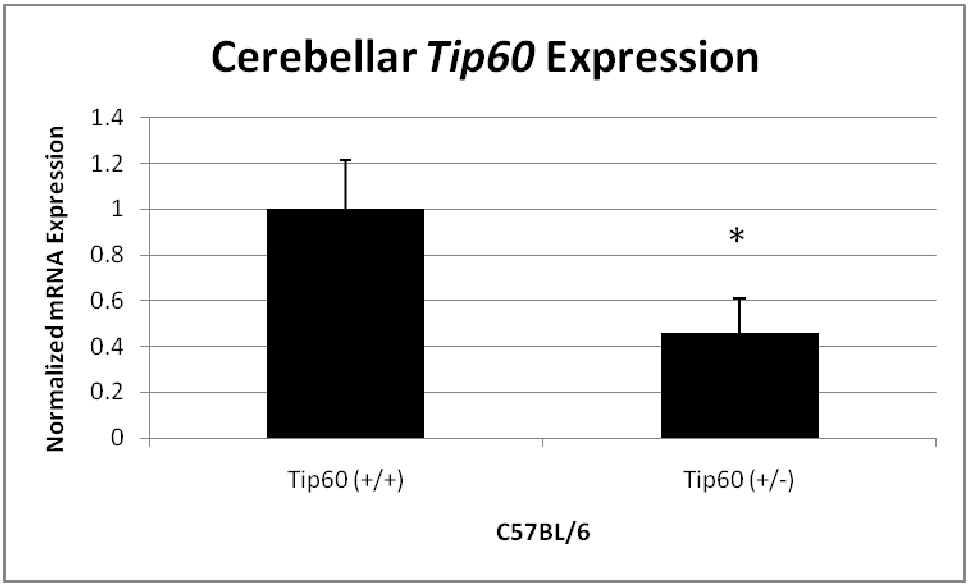

Figure 5. qRT-PCR of *Tip60* in cerebella of *Tip60*$^{+/+}$ and *Tip60*$^{+/-}$ C57BL/6 mice. *Tip60* expression was normalized to *GAPDH*. Error bars represent SEM; n=4 mice per genotype, *p=0.04.

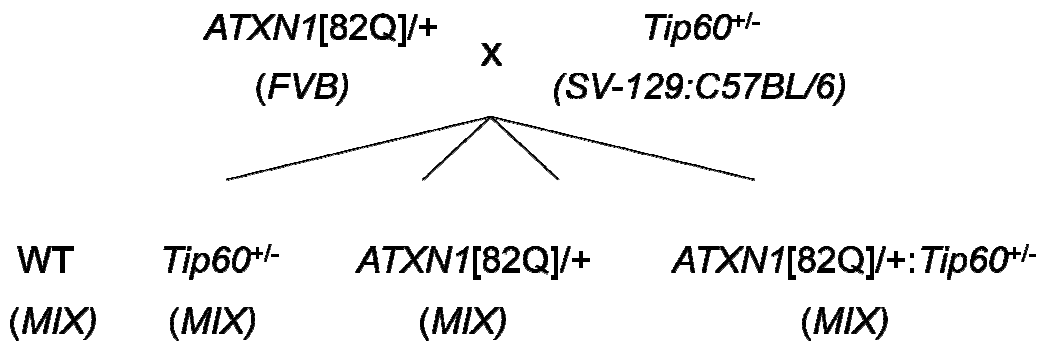

Figure 6. Breeding strategy for *ATXN1*[82Q]/+:*Tip60*$^{+/-}$ mice. The *ATXN1* mice were maintained on an FVB background; the *Tip60*$^{+/-}$ mice were generated from a cross between C57BL/6 and SV-129 mice. The F_1 genotypes used in this study were on a mixed genetic background of FVB;SV-129;C57BL/6.

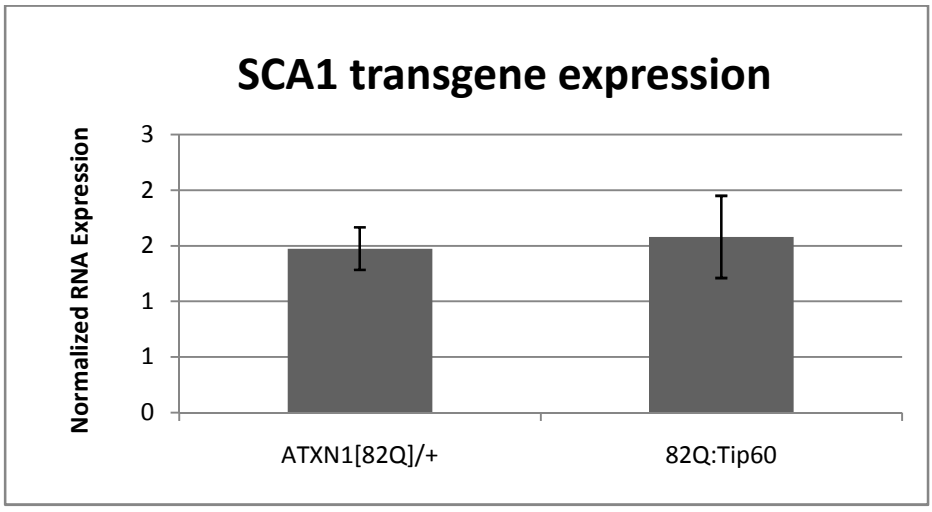

Figure 7. qRT-PCR of *ATXN1*, in *ATXN1*[82Q]/+:*Tip60*$^{+/-}$ and *ATXN1*[82Q]/+ mouse cerebella. RNA expression was normalized to *GAPDH.* Error bars represent SEM; n=3 mice per genotype.

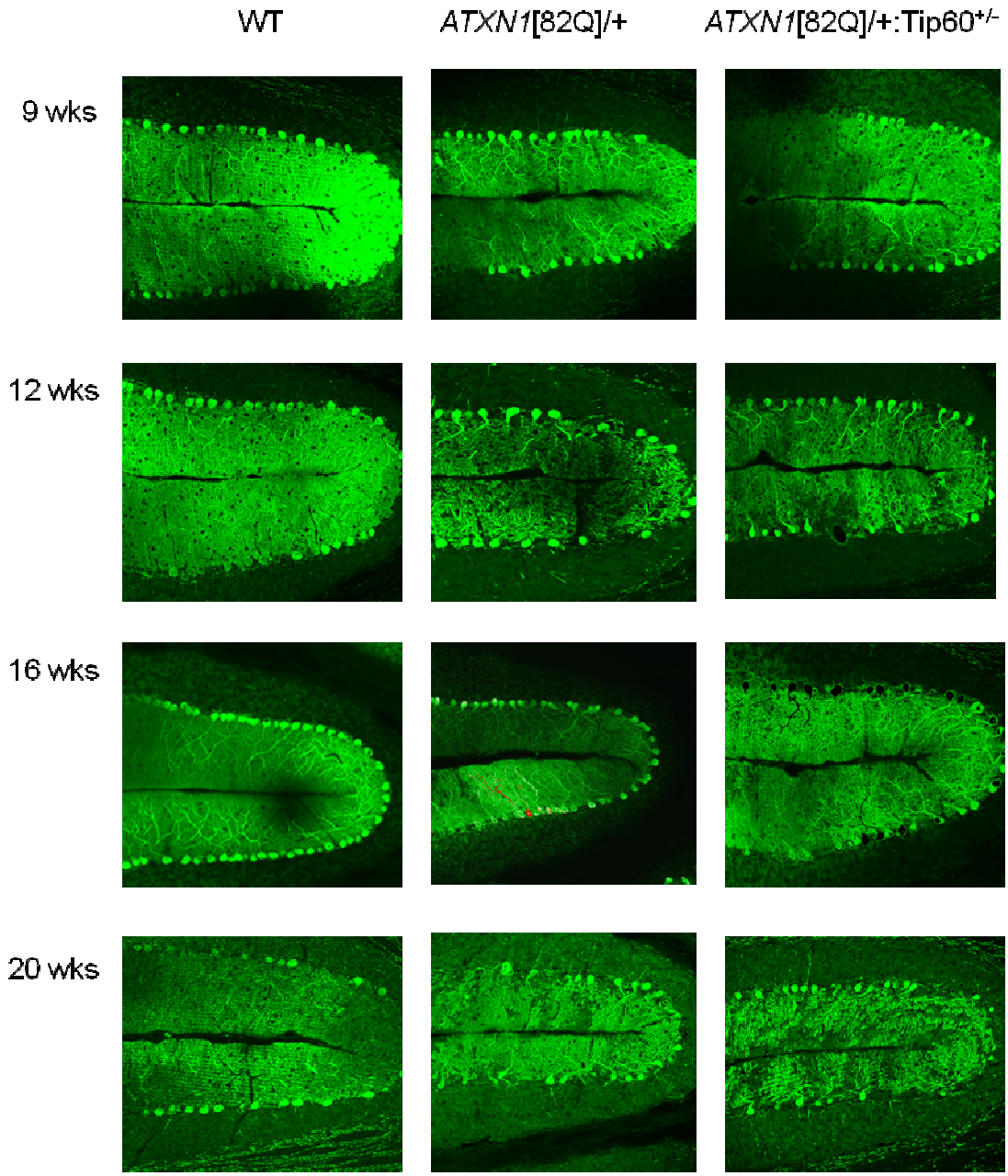

Figure 8. Cerebellar sections of wt, *ATXN1*[82Q]/+, and *ATXN1*[82Q]/+:*Tip60*$^{+/-}$ mice stained with anti-Calbindin D28K antibody to assess ML thickness at the primary fissure. Immunostained sections were visualized and measured with confocal laser scanning microscopy.

A.

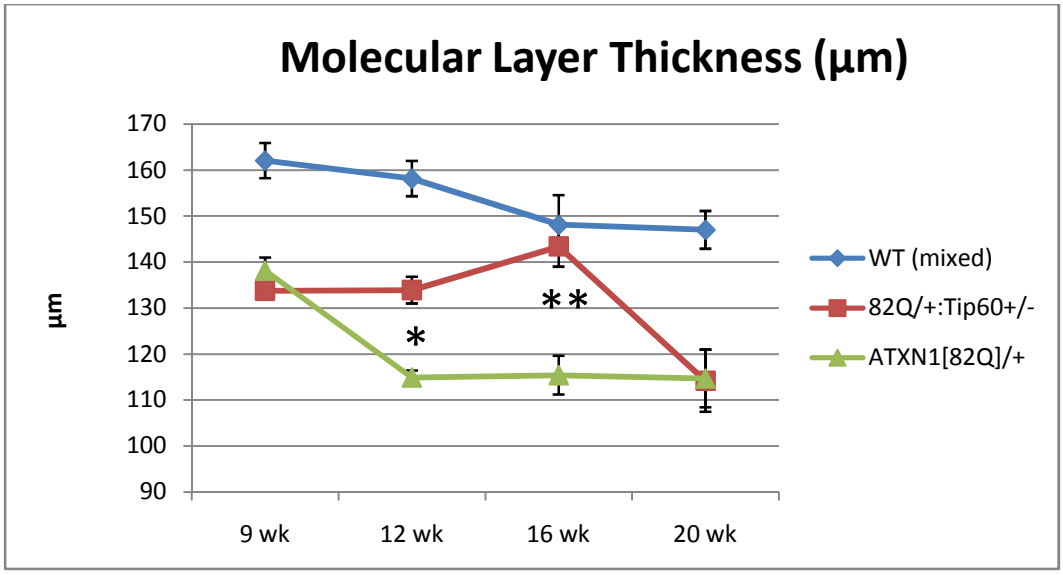

Figure 9. Molecular layer thickness quantification of wt, *Tip60*$^{+/-}$, *ATXN1*[82Q]/+, and *ATXN1*[82Q]/+:*Tip60*$^{+/-}$ mice, measured with anti-calbindin D28K immunostaining and confocal microscopy. Error bars represent the SEM between the average ML thickness of individual mice; n=3-7 mice per genotype at each timepoint. Statistical comparisons are *ATXN1*[82Q]/+ vs. *ATXN*1[82Q]/+:Tip60$^{+/-}$ *p=0.004; **p=0.009.

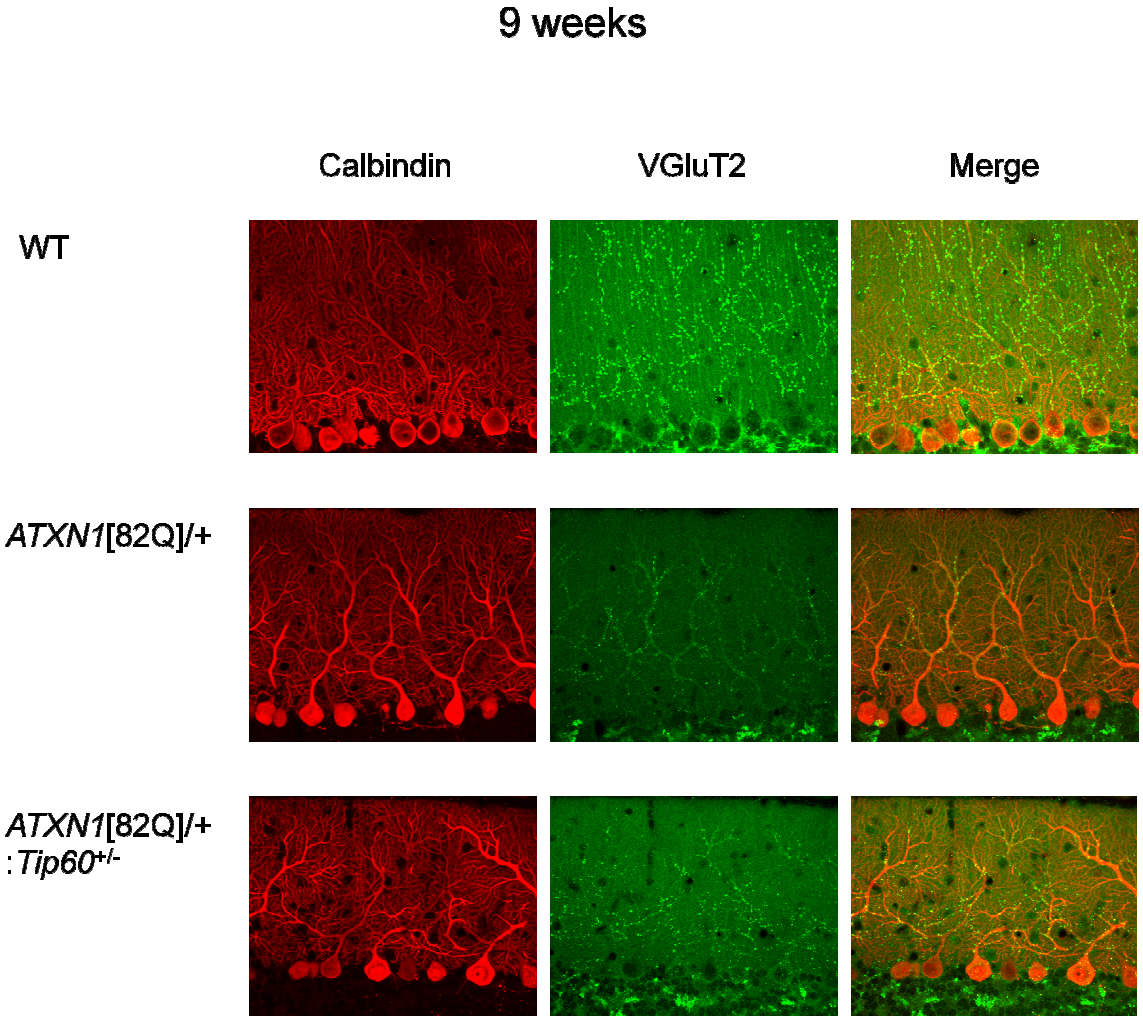

Figure 10. Climbing fiber-PC terminals in 9-week-old wt, *ATXN1*[82Q]/+, and *ATXN1*[82Q]/+:*Tip60*$^{+/-}$ mice were visualized at the primary fissure with calbindin D28K and VGluT2 antibodies. Immunostained cerebellar sections were visualized and measured with confocal laser scanning microscopy.

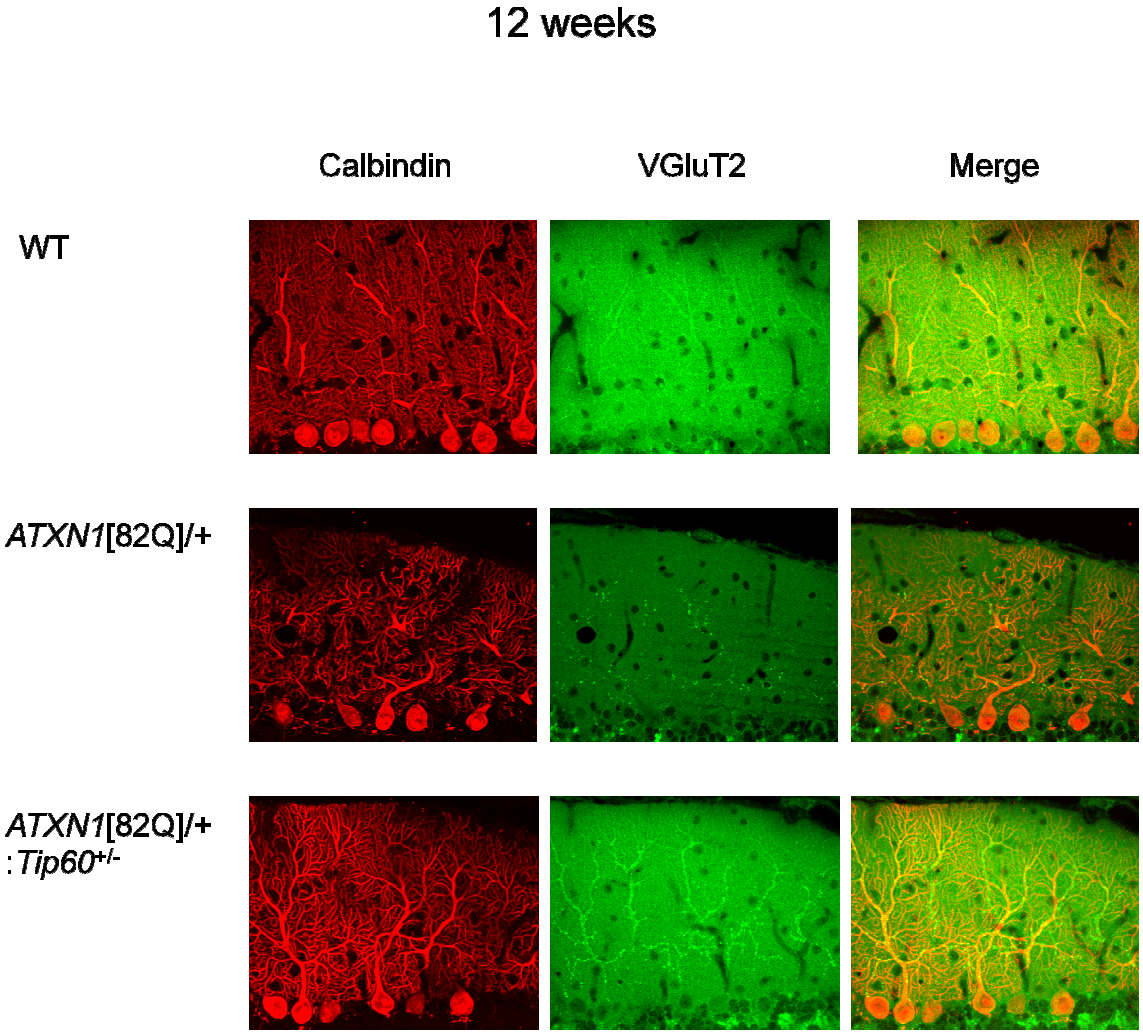

Figure 11. Climbing fiber-PC terminals in 12-week-old wt, *ATXN1*[82Q]/+, and *ATXN1*[82Q]/+:*Tip60*$^{+/-}$ mice were visualized at the primary fissure with calbindin D28K and VGluT2 antibodies. Immunostained cerebellar sections were visualized and measured with confocal laser scanning microscopy.

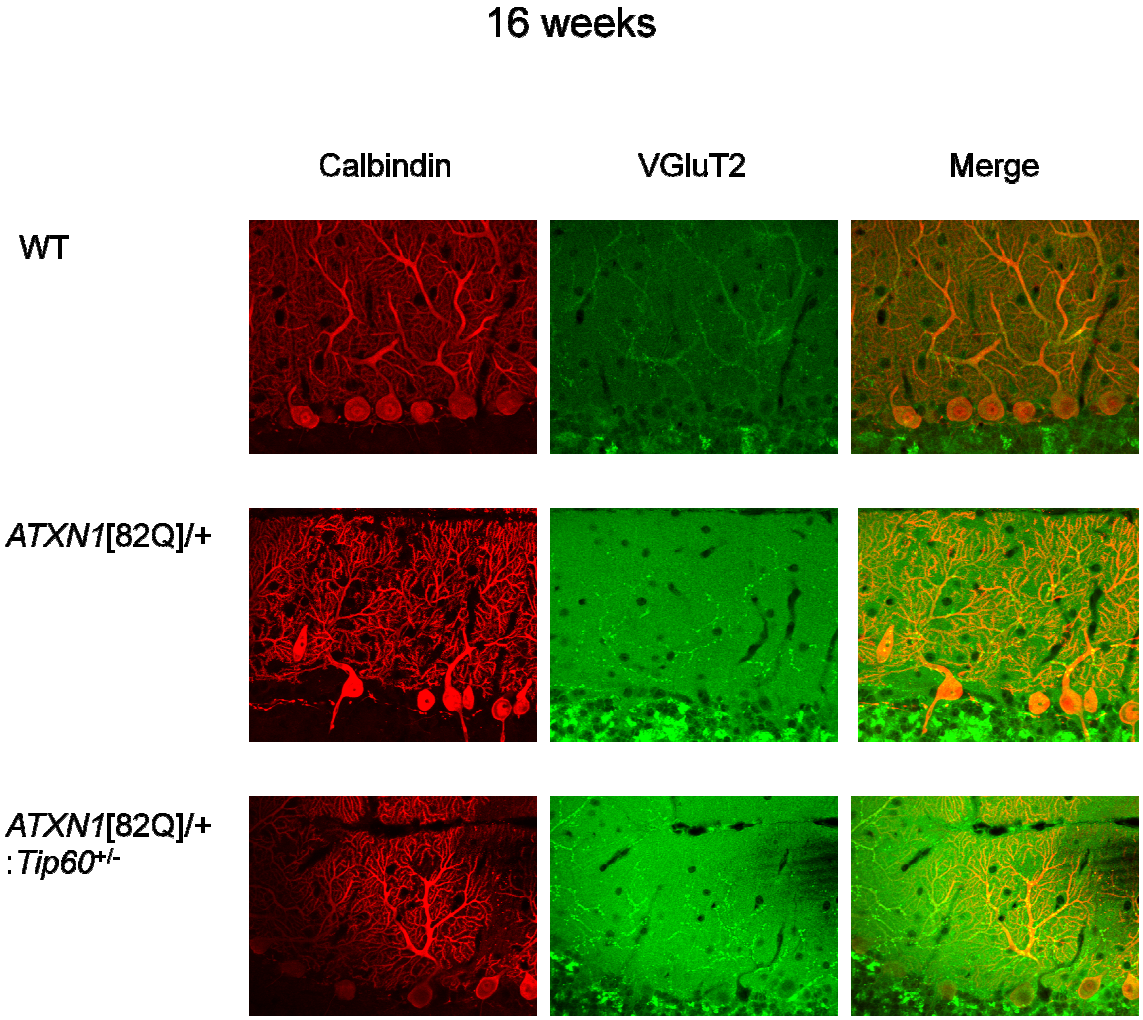

Figure 12. Climbing fiber-PC terminals in 16-week-old wt, *ATXN1*[82Q]/+, and *ATXN1*[82Q]/+:*Tip60*$^{+/-}$ mice were visualized at the primary fissure with calbindin D28K and VGluT2 antibodies. Immunostained cerebellar sections were visualized and measured with confocal laser scanning microscopy.

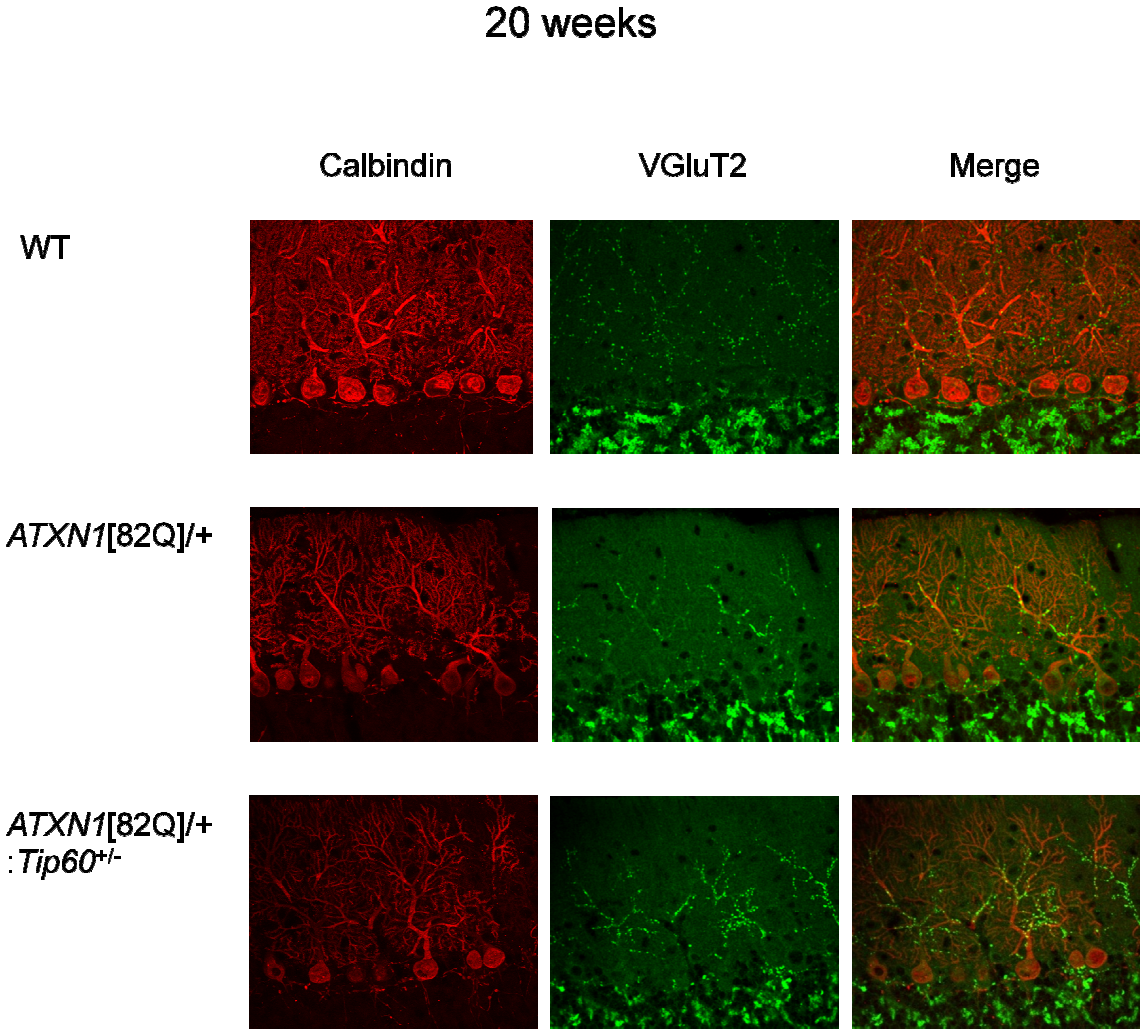

Figure 13. Climbing fiber-PC terminals in 20-week-old wt, *ATXN1*[82Q]/+, and *ATXN1*[82Q]/+:*Tip60*$^{+/-}$ mice were visualized at the primary fissure with calbindin D28K and VGluT2 antibodies. Immunostained cerebellar sections were visualized and measured with confocal laser scanning microscopy.

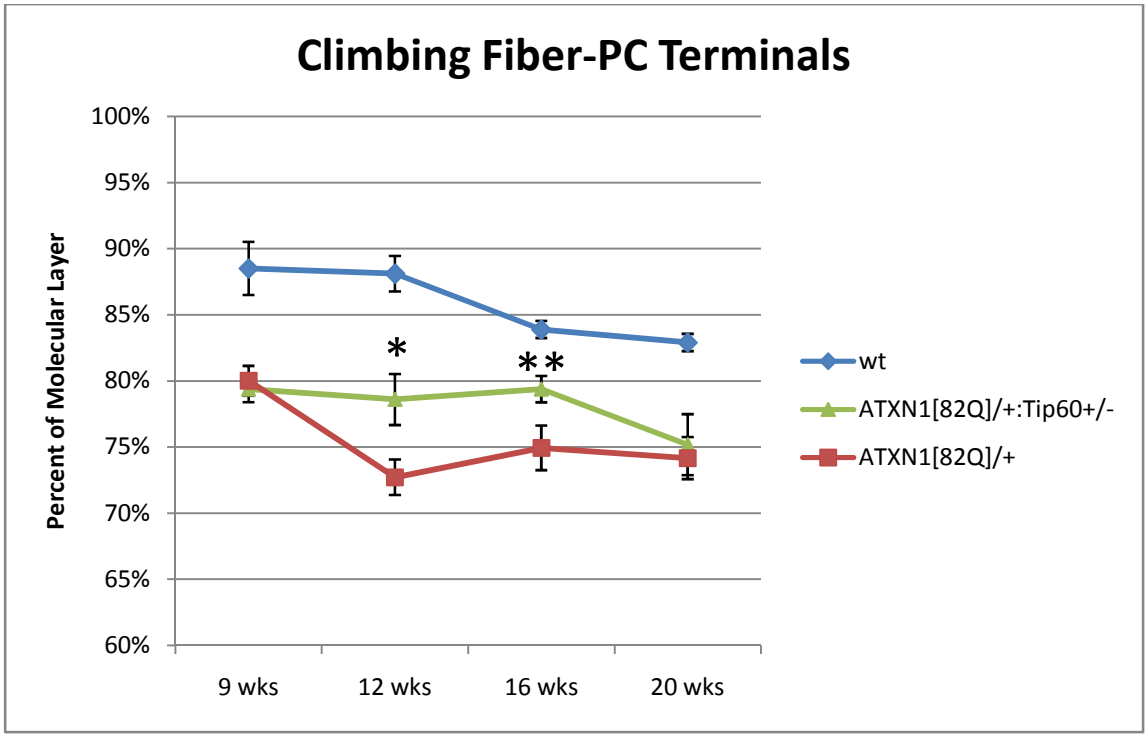

Figure 14. Climbing fiber-PC terminals in wt, *ATXN1*[82Q]/+, and *ATXN1*[82Q]/+:*Tip60*$^{+/-}$ mice. Percentage of the ML innervated by climbing fibers is represented (climbing fiber/ML). CFs were stained with VGluT2 antibody, and PC ML was visualized with calbindin antibody immunofluorescence. Error bars represent SEM; n=3-5 mice per genotype at each timepoint. (12 wk *ATXN1*[82Q]/+ vs. *ATXN1*[82Q]/+:*Tip60*$^{+/-}$ *p=0.02; 16 wk *ATXN1*[82Q]/+ vs. *ATXN1*[82Q]/+:*Tip60*$^{+/-}$ **p=0.04)

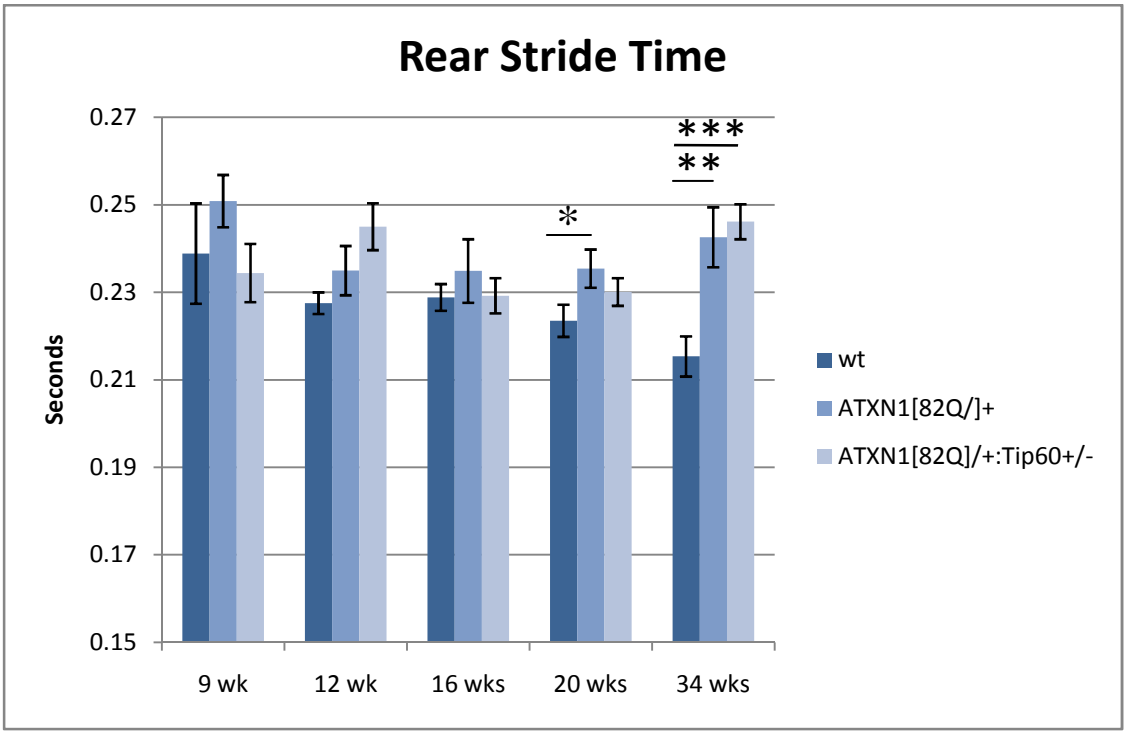

Figure 15. DigiGait analysis (rear stride time) of wt, *ATXN1*[82Q]/+, and *ATXN1*[82Q]/+:Tip60$^{+/-}$ mice at 9, 12, 16, 20, and 34 weeks. Error bars represent SEM; n=12-16 mice per genotype. (*p=0.043, **p=0.004, ***p=0.0001).

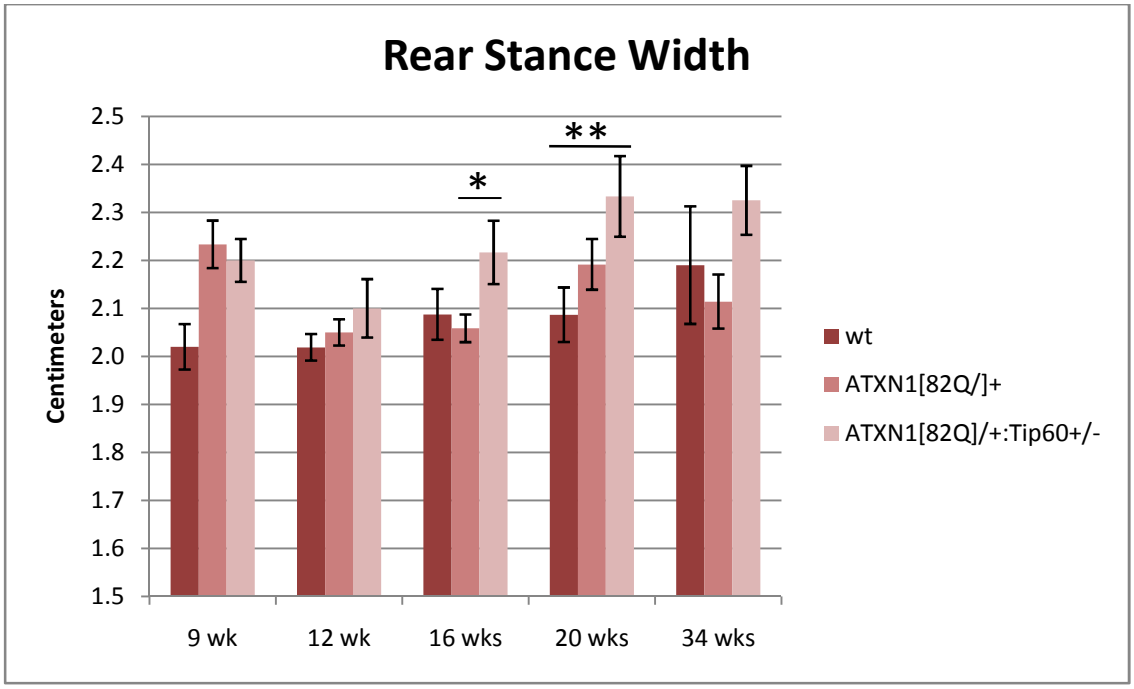

Figure 16. DigiGait analysis (rear stance width) of wt, *ATXN1*[82Q]/+, and *ATXN1*[82Q]/+:Tip60$^{+/-}$ mice at 9, 12, 16, 20, and 34 weeks. Error bars represent SEM; n=12-16 mice per genotype. (*p=0.034, **p=0.016).

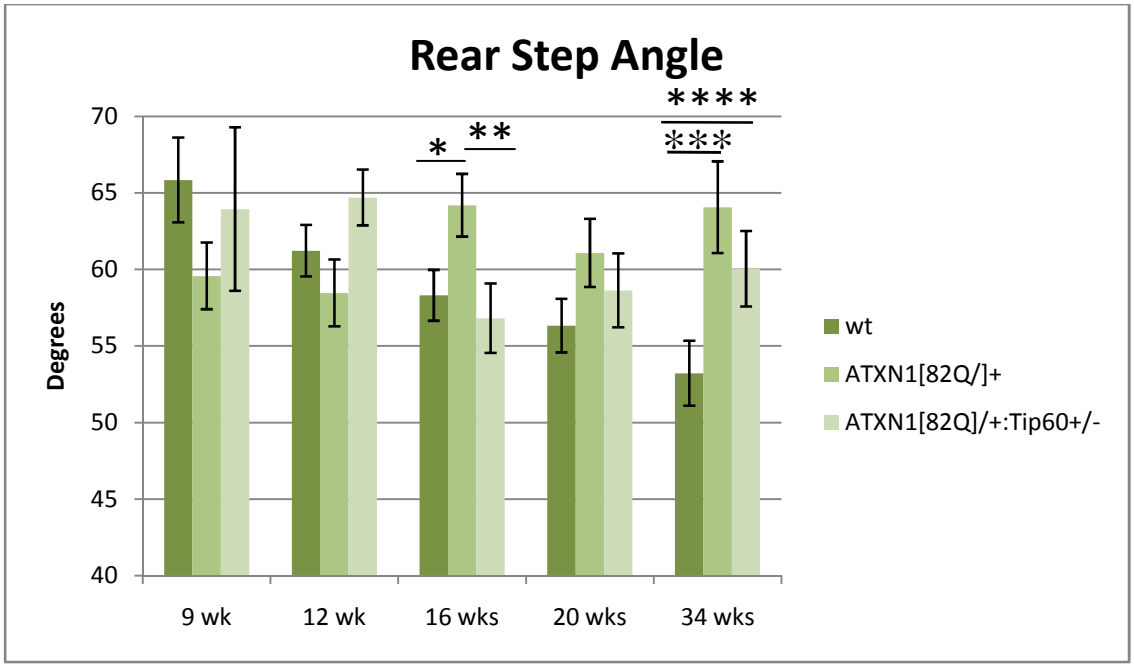

Figure 17. DigiGait analysis (rear step angle) of wt, *ATXN1*[82Q]/+, and *ATXN1*[82Q]/+:Tip60$^{+/-}$ mice at 9, 12, 16, 20, and 34 weeks. Error bars represent SEM; n=12-16 mice per genotype. Error bars represent SEM, n=12-16 mice per genotype. (*p=0.036, **p=0.025, ***p=0.002, ****p=0.05).

Table 1: DigiGait statistics for wt, *ATXN1*[82Q]/+, and *ATXN1*[82Q]/+:Tip60$^{+/-}$

Rear Stride Time p-values					
	9 wks	12 wks	16 wks	20 wks	34 wks
wt vs 82Q/+	0.52	0.18	0.43	**0.043**	**0.004**
82Q/+ vs. 82Q/+:Tip60+/-	0.11	0.67	0.52	0.38	0.63
wt vs. 82Q/+:Tip60+/-				0.24	**0.0001**

Rear Stance Width p-values					
	9 wks	12 wks	16 wks	20 wks	34 wks
wt vs 82Q/+	**0.011**	0.43	0.47	0.2	0.65
82Q/+ vs. 82Q/+:Tip60+/-	0.64	0.54	**0.034**	0.15	0.08
wt vs. 82Q/+:Tip60+/-				**0.016**	0.33

Rear Step Angle p-values					
	9 wks	12 wks	16 wks	20 wks	34 wks
wt vs 82Q/+	0.12	0.31	**0.036**	0.1	**0.002**
82Q/+ vs. 82Q/+:Tip60+/-	0.42	0.5	**0.025**	0.47	0.37
wt vs. 82Q/+:Tip60+/-				0.44	**0.05**

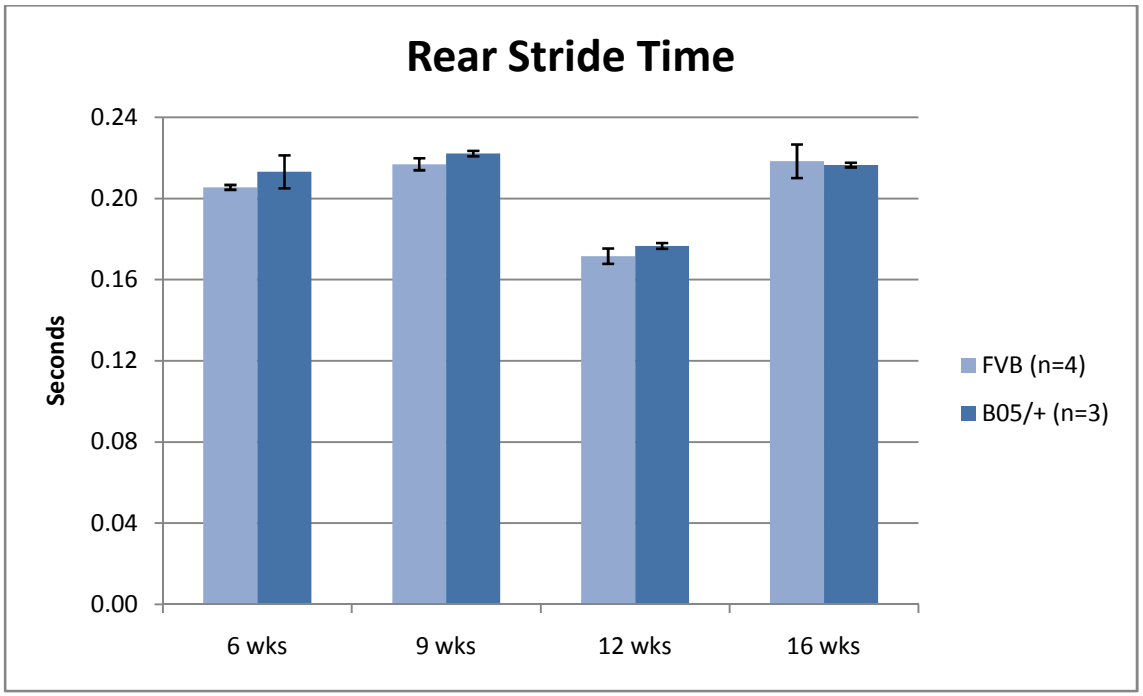

Figure 18. DigiGait analysis (rear stride time) of wt (FVB) and ATXN1[82Q]/+ (B05 on FVB background) mice at 6, 9, 12, and 16 weeks. Error bars represent SEM.

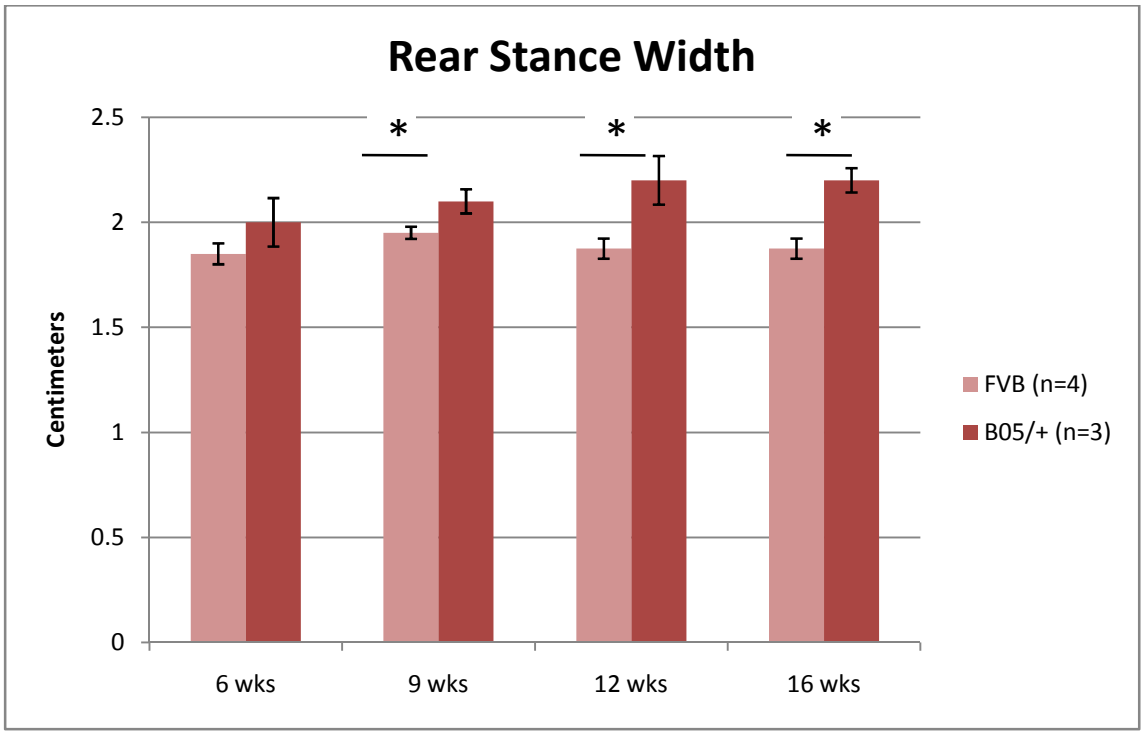

Figure 19. DigiGait analysis (rear stance width) of wt (FVB) and ATXN1[82Q]/+ (B05 on FVB background) mice at 6, 9, 12, 20, and 16 weeks. Error bars represent SEM. (9 wks *p=0.05, 12 wks *p=0.03, 16 wks *p=0.007).

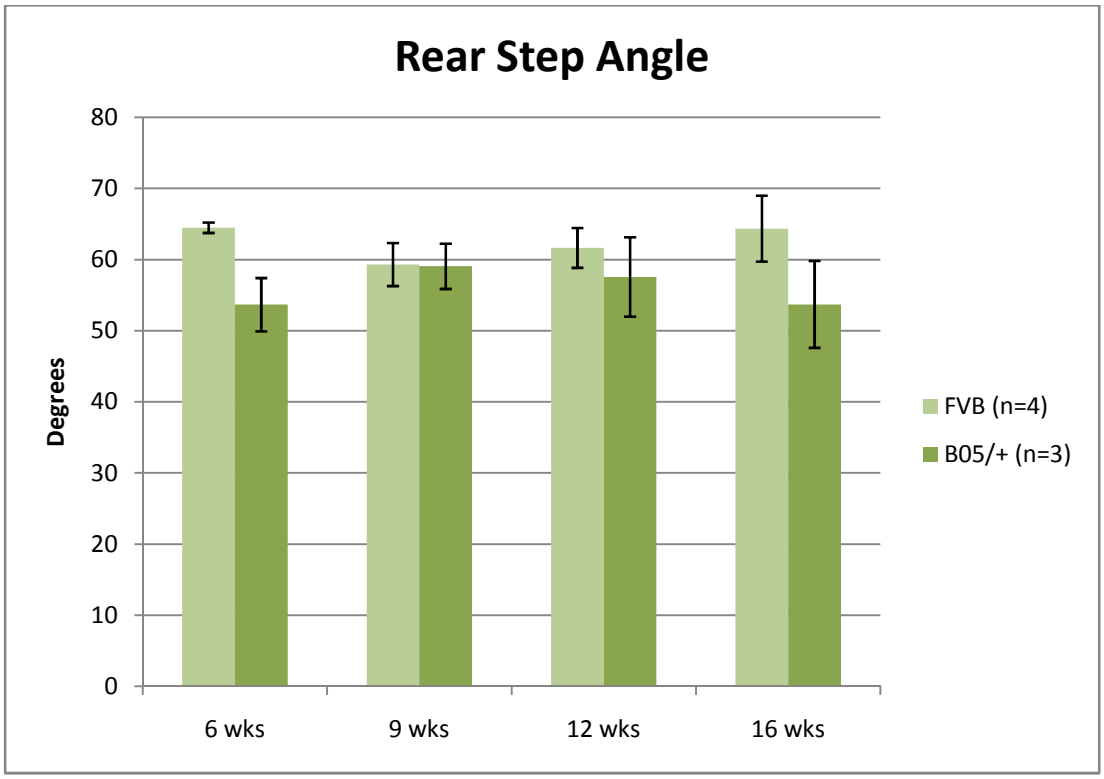

Figure 20. DigiGait analysis (rear step angle) of wt (FVB) and ATXN1[82Q]/+ (B05 on FVB background) at 6, 9, 12, 20, and 16 weeks. Error bars represent SEM.

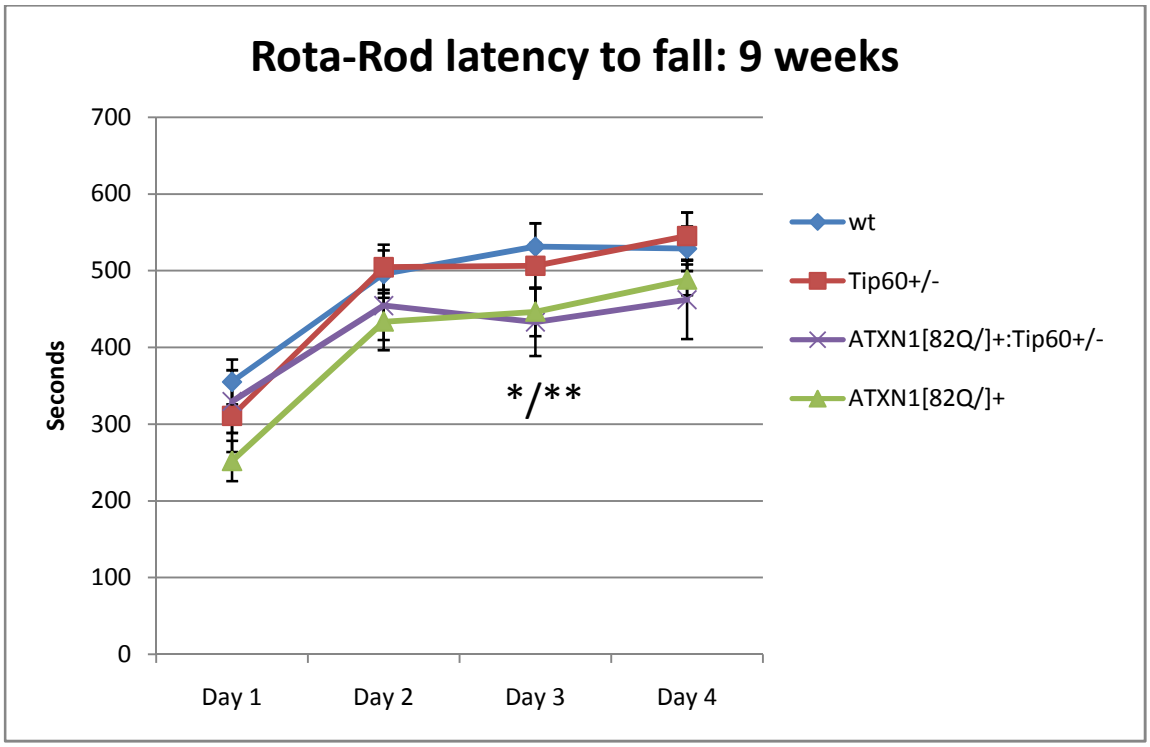

Figure 21. Rota-Rod performance of wt, Tip60$^{+/-}$, *ATXN1*[82Q]/+, and *ATXN1*[82Q]/+:Tip60$^{+/-}$ mice at 9 weeks. Mice were given four trials per day for four consecutive days. Error bars represent SEM. (wt n=13, Tip60$^{+/-}$ n=11, *ATXN1*[82Q]/+ n=14, and *ATXN1*[82Q]/+:Tip60$^{+/-}$ n=8). (Day 3: wt vs. *ATXN1*[82Q]/+ *p=0.05, *ATXN1*[82Q]/+ vs. *ATXN1*[82Q]/+:Tip60$^{+/-}$ **p=0.02).

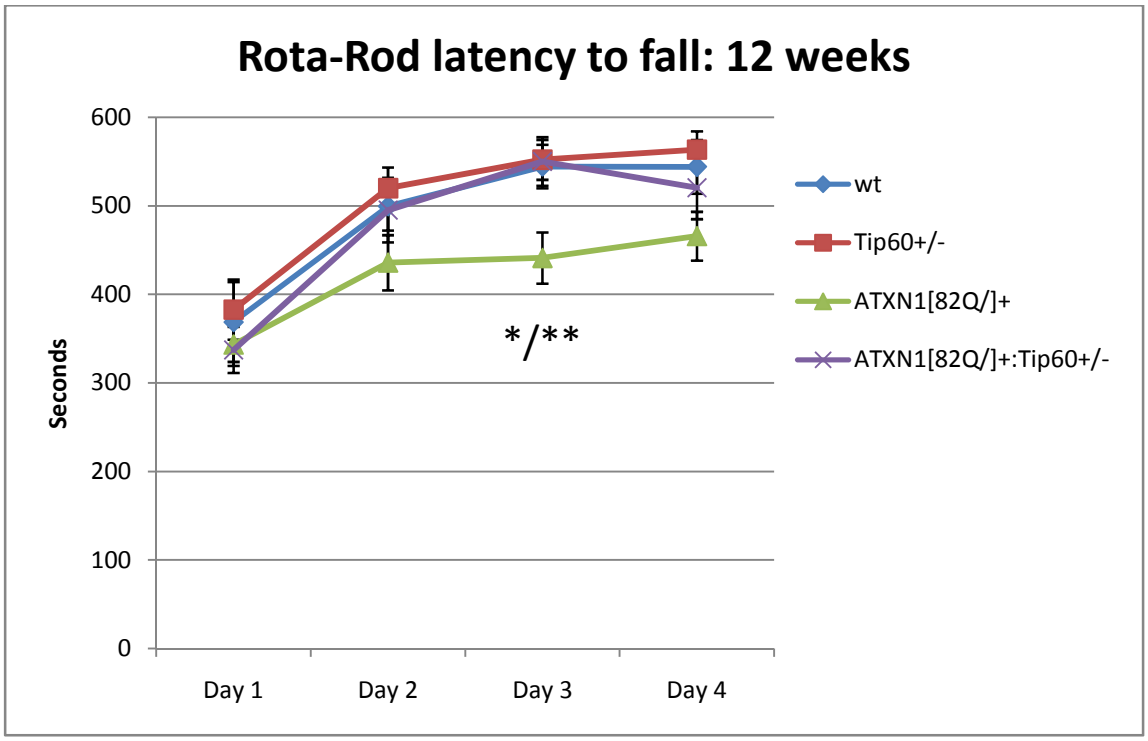

Figure 22. Rota-Rod performance of wt, Tip60$^{+/-}$, *ATXN1*[82Q]/+, and *ATXN1*[82Q]/+:Tip60$^{+/-}$ mice at 12 weeks. Mice were given four trials per day for four consecutive days. Error bars represent SEM. (wt n=11, Tip60$^{+/-}$ n=12, *ATXN1*[82Q]/+ n=12, and *ATXN1*[82Q]/+:Tip60$^{+/-}$ n=8) (Day 3: wt vs. *ATXN1*[82Q]/+ *p=0.01, *ATXN1*[82Q]/+ vs. *ATXN1*[82Q]/+:Tip60$^{+/-}$ **p=0.02).

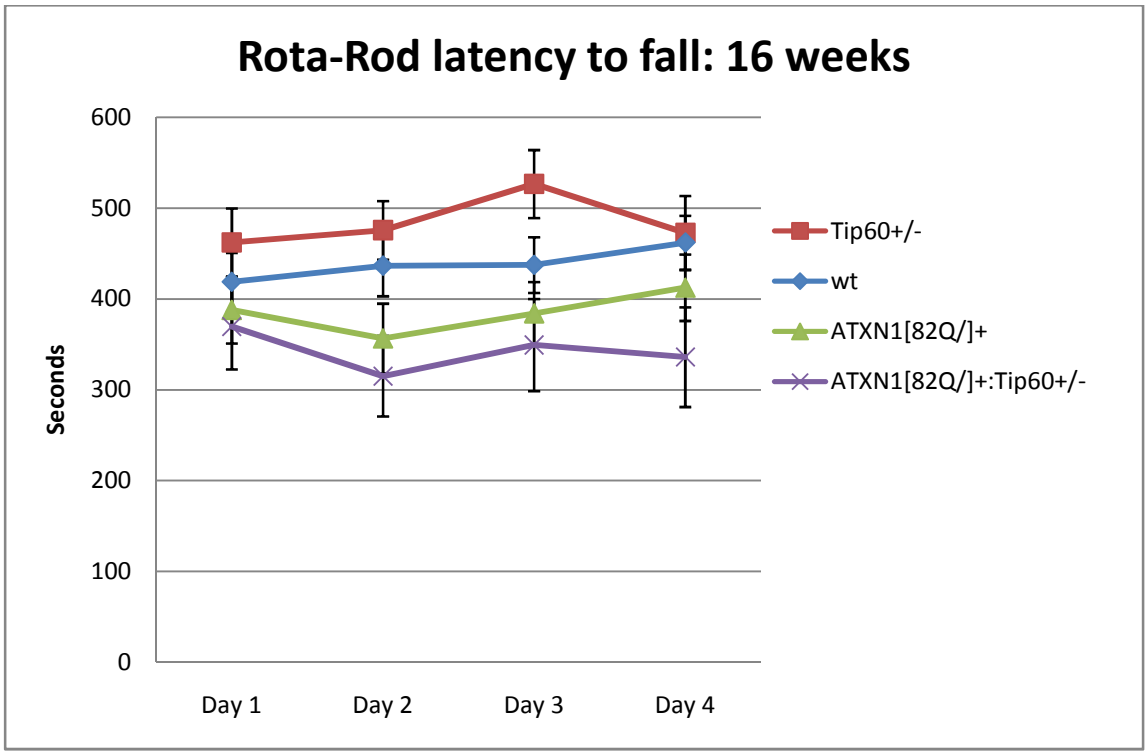

Figure 23. Rota-Rod performance of wt, Tip60$^{+/-}$, *ATXN1*[82Q]/+, and *ATXN1*[82Q]/+:Tip60$^{+/-}$ mice at 16 weeks. Mice were given four trials per day for four consecutive days. Error bars represent SEM. (wt n=12, Tip60$^{+/-}$ n=13, *ATXN1*[82Q]/+ n=12, and *ATXN1*[82Q]/+:Tip60$^{+/-}$ n=10).

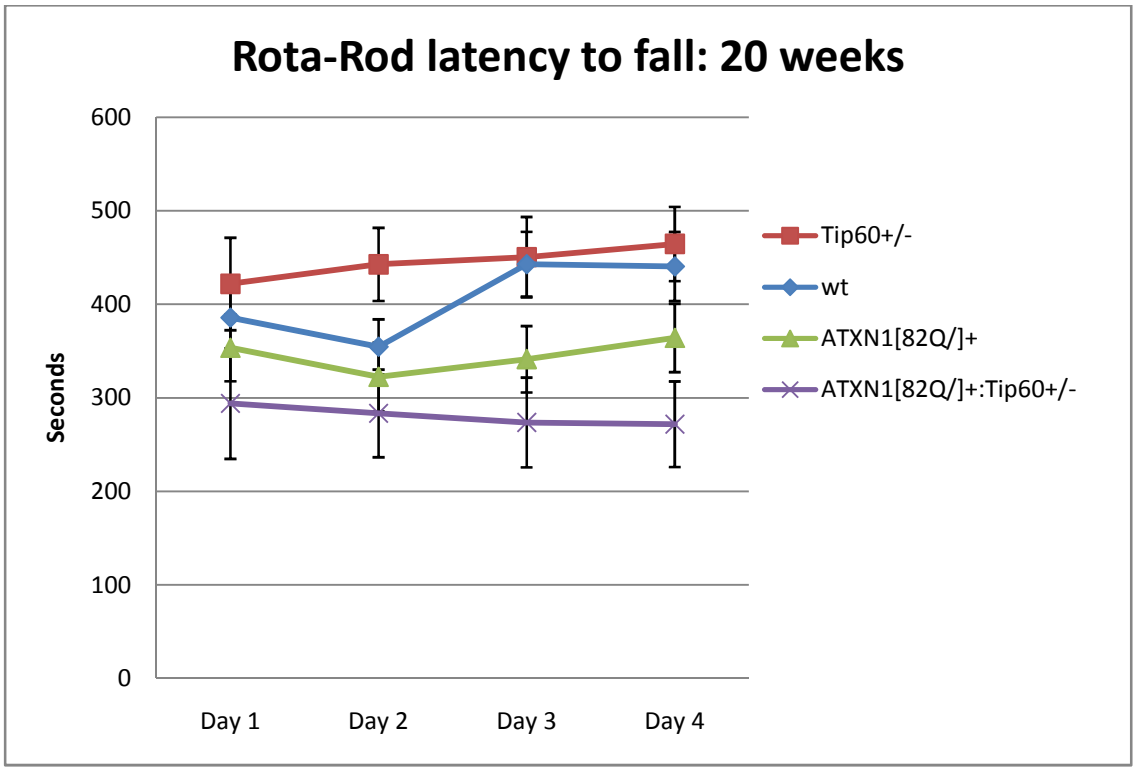

Figure 24. Rota-Rod performance of wt, Tip60$^{+/-}$, *ATXN1*[82Q]/+, and *ATXN1*[82Q]/+:Tip60$^{+/-}$ mice at 20 weeks. Mice were given four trials per day for four consecutive days. Error bars represent SEM. (wt n=12, Tip60$^{+/-}$ n=13, *ATXN1*[82Q]/+ n=12, and *ATXN1*[82Q]/+:Tip60$^{+/-}$ n=10).

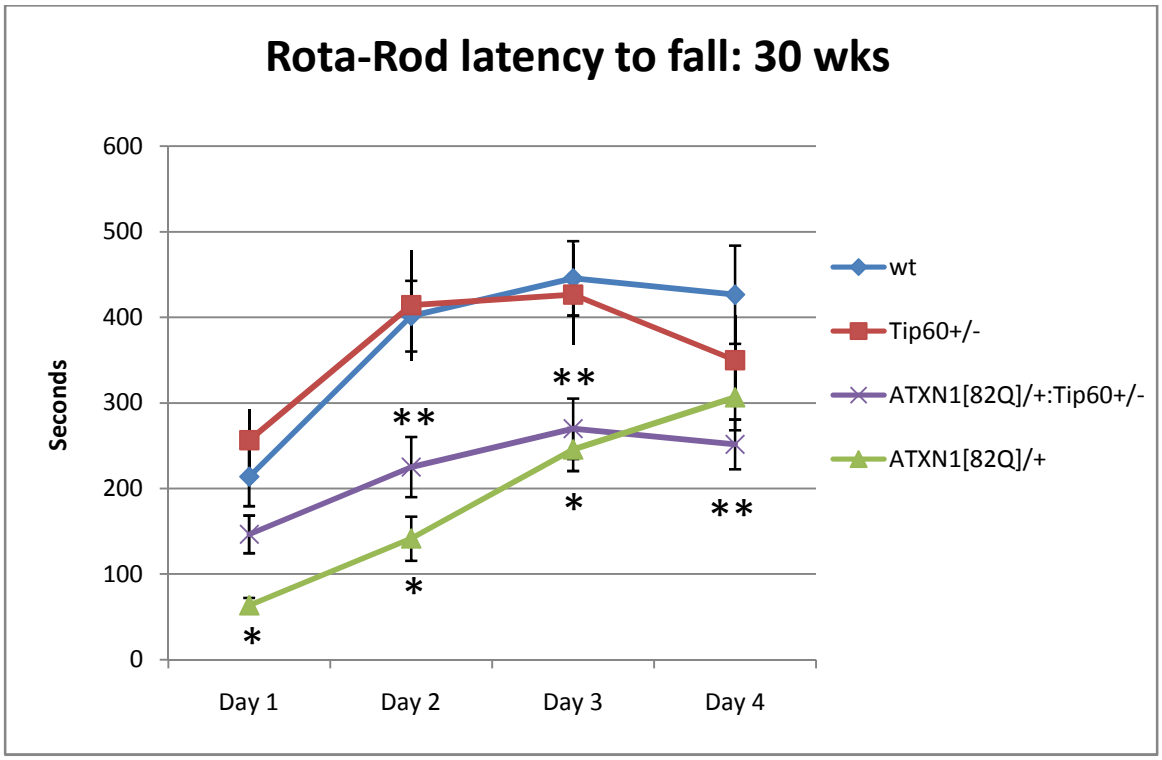

Figure 25. Rota-Rod performance of wt, Tip60$^{+/-}$, *ATXN1*[82Q]/+, and *ATXN1*[82Q]/+:Tip60$^{+/-}$ mice at 30 weeks. Mice were given four trials per day for four consecutive days. Error bars represent SEM. (wt n=10, Tip60$^{+/-}$ n=6, *ATXN1*[82Q]/+ n=6, and *ATXN1*[82Q]/+:Tip60$^{+/-}$ n=12). (* indicates wt vs. *ATXN1*[82Q]/+ and ** indicates wt vs. *ATXN1*[82Q]/+:Tip60$^{+/-}$. Day 1 *p=0.005, Day 2 *p=0.005; **p=0.0038, Day 3 *p=0.005; **p=0.004; Day 4 **p=0.009).

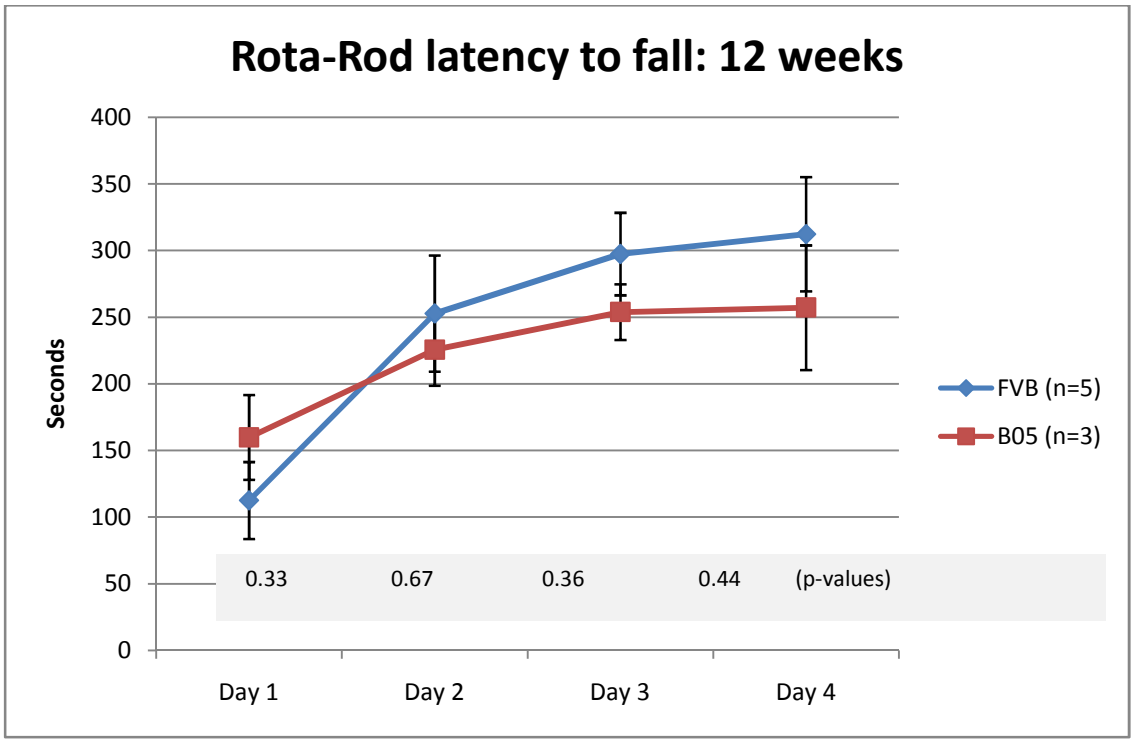

Figure 26. Rota-Rod performance of FVB and B05 (*ATXN1*[82Q]/+ on FVB background) mice at 12 weeks. Mice were given four trials per day for four consecutive days. Error bars represent SEM.

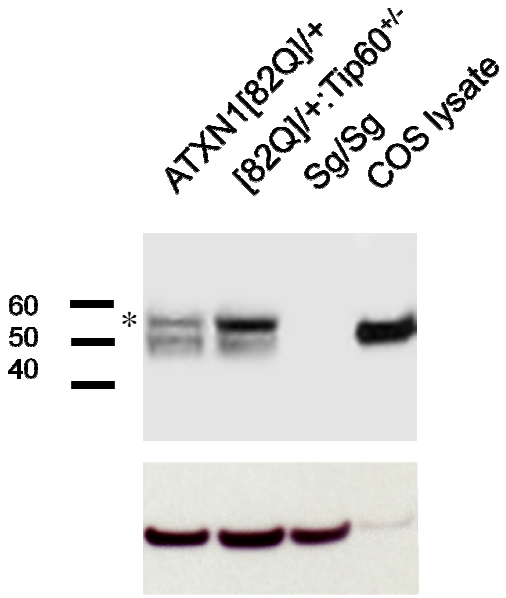

Figure 27. Upper panel: Western blot with mouse cerebellar lysates probed for RORα (55kD) (Santa Cruz H-65). Negative control: homozygous s*taggerer* ($Rora^{sg/sg}$) mouse cerebellar extracts. Positive control: Lysates from COS cells transfected with *Rora1*. Lower panel: GAPDH was used as a loading control. (Asterisk indicates the RORα4 isoform based on size and relative abundance.)

A.

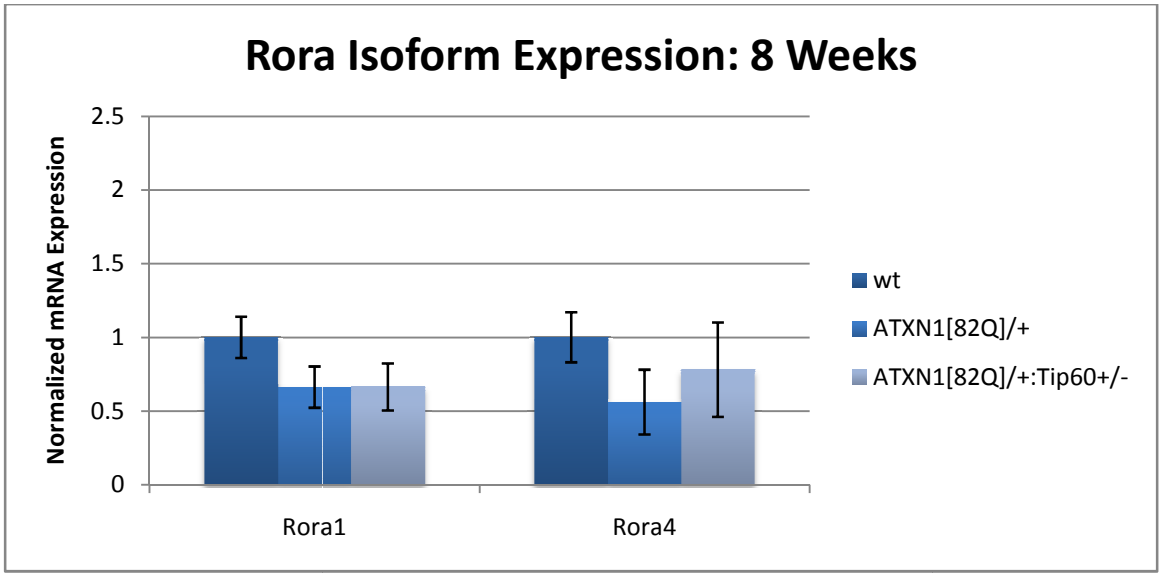
Rora Isoform Expression: 8 Weeks
Normalized mRNA Expression
2.5
2
1.5
1
0.5
0
Rora1
Rora4
wt
ATXN1[82Q]/+
ATXN1[82Q]/+:Tip60+/-

B.

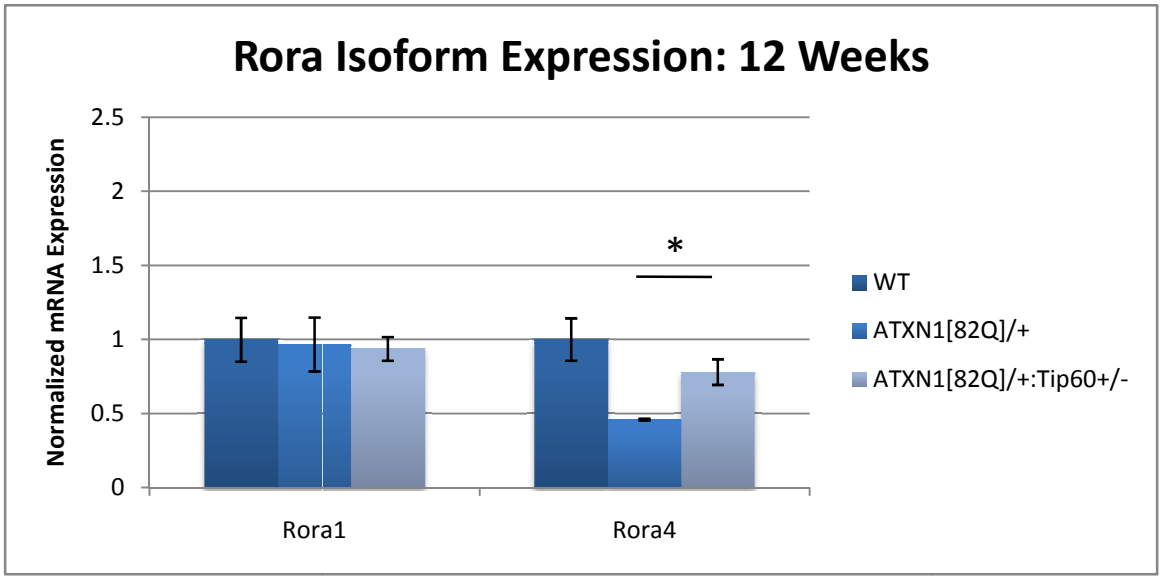
Rora Isoform Expression: 12 Weeks
Normalized mRNA Expression
2.5
2
1.5
1
0.5
0
*
Rora1
Rora4
WT
ATXN1[82Q]/+
ATXN1[82Q]/+:Tip60+/-

C.

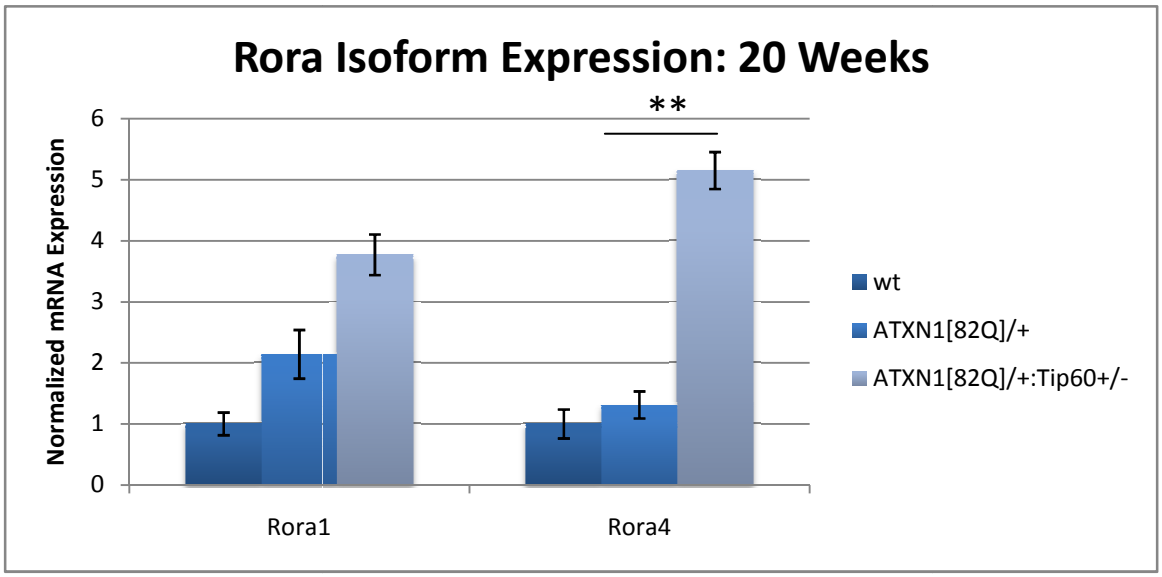

Figure 28. qRT-PCR of Rora isoforms 1 and 4 in cerebella of A) 8 week B) 12 week and C) 20 week old wt, *ATXN1*[82Q]/+, and *ATXN1*[82Q]/+:*Tip60*$^{+/-}$ mice. Of the four isoforms of *Rora* (1-4), *Rora1* and *Rora4* are expressed in the cerebellum (Nehls et al. 1997). Error bars represent SEM; n=3 mice per genotype. [p-values: B) *Rora4* *p=0.009; C) *Rora4* **p=0.03].

A.

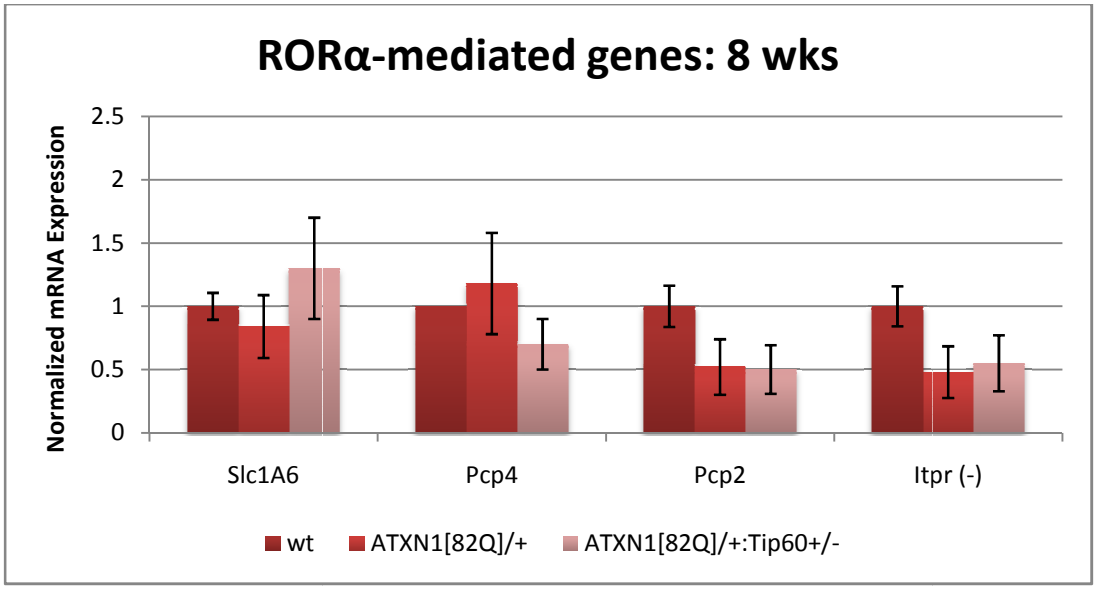
RORα-mediated genes: 8 wks
Normalized mRNA Expression
2.5
2
1.5
1
0.5
0
Slc1A6
Pcp4
Pcp2
Itpr (-)
wt
ATXN1[82Q]/+
ATXN1[82Q]/+:Tip60+/-

B.

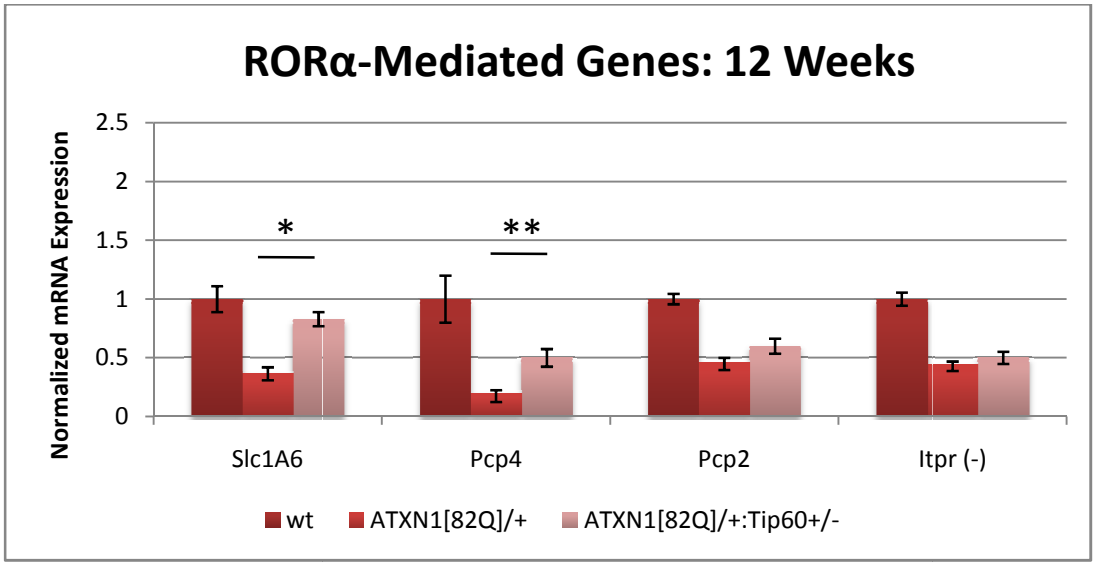
RORα-Mediated Genes: 12 Weeks
Normalized mRNA Expression
2.5
2
1.5
1
0.5
0
*
**
Slc1A6
Pcp4
Pcp2
Itpr (-)
wt
ATXN1[82Q]/+
ATXN1[82Q]/+:Tip60+/-

C.

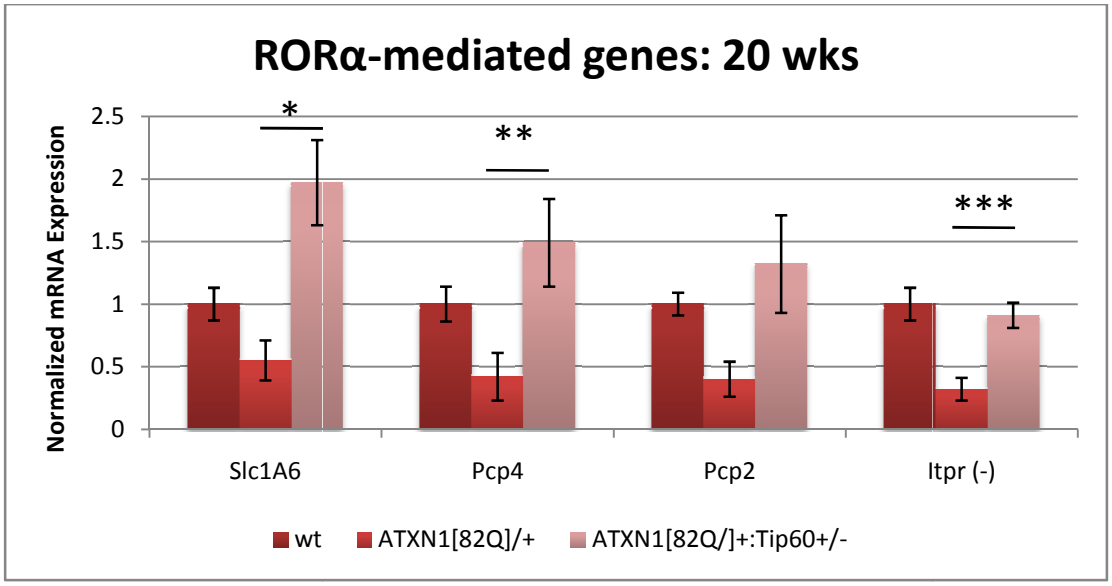

Figure 29. qRT-PCR of RORα-mediated genes in cerebella of A) 8 week B) 12 week and C) 20 week old wt, *ATXN1*[82Q]/+, and *ATXN1*[82Q]/+:*Tip60*$^{+/-}$ mice. Error bars represent SEM; n=3 mice per genotype. [p-values: B) *Slc1A6*: *p=0.004; *Pcp4*: **p=0.02 C) *Slc1A6*: *p=0.028; *Pcp4*: **p=0.028; *Itpr*: ***p=0.045]

	*Tip60 $^{+/+}$ *ATXN1*[82Q]	*Tip60 $^{+/-}$ *ATXN1*[82Q]
12 wks	low Rora4 low Slc1A6 low Pcp4 (low Itpr) Disease progression	high Rora4 high Slc1A6 high Pcp4 (low Itpr) DISEASE SUSPENSION
20 wks	low Rora4 low Slc1A6 low Pcp4 (low Itpr) Disease progression	high Rora4 high Slc1A6 high Pcp4 (high Itpr) Disease progression

Table 2. Gene expression summary of *ATXN1*[82Q]/+ (*Tip60*$^{+/+}$) versus *ATXN1*[82Q]/+:*Tip60*$^{+/-}$ mice. Differential gene expression begins at 12 weeks, which correlates with the slowing of ML thinning in *ATXN1*[82Q]/+:*Tip60*$^{+/-}$ mice. Partial *Tip60* loss restores *Rora* (isoform 4), *Slc1A6*, and *Pcp4* expression in *ATXN1*[82Q] mice. *Itpr* is included as a negative control; Day P0 data suggests that Tip60 is not present at the *Itpr* promoter (Gold et al., 2003).

Chapter 4

ATXN1 Modulates Tip60 Histone Acetylation

Part I: Introduction: Histone Acetyltransferases in Polyglutamine Disease

Histone modifications, especially acetylation and deacetylation, are major contributors to epigenetic gene regulation (Minucci and Pelicci, 2006). Histone acetyltransferases (HATs) and histone deacetylases (HDACs) are the enzymes responsible for adding and removing acetyl groups, respectively. While histones are traditionally thought of as targets, over 50 nonhistone targets have been discovered for HDACs (Minucci and Pelicci, 2006; Xu et al., 2007) and myriad HAT targets have been identified; many are nuclear receptors (Gaughan et al., 2002; Fu et al., 2004; Sun et al., 2005; Tang et al., 2006).

Huntington's Disease (HD) and SCA1 are polyglutamine disorders with cognitive effects and movement dysfunction. While HD and SCA1 have distinct pathology and mechanisms, they share the common feature of transcriptional dysregulation. Sp1, which interacts directly with ATXN1's AXH domain (Mizutani et al., 2005), also interacts with Huntingtin (Htt), the protein containing the expanded polyglutamine tract in HD (Dunah et al., 2002; Li et al., 2002). Many Sp1-driven genes are downregulated in HD human and mouse models (Luthi-Carter et al., 2000). Mechanisms implicated in HD include core transcription

machinery disruption (Freiman and Tjian, 2002; Zhai et al., 2005) and changes in posttranslational modifications (decreased acetylation with concomitant increased methylation) (Steffan et al., 2001; Ferrante et al., 2004; Ryu et al., 2006; Stack et al., 2007). The latter mechanism is probably linked to the Htt polyglutamine domain's interaction with CREB-binding protein's (CBP) and p300/CBP-associated factor's (P/CAF) acetyltransferase domains. The polyglutamine/acetyltransferase domain interaction may inhibit enzymatic HAT activity (Steffan et al., 2001).

Tip60 acetylates both histone and nonhistone proteins (Gaughan et al., 2002; Sun et al., 2005; Tang et al., 2006). Tip60's nonhistone targets include polyglutamine proteins and steroid nuclear receptors (Gaughan et al., 2001; Gaughan et al., 2002), suggesting that either ATXN1 or RORα may be Tip60 acetylation targets.

Part II: Results: *ATXN1*[82Q] Increases Histone Acetylation *in vitro*

Having demonstrated a role for partial *Tip60* loss in delaying SCA1 neurodegeneration, I hypothesized a mechanistic role for Tip60 acetyltransferase activity in SCA1 pathogenesis. I characterized Tip60 histone acetyltransferase activity in cells with either no *ATXN1*, *ATXN1*[30Q], or *ATXN1*[82Q] (Figure 30). Investigating an *ATXN1* polyglutamine effect on Tip60 activity is important, because the interaction between Tip60 and ATXN1 appears to be polyglutamine repeat-length independent (Serra et al., 2004). I performed histone acetyltransferase experiments with CHO cells, which do not express endogenous

Atxn1 or *Tip60*. CHO cells were transfected, without *ATXN1*, with and without *Tip60*, with *ATXN1*[30Q], with and without *Tip60*, and with *ATXN1*[82Q], with and without *Tip60*. All cells were treated with histone deacetylase inhibitor (HDACi), sodium butyrate, at 24 hours to prevent deacetylation. Whole cell protein lysates were isolated at 48 hours. Acetyl-histone H3 levels were determined by western blot and normalized to total histone H3 levels. Cells transfected with *Tip60* and either no *ATXN1* or *ATXN1*[30Q] had an approximately tenfold increase in acetyl-histone H3 compared to *ATXN1* and *ATXN1*[30Q] cells without exogenous *Tip60* (Figure 30B, lanes 1 vs. 2, and 3 vs. 4). However *ATXN1*[82Q] cells co-expressing *Tip60* had a thirtyfold increase in acetylation relative to no-*Tip60* *ATXN1*[82Q] controls (Figure 30B, lanes 5 vs. 6), triple that of their wt counterparts. In cells expressing *Tip60*, *ATXN1*[82Q] enhanced acetylation three times as much as *ATXN1*[30Q], suggesting an ATXN1 polyglutamine length effect on Tip60 activity.

Part III: Discussion: Tip60 Acetyltransferase Activity in the SCA1 Model

The aforementioned experiments suggest that Tip60's dysregulation in the presence of mutant *ATXN1*[82Q] *in vitro* causes increased total acetylation. The mechanism for SCA1 pathogenesis may involve (a) acetylation of histones, or (b) acetylation of other proteins.

If hypothesis (a) is true, the partial *Tip60* loss in the *ATXN1*[82Q]/+:*Tip60*$^{+/-}$ mouse may suppress pathogenic gene transcription. Disease-causing gene suppression during the protective window would contribute to the cerebellar

degeneration delay. Conversely suppressing genes that promote healthy PC function at 20 weeks may explain eventual degeneration in *ATXN1*[82Q]/+:*Tip60*$^{+/-}$ mice. I found no evidence in the *ATXN1*[82Q]/+:*Tip60*$^{+/-}$ mice for genes differentially regulated during and after the protective window. However my studies focused on genes that promote, rather than inhibit, PC signaling and function. Future studies investigating genes that inhibit PC function may reveal a role for Tip60 histone acetyltransferase activity in SCA1 pathology.

If hypothesis (b) is a mechanism of SCA1 cerebellar degeneration, one potential acetylation target is RORα, since it is both a nuclear receptor and present in an *in vivo* complex with Tip60 and ATXN1 (Serra et al., 2006). In this scenario, RORα acetylation is predicted to decrease transcriptional activity. The partial *Tip60* loss would decrease RORα acetylation and increase transcriptional activity. An increase in RORα-mediated transcription is seen in *ATXN1*[82Q]/+:*Tip60*$^{+/-}$ mice compared to *ATXN1*[82Q]/+ mice (Table 2). While Tip60 can function as a transcriptional co-activator, the effect of Tip60 activity seems to be context dependent. Tip60 often functions as a transcription repressor. For example, in the Alzheimer Disease model, Tip60 represses FE65 transcriptional activity (Yang et al., 2006). In T lymphoma cells, Tip60 augments HIV-1 Tat transactivation at the HIV long terminal repeat (LTR) promoter in HeLa cells, but inhibits transcription at the same promoter in Jurkat cells (Hlubek et al., 2001). Tip60 also negatively modulates transcription when it binds to the repressor, zinc finger E box binding protein (ZEB) (Postigo and Dean, 1997; Hlubek et al., 2001) and inhibits CD4-enhancer/promoter activity (Hlubek et al., 2001). Moreover

Tip60 has no intrinsic transactivation activity when brought to DNA by a heterologous DNA binding domain in COS-1 cells (African green monkey kidney cells)(Brady et al., 1999), but does activate transcription in the same system in yeast via a HAT-dependent mechanism (Gavaravarapu and Kamine, 2000). These studies suggest that Tip60 can function either as a transcriptional co-activator or co-repressor based on the cellular environment.

Part IV: A Brief Discussion of the Therapeutic Use of HDAC Inhibitors

Because HDACis have been shown to increase or decrease transcription of specific genes, and because Tip60 also can have disparate effects on transcription depending on the cellular context, I have included a brief discussion of a rapidly-growing area of new investigation: therapeutic HDACi use for neurodegenerative diseases.

The use of HDACis has been tested in HD mouse models (Thomas et al., 2008), Friedreich's ataxia (Herman et al., 2006; Rai et al., 2008), and in human hematologic and solid tumor malignancy trials (Bruserud et al., 2007; Mottet and Castronovo, 2008; Shankar and Srivastava, 2008). All together there are more than 100 ongoing clinical trials with HDACis as monotherapy or in combination with other therapies.

While several transcriptional dysregulation mechanisms have been identified in HD pathology, the precise role of each mechanism remains unclear (Okazawa, 2003; Sugars and Rubinsztein, 2003; Thomas, 2006). In the meantime, efforts

have been aimed at developing therapeutic strategies centered around transcription, namely histone deacetylase inhibitors (HDACis). HDACi 4b (a compound developed at the Scripps Research Institute for use in an HD mouse model) improves motor performance, decreases brain atrophy, and reverses downregulated gene expression. Notably the cerebellum is most responsive to HDACi 4b-induced transcription changes (Thomas et al., 2008).

Isoform-specific versus broad-spectrum HDACi utility is debatable. HDACis cause extensive deacetylation, affecting anywhere from less than 10% of the genome (Mariadason et al., 2000; Glaser et al., 2003) to 22% (Peart et al., 2005). Toxicity is an important HDACi side effect to consider and may be more pronounced with broad-spectrum inhibitors. Documented effects of HDACis include proapoptotic pathway activation, antiapoptotic pathway inhibition, increased cellular differentiation, and growth arrest (Kelly et al., 2002; Dokmanovic and Marks, 2005; Drummond et al., 2005). While helpful in treating cancer, these effects may prove detrimental in neurodegenerative models.

HDACis would be useful for SCA1 therapy if downregulated SCA1 genes were identified and could be targeted with selective HDACis. Other considerations for using HDACis in neurodegenerative diseases include choosing compounds that cross the blood-brain barrier and reducing toxic side effects.

A.

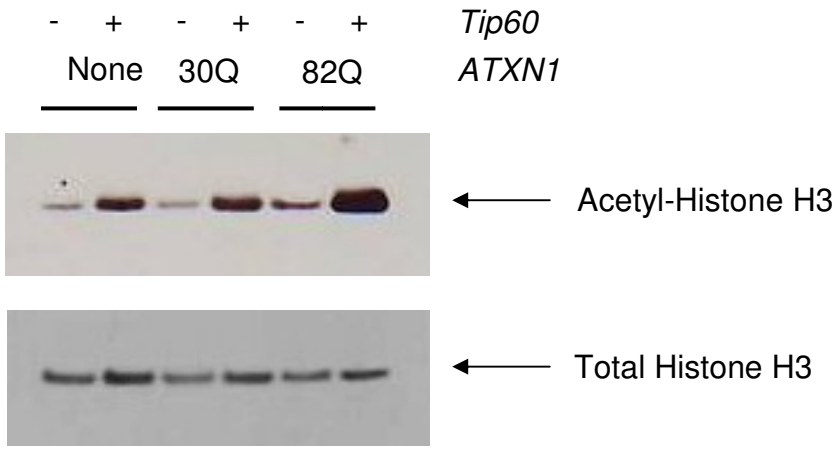

B.

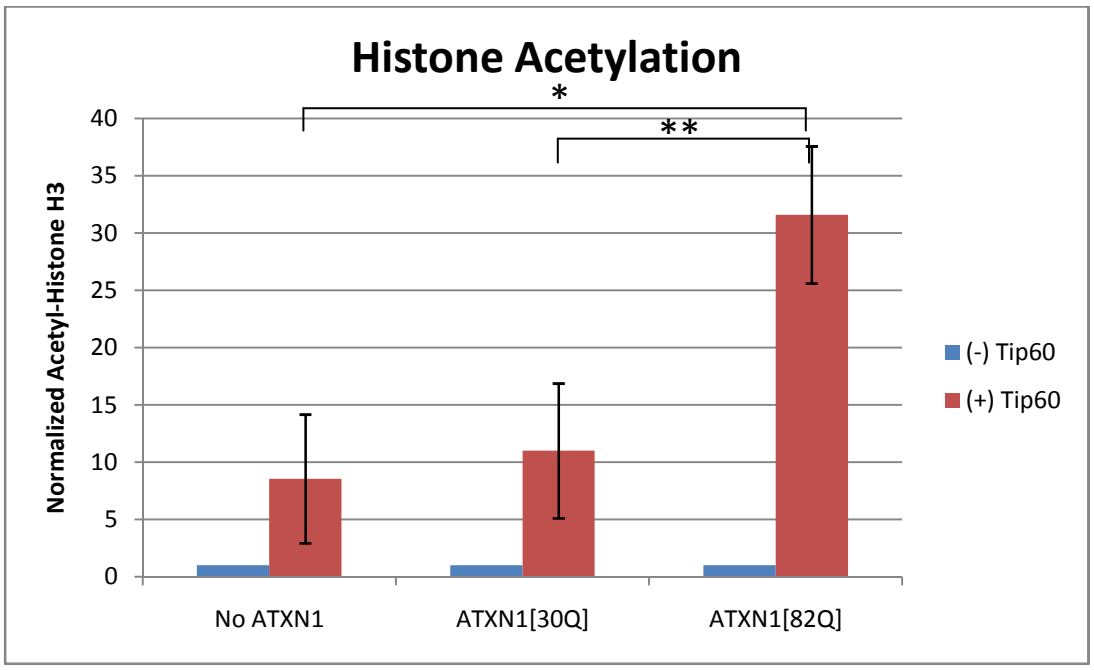

Figure 30. A) Western blots, B) with quantification of CHO cells transfected with no *ATXN1*, *ATXN1*[30Q], and *ATXN1*[82Q]; with or without Tip60; and probed with anti-acetyl-histone H3 antibody. Total histone H3 antibody was used as a loading control. (*p=0.03; **p=0.048).

Chapter 5

Tip60 miRNA

Part I: Introduction to the Use of Interfering RNA for SCA1

RNA interference (RNAi) is an attractive treatment option for progressive, intractable, and fatal diseases when mutant, gain-of-function genes have been identified. RNAi may be especially useful when a knockout mouse model has shown that mutant allele loss ameliorates the disease phenotype. In SCA1, the *Atxn1* knockout mice have no neuronal pathology and only a mild Rota-Rod phenotype (Matilla et al., 1998). Initial tissue culture and brain models suggest that RNAi has promise in treating polyglutamine diseases (Caplen et al., 2002; Xia et al., 2002; Miller et al., 2003; Davidson and Paulson, 2004). RNAi developed against *ATXN1* reduces RNA up to 60% and reduces protein up to 80% (Xia et al., 2004). Short hairpin RNAs (shRNAs) with a loop sequence derived from endogenously expressed micro-RNAs (miRNAs) improve transcript nuclear export and gene silencing (Kawasaki and Taira, 2003). *ATXN1* shRNAs were modified to contain the loop from mir23 (5'-CTTCCTGTCA-3'); this improves human *ATXN1*[30Q] and *ATXN1*[82Q] silencing from the pol III promoter (Xia et al., 2004). Both adeno-associated virus1 (AAV1) and AAV5 expression vectors, when injected into the cerebellum, show high cerebellar PC tropism (Alisky et al., 2000). For the *ATXN1* RNAi mouse model, shRNA

constructs were expressed in an AAV1 vector and delivered into murine cerebellum via stereotaxic injection. AAV1shSCA1 transduced PCs, improved motor coordination (tested with a Rota-Rod apparatus), protected the ML thickness, and resulted in greater resolution of PC nuclear inclusions relative to AAV1shLacZ controls (Xia et al., 2004).

Part II: Development and Validation of Tip60 miRNA Hairpin Constructs

Using the previously described SCA1 RNAi experiments as a model for stereotaxic injection of RNAi to treat neurodegeneration, I developed Tip60 miRNAs targeting the endogenous murine *Tip60* cDNA for *in vitro* screening (Figure 31). Plasmids expressing miRNA were cotransfected into 293T cells (derived from human embryonic kidney) along with Flag-tagged *Tip60*. The kidney has moderate *Tip60* expression (Lough lab, unpublished data), but 293T cells (derived from human renal epithelial cells) were supplemented with exogenous 3xFlag-*Tip60* to allow measurement of protein levels in the absence of a robust, commercially available Tip60 antibody. Plasmids encoding Tip60 miRNA were transfected alone into C2C12 cells (myogenic cells derived from mouse leg muscle) to measure endogenous *Tip60* RNA knockdown (Kioussi et al., 2002).

Candidate sequences, dispersed throughout the *Tip60* cDNA, were cloned into vectors downstream of the pol III U6 promoter. The vectors also expressed GFP driven by the pol II cytomegalovirus (CMV) promoter; GFP expression was used as an internal control. Hairpins were engineered to contain endogenously

expressed mir30 (similar to mir23) loop structures to increase nuclear export and gene silencing efficiency.

To measure the effect of Tip60 miRNA knockdown on endogenous Tip60 mRNA, mir30/Tip60 construct 3, 4, 5, or 6 was transfected into C2C12 cells. Empty vectors were transfected as a negative control. After 48 hours, cells were harvested to isolate RNA and protein. *Tip60* RNA knockdown was quantified with *Tip60* qRT-PCR; transcript levels were normalized to the housekeeping gene Glyceraldehyde 3-phosphate dehydrogenase (*GAPDH)*. *Tip60* mRNA levels in cells transfected with target miRNAs 3-6 were appreciably less than in the mock-transfected control (Figure 33).

Tip60 RNAi's ability to reduce protein levels *in vitro* was tested using western blot analysis on whole cell lysates from 293T cells transfected with 3xFlag-*Tip60* and either mock vector, GFP control miRNA, or miTip60 constructs 1-6. 3xFlag-Tip60 was transfected into cells; anti-Flag antibody blots detected exogenous Tip60 (Figure 34). The most effective *Tip60* miRNAs were constructs miTip60-3 and miTip60-6. The miTip60-3 target sequence is near the transcript's center, upstream from the zinc-finger domain. The miTip60-6 target is located between the histone acetyltransferase domain and the nuclear receptor box (Figure 32). Both miTip60-3 and miTip60-6 achieved almost complete Tip60 protein knockdown by western blot. These miRNAs may be useful for future applications, including stereotaxic miTip60-encoding AAV viral vector injection to study *in vivo* *Tip60* knockdown.

Part III: Discussion of miRNA for Therapeutic Knockdown Applications

RNAs were previously thought to have two major functional roles, the transfer of genetic information from DNA to protein and protein synthesis. RNA also is known to perform more complex functions. Short, double-stranded RNAs interfere with gene expression (Fire et al., 1998) and can be used as a tool to knock down target RNA. RNAi is a proposed treatment for many diseases, including cancer (Christopher S. Gondi, 2009), HIV (Martinez, 2009), Huntington's Disease (Pfister et al., 2009), amyotrophic lateral sclerosis (ALS) (Wu et al., 2009), and a variety of liver diseases (Arbuthnot et al., 2009).

Tip60 is an attractive target for RNAi. Although a complete and global *Tip60* loss is not compatible with embryonic development, a *Tip60* half dose results in a phenotypically normal mouse. In my *ATXN1*[82Q]/+:*Tip60*$^{+/-}$ mouse model, a *Tip60* half dose slowed the cerebellar neurodegenerative progression. Systemic *Tip60* miRNAs with an approximately 50% targeting efficiency, or more potent miRNAs delivered locally to the cerebellum, would likely have a similar effect. Cerebellar specificity can be achieved with selective PC-tropic vectors and promoters. Photocaged siRNAs, a modification that silences oligonucleotides until exposed to near-ultraviolet light, spatially and temporally control RNAi activation (Casey et al., 2009). Initial studies suggest a therapeutic benefit for treating neurodegenerative diseases with RNAi, but further work is needed to develop targeting and delivery strategies appropriate for clinical use.

1 atggcggagg tgggggagat aatcgagggc tgccgcctgc ccgtgctgcg gc**gcaaccag**

61 **gacaacgaag at**gagtggcc cctggctgag atcctgagcg tgaaggacat cagtggccga

121 aagcttttct atgt**ccatta cattgacttc aaca**aacgtc tggatgaatg ggtgactcac

181 gagcggctgg acttaaagaa gatccaattt cccaagaaag aggccaagac acctaccaag

241 aacggacttc ctgggtcccg ccccggctct cccgaaagag aggtgaaacg gaaggtggag

301 gtggtttcac cagcaacccc agtgcccagc gagacagccc cagcctcggt tttccctcag

361 aatgggtcag cccgtagggc agtggcagcc cagcctggac ggaagcggaa atctaattgc

421 ttgg**gcactg atgaggattc tcag**gacagc tcagatggaa taccgtcagc accacgaatg

481 actggcagtc tggtgtctga ccggagccac gacgacattg tcacccggat gaagaacatt

541 gagtgtattg agcttggccg gcaccgcctc aagccgtggt acttctcccc gtacccacaa

601 gagcttacca cgctacccgt cctctacctg tgcgaatttt gcctcaaata tggccgtagc

661 ctcaagtgtc tgcaac**gcca cttgaccaaa tgtgat**cttc ggcaccctcc aggcaatgaa

721 atttaccgca agggcaccat ctccttttt gagattgatg gacggaaaaa caagagttac

781 tcacaaaacc tgtgtcttct ggccaagtgt ttcctggacc acaaaacact gtactatgac

841 actgacccct tcctcttct**a cgtaatgacg gagtatgact** gcaaaggttt ccacatcgtg

901 ggctacttct ccaaggaaaa ggaatccaca gaagattaca atgtggcctg catcttgact

961 ctgcctccct accagcgccg gggctatggc aagctgctta ttgagttcag ctatgaactc

1021 tcgaaagtag aagggaagac cggaactcct gagaaacccc tgtcagatct tggcctccta

1081 tcct**accgaa gttactggtc ccaaa**ccatc ttggagatcc tgatggggct gaagtcggag

1141 agcggggaga ggccacagat caccatcaat gagatcagtg aaatcactag tatcaagaaa

1201 gaagatgtca tctccacact gcagtatctc aacctcatca attactacaa gggccagtat

1261 atcctaactc tgtcagaaga catcgtggat gggcatgagc gggctatgct caagcggctc

1321 cttcggattg actccaagtg tctgcacttc actcccaaag actggagcaa gagaggaaag

1381 tggtga

Figure 31. *Tip60β* cDNA (1386 b.p.). GenBank: AF528196.1. Sequence from *Mus musculus* strain C57BL/6. The six 20-21 base pair miRNA target sequences are bolded and underlined.

A.

1 maevgeiieg crlpvlr**rnq dned**ewplae ilsvkdisgr klfy**vhyidf n**krldewvth

61 erldlkkiqf pkkeaktptk nglpgsrpgs perevpasaq asgktlpipv qitlrfnlpk

121 ereaipggep dqplsssscl qpnhrstkrk vevvspatpv psetapasvf pqngaarrav

181 aaqpgrkrks ncl**gtdedsq** dssdgipsap rmtgslvsdr shddivtrmk niecielgrh

241 rlkpwyfspy pqelttlpvl ylcefclkyg rslkclq**rhl tkcd**lrhppg neiyrkgtis

301 ffeidgrknk sysqnlclla kcfldhktly ydtdpflf**yv mteyd**ckgfh ivgyfskeke

361 stedynvaci ltlppyqrrg ygklliefsy elskvegktg tpekplsdlg lls**yrsywsq**

421 tileilmglk sesgerpqit ineiseitsi kkedvistlq ylnlinyykg qyiltlsedi

481 vdgheramlk rllridskcl hftpkdwskr gkw

B.

Tip60 miRNA target #	amino acid #
1	18-24
2	45-52
3	194-200
4	278-284
5	339-345
6	414-420

Figure 32. A) Tip60 amino acid sequence with miRNA targets bolded and underlined and B) corresponding peptides targeted by *Tip60* miRNAs 1-6.

C.

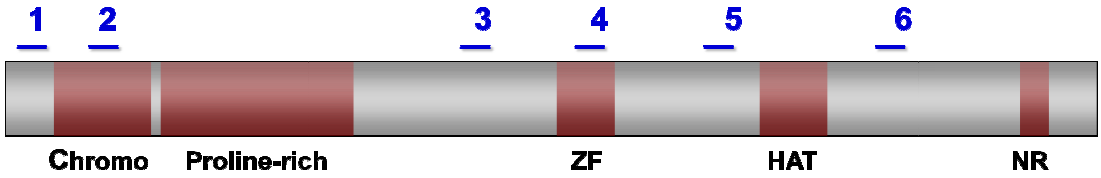

Figure 32 (cont'd). C) *Tip60* miRNA target locations in relation to Tip60 protein functional domains (chromodomain [chromo], zinc finger [ZF], histone acetyltransferase [HAT], and nuclear receptor domain [NR]).

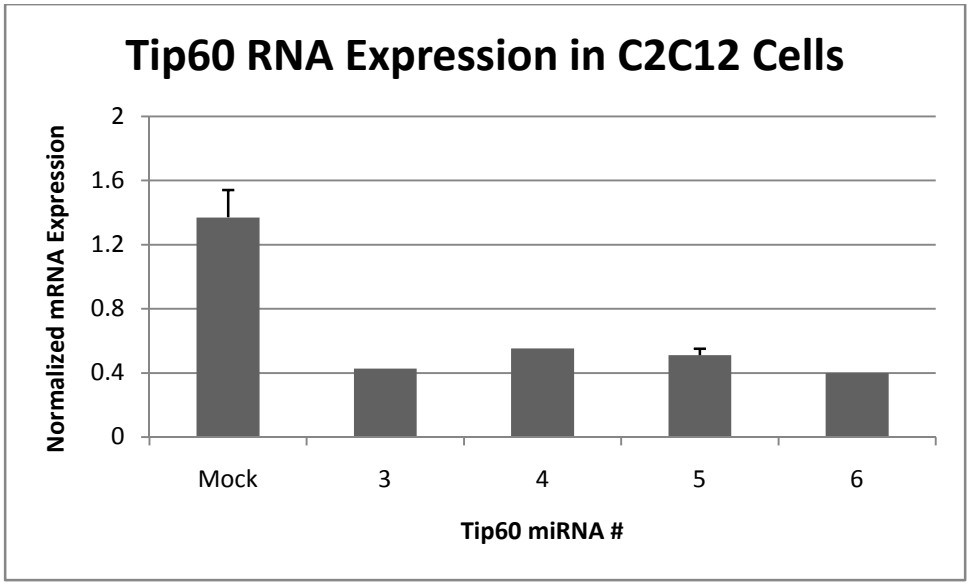

Figure 33. qRT-PCR of endogenous *Tip60* after empty vector or Tip60 miRNA constructs 3-6 transfection. *Tip60* expression was corrected for transfection efficiency and normalized to *GAPDH*.

A.

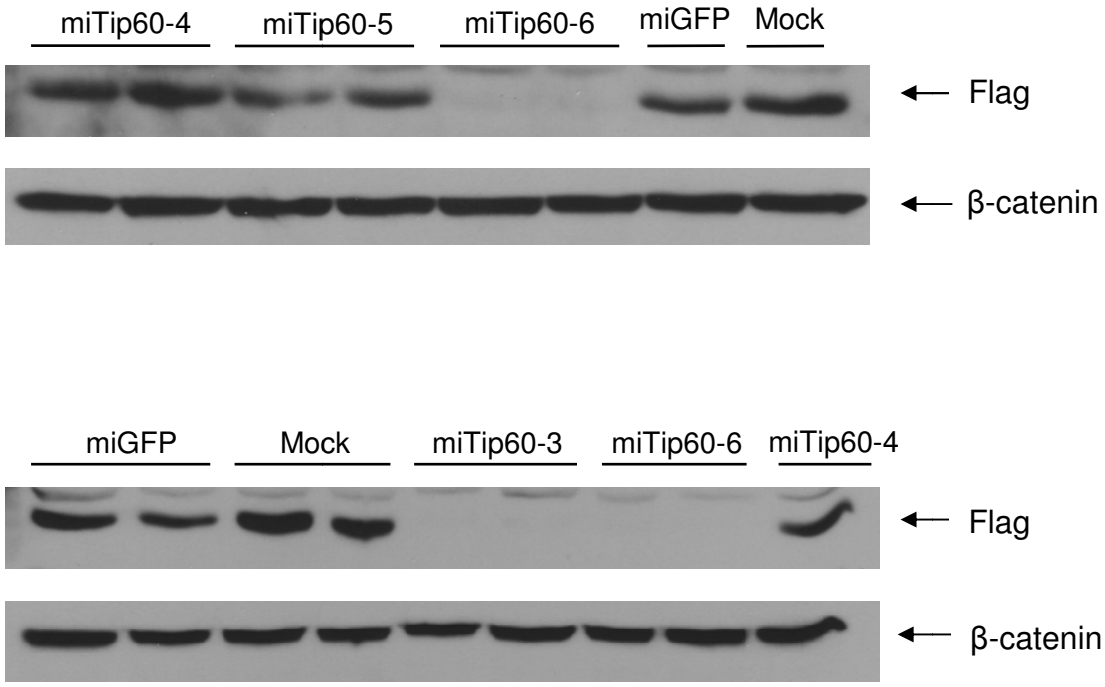
miTip60-4
miTip60-5
miTip60-6
miGFP
Mock
Flag
β-catenin
miGFP
Mock
miTip60-3
miTip60-6
miTip60-4
Flag
β-catenin

B.

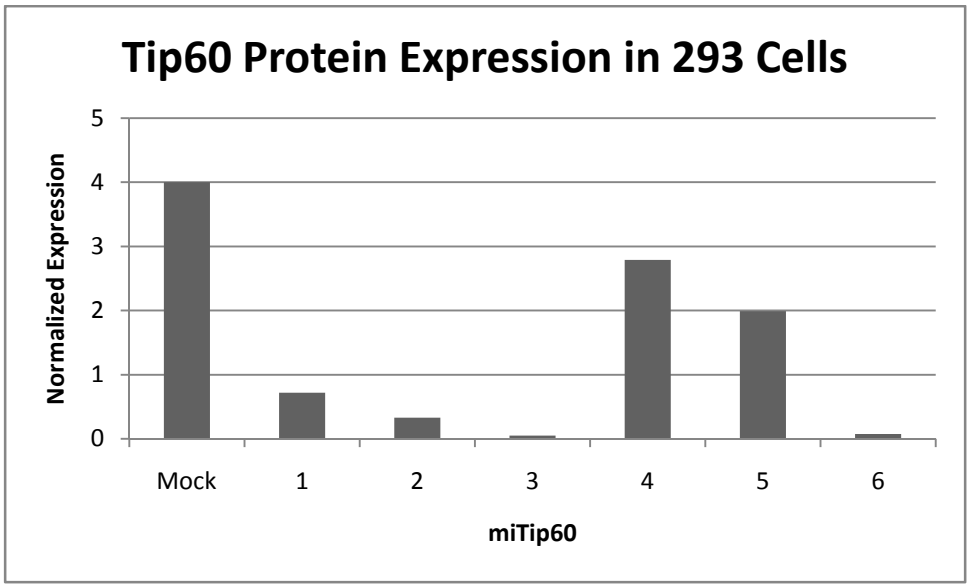

Figure 34. A) Western blots B) with quantification of 3xFlag-Tip60 knockdown using miRNA constructs 1-6. Western blots were probed with anti-Flag antibody. β-catenin was used as a loading control.

Chapter 6

Conclusions and Future Directions

Significant pathologic improvements result from partial *Tip60* loss in *ATXN1*[82Q]/+:*Tip60*$^{+/-}$ mice compared to *ATXN1*[82Q]/+ littermates on the FVB;SV-129;C57BL/6 background. Pathologic and biochemical changes were observed without significant behavioral phenotype differences. Future efforts to characterize the mouse model would include (a) identifying genes that are differentially regulated during and after cerebellar degeneration slows in *ATXN1*[82Q]/+:*Tip60*$^{+/-}$ mice, and (b) identifying mutant ATXN1[82Q] toxic effects that overcome partial *Tip60* protective effects at 20 weeks. Since this study focused on calcium and glutamate signaling genes, which are necessary for PC development, additional studies should focus on genes that negatively impact PCs, including neuronal dysfunction, cell cycle arrest, and apoptosis genes. ATXN1[82Q] toxic effects may involve the ubiquitin/proteasome pathway (Skinner et al., 2001), RNA splicing (Lim et al., 2008), or transcription dysregulation (Okazawa et al., 2002).

The FVB;SV-129;C57BL/6 strain resulted in a more rapid *ATXN1*[82Q]/+ transgene-mediated ML thinning and a delayed behavioral phenotype compared to the FVB background. Isolating genes with differential expression or single

nucleotide polymorphisms (SNPs) among the FVB, SV-129, and C57BL/6 strains may identify cerebellar degeneration modifier genes, especially if the genes are linked to *Tip60* or disrupted by *ATXN1*[82Q]/+ transgene insertion. Genetic strain analysis would involve extensive characterization by comparative gene array. *ATXN1*[82Q]/+:*Tip60*$^{+/-}$ mice could also be backcrossed onto the FVB background to minimize SV-129;C57BL/6 background strain effects.

Partial *Tip60* loss is linked to slowing of cerebellar degeneration, but a partial *Tip60* dose cannot sustain long-term protection. It may be that cerebellar Tip60 accumulates over time or that Tip60-dependent changes persist in the PC until the benefit of *Tip60* loss is silenced. A cerebellar specific *Tip60* homozygous knockout would illuminate this possibility. Although generating a floxed *Tip60* mouse has proven technically challenging for our collaborators (Lough lab, Medical College of Wisconsin), a mouse with a floxed allele could be linked to the Pcp2/L7 to generate PC-specific *Tip60* null mice.

Mutant ATXN1[82Q] increased Tip60 histone acetyltransferase activity over wild-type ATXN1[30Q] *in vitro*. Tip60 acetyltransferase activity at nonhistone targets should be determined. RORα and ATXN1 may be stabilized or inhibited by posttranslation acetylation, and the downstream effects may hold the key for SCA1 pathogenesis. Another Tip60 acetylation target mediating the SCA1 degenerative pathway may be p53. Tip60 is known to acetylate p53. Acetylated p53 and nonacetylated p53 activate distinct cell-cycle arrest and apoptotic pathways (Tang et al., 2006). *ATXN1*[82Q]/+ mice with a targeted deletion of *p53*

(ATXN[82Q]/+;*p53*$^{-/-}$) have significantly thinner MLs at 15 and 20 weeks compared to ATXN[82Q]/+;*p53*$^{+/+}$ controls, without an improvement in motor coordination by Rota-Rod analysis at 6, 9, or 12 weeks. p53 is hypothesized to act at an intermediate stage of SCA1 disease (between 6 and 15 weeks) to promote disease progression (Shahbazian et al., 2001). Parallels between my *ATXN1*[82Q]/+;*Tip60*$^{+/-}$ model and the *ATXN1*[82Q]/+;*p53*$^{-/-}$ model, along with the knowledge that (a) p53 regulates neuronal survival (Hughes et al., 1997), (b) polyglutamine proteins increase p53 levels (Trettel et al., 2000; Jana et al., 2001), and (c) Tip60 acetylates p53 (Tang et al., 2006), identify p53 as a rational focus for future Tip60 experiments.

Model of Tip60 Activity in SCA1 Pathogenesis

Tip60 and ATXN1 interact directly *in vivo*. Although polyglutamine tract length does not affect GST-ATXN1/Tip60 interaction (Serra et al., 2006), it may impact Tip60 activity. I have shown an ATXN1 polyglutamine length effect on Tip60 histone acetyltransferase activity *in vitro*; mutant ATXN1[82Q] increases Tip60's activity. It is not known whether Tip60 nonhistone protein acetylation is a regulatory step in SCA1 pathogenesis. Tip60 does acetylate other proteins, including nuclear receptors, transcription factors, and cell-cycle regulators (Kouzarides, 2000; Gaughan et al., 2001). Acetylation is known to regulate phosphorylation; these modifications stabilize the substrate protein, promote protein-protein interactions, and regulate DNA binding affinity (Kouzarides, 2000; Chen et al., 2005; Matsuzaki et al., 2005; Yuan et al., 2005). Additionally

acetylation of nuclear receptors is known to increase transactivation (Yamamoto and Horikoshi, 1997; Brady et al., 1999; Gaughan et al., 2001; Gold et al., 2003). Within the ATXN1/Tip60/RORα complex, a direct interaction has been shown for ATXN1-Tip60, but not for Tip60-RORα or ATXN1-RORα (Serra et al., 2006). Direct interaction suggests ATXN1 as a putative Tip60 acetylation target; precedence for Tip60 nuclear receptor acetylation points to RORα as another putative substrate. Other unidentified proteins in the ATXN1/RORα/Tip60 complex cannot be ruled out as Tip60 substrates. If decreased RORα-mediated gene transcription is the direct result of acetylation by Tip60, this would demonstrate a new effect of nuclear receptor acetylation. Another possibility is that acetylation destabilizes RORα. Finally acetylation may decrease RORα's DNA binding affinity, a function that has been shown for acetylation of p53, E2F1, EKLF, and GATA1 transcription factors (Gu and Roeder, 1997; Boyes and Byfield, 1998; Zhang and Bieker, 1998; Martinez-Balbas et al., 2000).

I propose a model in which mutant ATXN1 increases Tip60 acetyltransferase activity in the PC nucleus (Figure 35A). ATXN1 enters the nucleus and forms a complex that also contains RORα and Tip60 (Figure 35A, 1). Tip60 and ATXN1 interact directly within the complex, and Tip60 can acetylate other proteins, including ATXN1 and/or RORα (Figure 35A, 2). Acetylation and phosphorylation are known to be linked and co-regulated (Barak and Eisenbach, 2004). For instance Forkhead box O1 (FOXO1) transcription factor acetylation increases its phosphorylation levels (Matsuzaki et al., 2005). Acetylation may also be a precursor to subsequent ATXN1 phosphorylation and stabilization (via decreased

degradation or increased protein-protein interactions, shown in orange) (Figure 35A, 3). While S776 phosphorylation is known to regulate ATXN1's stabilizing interaction with 14-3-3 (Chen et al., 2003), recent *in vitro* evidence suggests most ATXN1-associated kinase activity may be in the cytoplasm (Orr lab, unpublished data), so it is also possible that acetylation and phosphorylation take place in the cytoplasm before nuclear translocation. Previous work in a conditional model of mutant *ATXN1*[82Q] shows that turning off *ATXN1*[82Q] restores RORα expression without simultaneous RNA restoration (Serra et al., 2006). In Figure 35A (4), stable mutant ATXN1 exerts its deleterious effects by depleting RORα from the PC nucleus. Mutant ATXN1 destabilizes RORα protein (Figure 35A, 5) by a mechanism separate from decreasing *Rora* transcription (Figure 35A, 6). Both mechanisms result in decreased RORα-mediated gene transcription (Figure 35A, 7). In the *ATXN1*[82Q]/+:Tip60$^{+/+}$ model, downstream Tip60 acetylation effects can include ATXN1 stabilization, RORα depletion, and decreased expression of RORα-mediated genes. Ultimately PC dysfunction results.

In a model of partial *Tip60* loss in SCA1 pathogenesis (*ATXN1*[82Q]/+:Tip60$^{+/-}$) (Figure 35B), I hypothesize the opposite effect. Mutant ATXN1 enters the nucleus and forms a complex that also contains RORα and a decreased amount of Tip60 (Figure 35B, 1). Decreased Tip60 target acetylation (potentially including, but not limited to, ATXN1 and RORα) (Figure 35B, 2) may decrease subsequent phosphorylation and ATXN1-stabilizing interactions (Figure 35B, 3). RORα may be directly stabilized by decreased acetylation. Alternatively a decrease in mutant ATXN1 may protect RORα from degradation (Figure 35B, 4),

increasing RORα-mediated gene transcription (Figure 35B, 5). In the *ATXN1*[82Q]/+:Tip60$^{+/-}$ model, decreased acetylation by Tip60 can lead to ATXN1 destabilization, increased RORα, and increased RORα-mediated gene expression, promoting PC function.

Consider SCA1 disease as occurring in the following stages: early stage disease, which includes cerebellar development (9 weeks and earlier); midstage disease or disease progression, after 9 weeks but before 20 weeks (12-16 weeks in this study); and an advanced stage, including 20 weeks and beyond (Fig. 36). Characterization of the conditional *ATXN1*[82Q]/+ mice demonstrates that mutant *ATXN1*[82Q] expression is important at each SCA1 stage. Furthermore early-, mid-, and late-stage disease recovery are unique when the mutant gene is turned off (Zu et al., 2004). Not only does SCA1 disease have at least three unique stages, ATXN1 plays a role in the pathology of each stage.

The *Rora*$^{sg/sg}$ mouse has a partial cerebellar agenesis, while the *Rora*$^{sg/+}$ mouse has an age-dependent cerebellar degeneration (Zanjani et al., 1992). The s*taggerer* mouse, along with gene expression profiling at 5 and 12 weeks (Lin et al., 2000; Hadj-Sahraoui et al., 2001; Serra et al., 2004; Serra et al., 2006), suggests that RORα is important during two SCA1 stages: early (development) and midstage (progression) disease.

Partial *Tip60* loss plays a specific, temporal disease role, slowing the neurodegenerative rate specifically during midstage disease progression. Midstage pathologic protection by ML and CF-PC analysis correlates with the time (12 weeks) when transcriptional changes are first measurable in *Rora4* and RORα-mediated genes (*Slc1A6 and Pcp4*). Increased expression of genes that promote PC function may contribute to the onset of the protective window in *ATXN1*[82Q]/+:*Tip60*$^{+/-}$ mice. However transcription upregulation continues at 20 weeks, when ML protection is lost. *Rora4, Pcp4, and Slc1A6* expression may be a compensatory mechanism that is not sufficient to overcome mutant ATXN1 or other signaling pathways' deleterious neurodegenerative effects.

In summary I conclude the Tip60-ATXN1 interaction is important for SCA1 pathogenesis and *Tip60* loss delays cerebellar degeneration in an SCA1 mouse model, specifically during midstage disease. I also show a genetic background effect on degenerative rate and suggest a potential role for acetylation in SCA1 disease mechanisms.

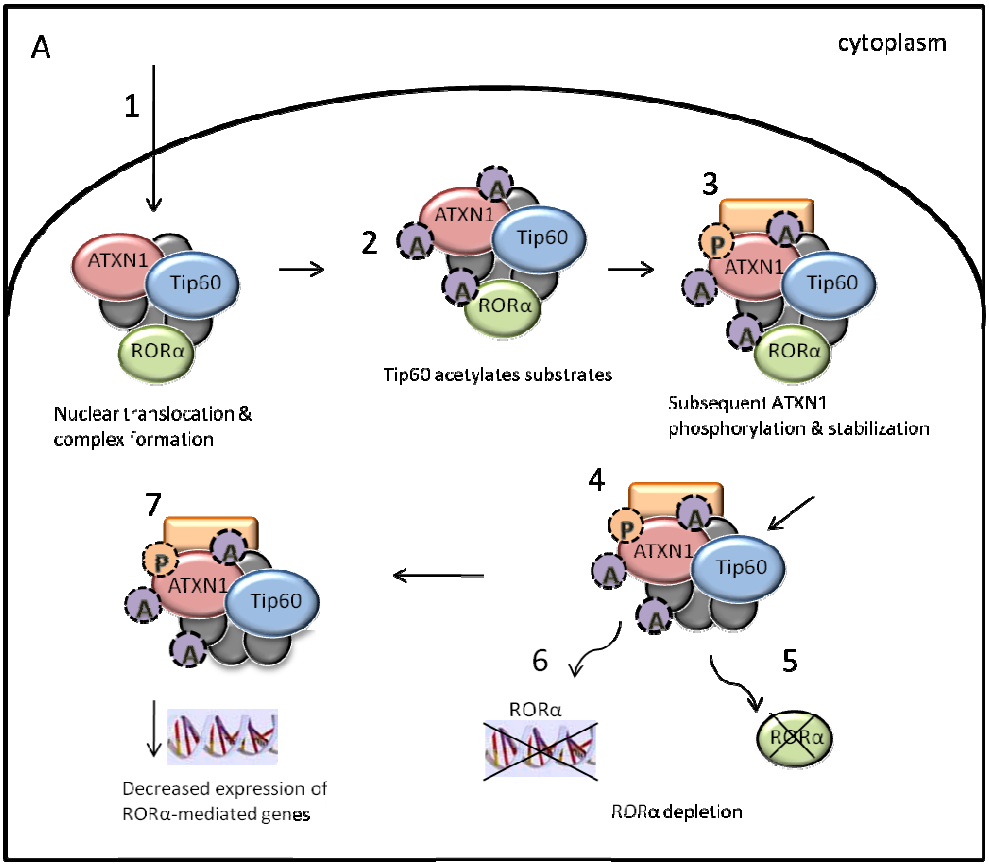

Figure 35A. Proposed model of Tip60 acetylation in SCA1 pathogenesis (*ATXN1*[82Q]/+:*Tip60*$^{+/+}$).

1) ATXN1 forms a nuclear complex with RORα and Tip60. 2) Tip60 can acetylate interacting proteins (including ATXN1 and RORα), which leads to ATXN1 phosphorylation and 3) subsequent stabilizing interactions. RORα acetylation may also destabilize RORα or decrease RORα-mediated transcription directly. 4) Stable ATXN1 depletes RORα from the PC nucleus by 5) degrading RORα protein or 6) decreasing *Rora* transcription, which both lead to 7) decreased RORα-mediated gene transcription and PC dysfunction.

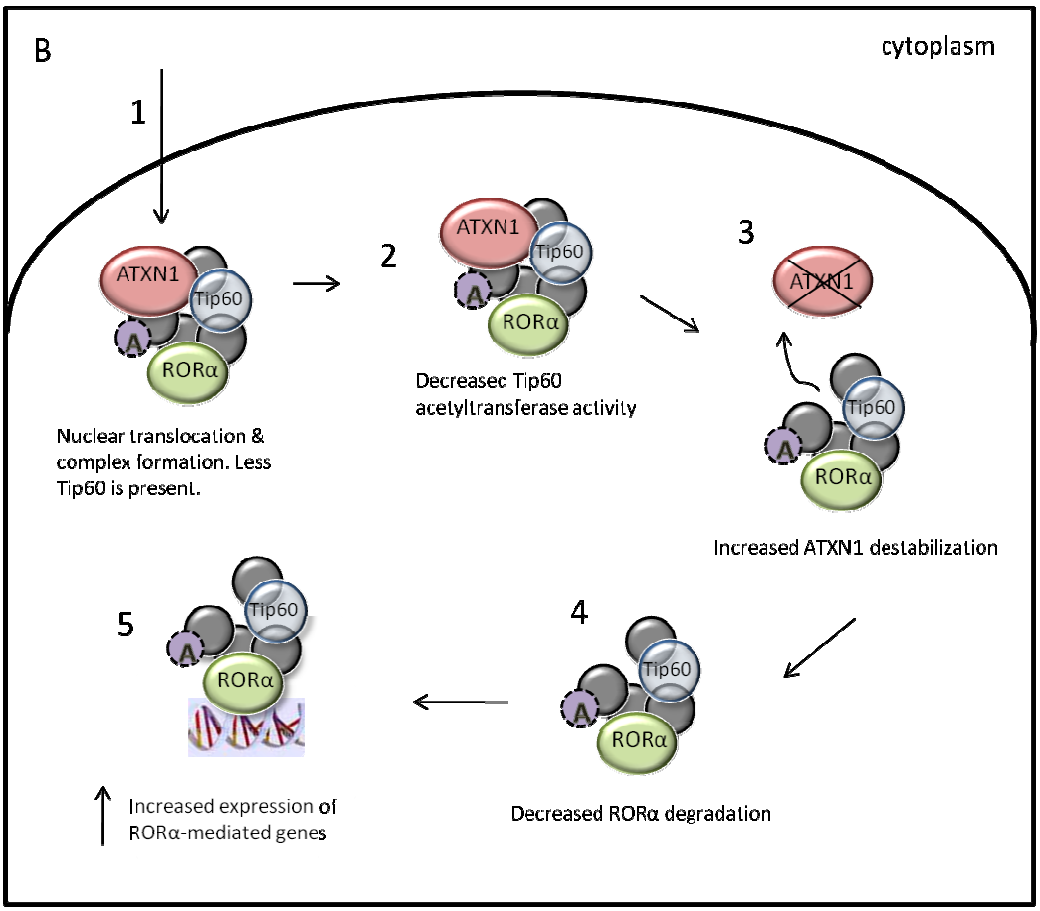

Figure 35B. Proposed model of partial *Tip60* loss in SCA1 pathogenesis (*ATXN1*[82Q]/+:*Tip60*$^{+/-}$).

1) ATXN1 forms a complex with RORα and a half-normal amount of Tip60. 2) Decreased Tip60 can lead to decreased ATXN1 acetylation, which 3) destabilizes ATXN1. 4) Less ATXN1 prevents RORα depletion and 5) increases RORα-mediated gene transcription, promoting PC function.

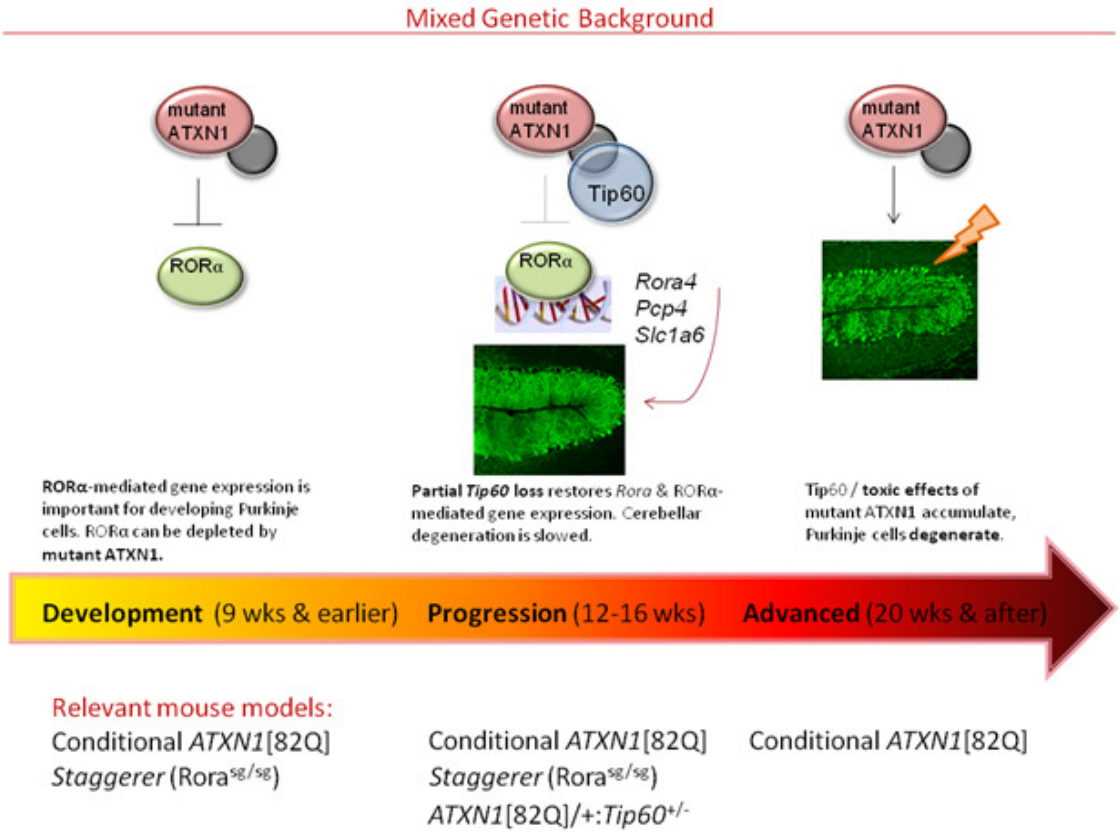

Figure 36. Model of SCA1 disease stages: early (including development), middle (progression), and late (advanced disease). ATXN1 expression is important for pathogenesis at each stage. RORα has demonstrated importance during early and midstage disease. Midstage disease pathology can be slowed by partial *Tip60* loss in the *ATXN1*[82Q]/+:*Tip60*$^{+/-}$ mouse model.

Chapter 7

Methods

Part I: Mouse Genotyping

Animal care and breeding. Wild-type, Tip60$^{+/-}$, *ATXN1*[82Q]/+, *ATXN1*[82Q]/+:Tip60$^{+/-}$ mice were the F_1 progeny (1:1:1:1) resulting from breeding *ATXN1*[82Q] and Tip60 heterozygous mice. The ATXN[82Q]/+ mice were maintained on an FVB background and the Tip60+/- mice were maintained on an SV-129;C57BL/6 background. The *ATXN1*[82Q]/+, Tip60$^{+/-}$, and *ATXN1*[82Q]/+:Tip60$^{+/-}$ (FVB;SV-129;C57BL/6) hybrid mice had access to standard chow and water ad libitum, were housed with controlled temperatures (68ºF–74ºF), and had a 12/12-hour diurnal light/dark cycle.

Isolation of murine DNA. Murine DNA was isolated using Promega Wizard® SV Genomic DNA Purification System (Promega #A2361). Tail clips (5mm from the tail tip, up to 20 mg) or ear punches (~6mm^2, up to 20mg) were cut into two equal pieces to allow for efficient digestion, placed in 1.5 mL microcentrifuge tubes (one tube per mouse), and incubated overnight (16-18 hours) at 55℃ (without shaking) in 275 µL digestion solution. Digestion solution components (except Proteinase K) were provided in the Promega purification system and added to each tissue sample in the following amounts: nuclei lysis solution (200µL/sample tube), 0.5M ethylenediaminetetraacetic acid (EDTA) pH 8.0 (50µL/sample tube),

Rnase A solution (5µL/sample tube). A 20mg/mL Proteinase K stock solution (Promega #V3021) was made with nuclease-free water and added at 20µL/sample tube. Proteinase K was stored at -20℃ and thawed on ice; RNAase inhibitor and all other components were stored at 22ºC. After overnight incubation, samples were centrifuged at 2500 times the force of gravity (x *g)* to pellet undigested hair or cartilage. Supernatants were transferred to a new 1.5 mL microcentrifuge tube, 250 µL of Wizard® SV Lysis buffer was added to each sample, and the tubes were briefly vortexed. At this step, samples were frozen at -80℃ (and later thawed and warmed at 55℃ x 1 hour), or warm lysates were immediately processed. All subsequent steps were performed at 22ºC. Sample lysates were transferred from 1.5 mL microcentrifuge tubes to a Wizard® SV minicolumn assembly. Loaded minicolumns were spun at 13,000 x *g* for 3 minutes to bind the DNA to the column filter. Flow-through was discarded from each minicolumn assembly, and 650 µL Wizard® SV wash solution (95% ethanol (EtOH)) was added to each minicolumn. Samples were then spun at 13,000 x *g* for 1 minute and flow-through was discarded. The EtOH wash was repeated three more times (four total washes). A final spin at 13,000 x *g* for 2 minutes dried the binding matrix. The minicolumn was placed in another 1.5 mL microcentrifuge tube for elution, and 250 uL of 65℃ nuclease-free water was added to the minicolumn. After 2 minutes of 22ºC incubation, samples were centrifuged at 13,000 x g for 1 minute. The final step was repeated for a 500 µL DNA elution volume. Purified genomic DNA was stored at -20℃.

Tip60 PCR conditions. The following *Tip60* primers were used: Neo 1621 (GGCCAGCTCATTCCTCCACTCATGATCTAT), Tip5006 (AAGCCTAAACATGATCTGAGTGACCGGCGT), and Tip5438c (CACGCCACTCATCTTCGTTGTCCTGGTT). In the wt mouse, these primers resulted in a single amplified band. In the *Tip60* heterozygote, targeted *Tip60* disruption by a Neo cassette led to two amplified bands.

Part II: Indirect Cerebellar Immunofluorescence

The mice were anesthetized with ketamine (100 mg/mL) and xylazine (20 mg/mL). Mice were dosed based on body weight at 100 mg/kg ketamine and 10 mg/kg xylazine, according to University of Minnesota Institutional Animal Care and Use Committee guidelines. Sedated mice were perfused transcardially with 10% phosphate buffered formalin (Fisher #SF100-4). Perfused brains were extracted, stored overnight in 10% phosphate buffered formalin, and then stored long-term in PBS at 4ºC. Midline sagital sections (50 µm) were made on a Vibratome Series 1000 Sectioning System at a speed of 3.0 and amplitude of 3.0. Floating cerebellar slices were placed in PBS immediately after sectioning. To unmask protein epitopes, PBS was replaced with 0.01M urea, and sections were heated to just under boiling (approximately 45 seconds in a microwave on high power). After unmasking, 0.01M urea was replaced with blocking solution (2% goat sera, 0.3% Triton-X, in PBS), and cerebellar slices were blocked on a rocker overnight at 4ºC. After overnight incubation, primary antibody was added to blocking solution at the following dilutions: goat calbindin D28K (Santa Cruz [c-

20] sc7691) at 1:500, rabbit 11750/ataxin-1 (Zoghbi lab) at 1:500, and goat VGluT2 (Millipore MAB5504) at 1:1000. Cerebellar slices were incubated with primary antibody for 48-72 hours at 4ºC, washed 4 times for 20 minutes each in PBS on a rocker at 22ºC, and incubated with secondary antibodies for 48 hours at 4ºC. Secondary antibody dilutions were made with blocking solution in the following concentrations: donkey anti-goat Cy3 (Jackson Immunoresearch #705-165-147) at 1:500, donkey anti-rabbit Cy2 (Jackson Immunoresearch #711-225-152) at 1:500, and donkey anti-mouse Cy5 (Jackson Immunoresearch #115-175-146) at 1:500. After incubation with secondary antibodies, sections were washed 4 times for 20 minutes each in PBS on a rocker at 22ºC. Washed sections were mounted on Thermo Scientific 24x40 slides with 55ºC glycerol gelatin (Sigma #GG1-15ML) containing 4 mg/mL n-Propyl Gallate (n-PG). All steps after the addition of secondary antibodies were performed with cerebellar sections covered in aluminum foil to protect the fluorescent labels' light-sensitive properties. Slides were visualized on a FluoView inverted confocal, laser-scanning microscope (Olympus #FV1000 IX2). Molecular layer thickness was measured with FluoView software. Mounted slides were stored at -20ºC when not in use.

Part III: Gait Analysis

DigiGait. To test multiple gait parameters, mice were placed on a DigiGait™ Imaging System (Mouse Specifics, Inc., Quincy, MA) and run at a 25 cm/sec belt speed for 10 seconds. Gait analysis from each mouse's ventral side was captured and analyzed with DigiGait proprietary software. Relevant specific parameters included rear stance width, stride time (stance and swing components), and rear paw angle. Student's *t* test was used to assess statistical significance.

Rota-Rod. To test motor coordination and balance, mice were placed on a Rota-Rod apparatus (Model #7650, Ugo Basile, Comerio, VA, Italy), which consists of a 3 cm diameter central rotating drum suspended 16 cm above a platform and separated by opaque disks into five sections for testing mice simultaneously without distraction. Mice were run on an accelerating protocol, where the trial was started at minimum velocity (4 rpm), accelerated for 5 minutes to maximum velocity (40 rpm), and maintained at maximum velocity. For each mouse, the trial continued until the mouse fell off the Rota-Rod or 10 minutes had elapsed. The latency to fall (up to 600 seconds) was recorded. The Rota-Rod protocol was continued for 4 consecutive days. Four trials were run per mouse, per day, for a total of 16 trials; the mice were given a 10 minute recovery period between trials. Each mouse's average daily latency to fall was reported. Student's *t* test was used to assess statistical significance.

Part IV: Mouse Cerebella

Cerebellar protein lysates. Mice were sacrificed with CO_2 according to University of Minnesota Institutional Animal Care and Use Committee guidelines. Fresh cerebella were bisected into hemispheres, placed in 1.5 mL microfuge tubes (one hemisphere per tube), flash frozen in liquid nitrogen, and stored at -80ºC. For protein extraction, brain extraction buffer (0.25 M Tris-HCl pH 7.5) was supplemented with phosphatase inhibitor cocktail I (Sigma-Aldrich #P2850) at a 1:100 dilution (100µL/10mL); phosphatase inhibitor cocktail II (Sigma-Aldrich #P5726) at a 1:100 dilution (100µL/10mL); and complete, mini, EDTA-free protease inhibitor (Roche #11836170001) at one mini tablet/10mL buffer. Cerebella were homogenized into a 500 µL supplemented brain extraction buffer with a cordless motor pestle (VWR #A6-LP-A0001) and 3" disposable pellet mixers (VWR #A6-PL-A0002). Homogenized cerebellar tissue was freeze-thawed three times in alternating liquid nitrogen followed by a 37℃ water bath. After three freeze-thaw cycles, lysates were centrifuged at 2500 x *g* for 10 minutes at 4℃. The supernatant was transferred to a new 1.5 mL microfuge tube and kept on ice.

Part V: Western Blot Analysis

Bradford assay. Protein Assay Dye Reagent (Bio-Rad #500-0006) was diluted 1:5 in water. Protein lysates were added to the dye reagent and incubated at 22ºC for 5 minutes. Concentrations were measured with a spectrophotometer at 595 nm.

Protein transfer. Prepared cerebellar tissue-culture lysates were reduced with NuPAGE® Sample Reducing Agent (Invitrogen #NP0004), heated for 10 minutes at 90℃, and loaded on 4-12% gradient NuPAGE® Novex Bis-Tris gels (Invitrogen #NP0321BOX). Gels were run in NuPAGE® MES SDS buffer (Invitrogen #NP0002) with NuPAGE® Antioxidant (Invitrogen #NP0005) at 100V. Gels were transferred in NuPAGE® Transfer Buffer (Invitrogen #NP00061) to nitrocellulose membranes (Whatman Protran BA 85) and kept overnight at a constant 100V.

Blocking and antibody probing. For GAPDH, anti-acetylated Histone H3, and anti-total Histone H3 western blots, membranes were blocked for 2 hours at 22ºC in 5% weight/volume (w/v) low-fat, powdered milk in phosphate buffered saline (PBS) with 0.1% volume/volume (v/v) Tween-20 (PBST) made with deionized water. Blocked membranes were incubated with mouse anti-GAPDH antibody (Chemicon #MAB374), rabbit anti-acetylated Histone H3 antibody (Active Motif #39129), or rabbit anti-total Histone H3 antibody (Cell Signaling #9715) for 1 hour at 22ºC, washed three times with PBST (0.1%), incubated with secondary antibody (anti-mouse HRP (GE Healthcare #NA931V) or anti-rabbit HRP (GE Healthcare (#NA934V)) for 45 minutes at 22ºC, washed three times with PBST (0.1%), incubated with SuperSignal® West Pico Chemiluminescent substrate (Pierce #34080) for 5 minutes at 22ºC, and then exposed to film (Kodak #165-1454).

For RORα western blots, membranes were blocked overnight at 4ºC with 10% blotto (10% w/v milk in 1x TBS) with 0.1% v/v Tween-20. Blocked membranes were incubated with RORα antibody (Santa Cruz H-65 #sc-28612) for 1 hour at 22ºC, washed three times with 0.1% PBST, incubated with anti-goat HRP secondary antibody for 45 minutes at 22ºC, washed three times with 0.1% PBST, incubated with SuperSignal® West Pico Chemiluminescent substrate (Pierce #34080) for 5 minutes at 22ºC, and then exposed to film (Kodak #165-1454).

Densitometry. To quantitate protein expression levels from western blot, films were scanned with a BioRad Gel Dock GS700 600 dpi flatbed densitometer and analyzed with ImageQuant software. RORα levels were normalized to GAPDH; acetylated Histone H3 levels were normalized to total Histone H3.

Part VI: Quantitative RT-PCR

Cerebellar RNA isolation. Isolated, frozen cerebella were placed on wet ice and 500 uL of TRIzol (Invitrogen #15596-026) was added to each sample. Cerebella were homogenized in 1.5 mL microfuge tubes with a cordless motor pestle (VWR #A6-LP-A0001) and 3" disposable pellet mixers (VWR #A6-PL-A0002). An additional 500 uL of TRIzol was added after complete homogenization and samples were centrifuged at 12,000 x *g* for 10 minutes at 4℃. Supernatant (cleared homogenate) was transferred to fresh DNase-free, RNase-free 1.5 mL tubes. After 5 minute incubation on ice, 200 uL chloroform was added to each sample. Samples were shaken vigorously by hand for 15 seconds, incubated on ice for 3 minutes, and centrifuged at 12,000 x *g* for 15 minutes at 4℃. The upper,

colorless, aqueous sample phase (containing the RNA) was transferred to another DNase-free, RNase-free test tube. After adding 500 µL of 100% isopropanol, the tubes were rocked by hand three times and incubated at 22ºC for 10 minutes. Samples were then centrifuged at 12,000 x *g* for 10 minutes at 4℃ to pellet the RNA. The supernatant was decanted, leaving the RNA in the pellets, and 1 mL of 75% RNase-free EtOH (dilutions made with deionized, diethylpyrocarbonate [DEPC] water) was added to each sample. Tubes were briefly vortexed to wash the pellets and centrifuged at 7500 x *g* for 5 minutes at 4℃. The EtOH wash was decanted; pellets were air-dried for 5-10 minutes at 22ºC, then dissolved in 50 µL of nuclease-free water. RNA was quantified on a spectrophotometer (Thermo Scientific #NanoDrop 8000), and RNA was stored at -80℃.

Part VII: Cell Culture

Cell growth and transfection. Tip60 RNAi and 3xFlag-Tip60 were transfected into 293T cells. Without a reliable commercial anti-Tip60 antibody, Tip60 protein levels were assessed with an anti-Flag antibody. RNAi alone was transfected into C2C12 cells, which express endogenous Tip60. 293T cells and C2C12 cells were grown in Dulbecco's Modified Eagle Medium (DMEM) (Invitrogen #12430-104). miRNAs were transfected using Opti-MEM (Invitrogen #11058-021) and Lipofectamine 2000 (Invitrogen #11668019) at a high cell density (90-95% by plating 0.5-2 x 10^5 cells in 24 well plates). Plates for C2C12 cells were precoated with 0.1 mg/mL Poly-L-ornithine (Sigma #P4957).

For RORα and histone acetyltransferase experiments, CHO cells were grown in Gibco™ Minimum Essential Medium (MEM) and Alpha Medium (Invitrogen #32561037). All media was supplemented with 10% fetal bovine serum (FBS) (Invitrogen #10091-148) and 1% penicillin-streptomycin liquid (Invitrogen #15140-122), supplied as 10,000 units Penicillin G (sodium salt), 10,000 µg Streptomycin (base)/mL, and Streptomycin sulfate in 0.85% saline, prior to transfection. Cells were grown at 37℃ with 5% carbon dioxide (CO_2). Cells were plated in media without antibiotics 24 hours before transfection at 10^5 cells/mL in 60mm tissue culture dishes (BD Biosciences #356401) unless otherwise specified. Cells were transfected with Lipofectamine Plus (Invitrogen #11514-015) and 3 µg of DNA. At transfection, supplemented media was replaced with serum- and anitbiotic-free media. At 3 hours posttransfection, 10% FBS was added to the media. At 24 hours posttransfection, sodium butyrate (Sigma-Aldrich #303410-5G), a histone deacetylase inhibitor (HDACi), was added to the cells (250 µL of 100mM stock to 5 mL media, resulting in a 5mM sodium butyrate concentration).

Cell culture lysates. At 48 hours posttransfection, cells were rinsed with PBS at 22ºC. Tris-Triton lysis buffer (50mM Tris-HCl pH 7.5, 2.5mM $MgCl_2$, 100mM NaCl, 0.5% Triton) was supplemented with phosphatase inhibitor cocktail I (Sigma #P2850) and phosphatase inhibitor cocktail II (Sigma #P5726), each at a 1:100 dilution (100µL inhibitor/10 mL lysis buffer); complete, mini, EDTA-free protease inhibitor (Roche #11836170001) at one mini tablet/10mL buffer; and

100 mM sodium butyrate (at 500uL/10 mL lysis buffer) to achieve a 5 mM sodium butyrate concentration.

Supplemented 4℃ Tris-Triton lysis buffer (400µL per 60mm tissue culture dish) was added to cells that had been rinsed with PBS. Dishes were incubated at 4℃ for 20 minutes on a rotator. Lysates were transferred to cold, 1.5 mL gel-slick Eppendorf tubes and kept on ice. Lsyates were spun at 2500 x *g* at 4℃, the supernatant was transferred to a new gel-slick tube, and the pellet was discarded.

Part VIII: Tip60 miRNA Constructs

Putative miRNA target sequences 20-21 base pairs long were identified from murine sequence (Genbank #AF528196) and chosen based on strand-biasing preferences and 30-50% GC content. Locus AF528196 includes sequence information present in TIP60β/Tip53 and TIP60α/Tip60, as Tip53 is a Tip60 splice variant that excludes exon 5 (Ran and Pereira-Smith, 2000). Green fluorescent protein (GFP) was used as a control. RNA folds were generated using mFold software (Integrated DNA Technologies). Oligos were generated which contained sense/antisense hairpins based on identified miRNA targets joined by a common loop region from the endogenously expressed miRNA mir30 (Li et al., 2007). An miRNA shuttle cloning strategy was used to generate hairpin constructs as follows: oligos were subjected to overlapping polymerase extension, cleaned with restriction digest, ligated with a Tb:U6 vector which also contained a GFP cassette expressed from a modified CMV promoter,

transformed into DH5-α *Escherichia coli* cells, and selected with Kanamycin. Plasmid DNA was isolated from selected colonies and sequenced. Purified Tip60 miRNA hairpins #3-6 were transfected into tissue culture cells +/- exogenous Tip60. Exogenous and endogenous Tip60 RNA knockdown and protein levels were assessed by Q-PCR and western blot, respectively, at 24 hours posttransfection.

Part IX: Statistical Analysis

Data were expressed as the mean ± standard error of the mean (SEM). Statistical comparisons were made with a student's *t* test unless otherwise noted.

Bibliography

Aiba A, Kano M, Chen C, Stanton ME, Fox GD, Herrup K, Zwingman TA, Tonegawa S (1994) Deficient cerebellar long-term depression and impaired motor learning in mGluR1 mutant mice. Cell 79:377-388.

Airaksinen MS, Eilers J, Garaschuk O, Thoenen H, Konnerth A, Meyer M (1997) Ataxia and altered dendritic calcium signaling in mice carrying a targeted null mutation of the calbindin D28k gene. Proceedings of the National Academy of Sciences of the United States of America 94:1488-1493.

Alisky J, Hughes S, Sauter S, Jolly D, Dubensky TJ, Staber P, Chiorini J, Davidson B (2000) Transduction of murine cerebellar neurons with recombinant FIV and AAV5 vectors. Neuroreport 11:2669-2673.

Altman J (1972a) Postnatal development of the cerebellar cortex in the rat. II. Phases in the maturation of Purkinje cells and of the molecular layer. J Comp Neurol:399-463.

Altman J (1972b) Postnatal development of the cerebellar cortex in the rat. III. Maturation of the components of the granular layer. J Comp Neurol:465-513.

Amende I, Kale A, McCue S, Glazier S, Morgan J, Hampton T (2005) Gait dynamics in mouse models of Parkinson's disease and Huntington's disease. Journal of NeuroEngineering and Rehabilitation 2:20.

André E, Gawlas K, Steinmayr M, Becker-André M (1998) A novel isoform of the orphan nuclear receptor ROR[beta] is specifically expressed in pineal gland and retina. Gene 216:277-283.

Arbuthnot P, Ely A, Weinberg M (2009) Hepatic delivery of RNA interference activators for therapeutic application. Curr Gene Ther 9:91-103.

Banfi S, Servadio A, Chung M, Capozzoli F, Duvick LA, Elde R, Zoghbi HY, Orr HT (1996) Cloning and developmental expression analysis of the murine homolog of the spinocerebellar ataxia type 1 gene (Sca1). Hum Mol Genet 5:33-40.

Barak R, Eisenbach M (2004) Co-regulation of Acetylation and Phosphorylation of CheY, A Response Regulator in Chemotaxis of Escherichia coli. Journal of Molecular Biology 342:375-381.

Batini C (1990) Cerebellar localization and colocalization of GABA and calcium binding protein-D28K. Arch Ital Biol 128:127-149.

Becker-Andre M, Andre E, DeLamarter JF (1993) Identification of nuclear receptor mRNAs by RT-PCR amplification of conserved zinc-finger motif sequences. Biochem Biophys Res Commun 194:1371-1379.

Bellocchio EE, Reimer RJ, Fremeau RT, Jr., Edwards RH (2000) Uptake of Glutamate into Synaptic Vesicles by an Inorganic Phosphate Transporter. Science 289:957-960.

Bianchi-Frias D, Pritchard C, Mecham B, Coleman I, Nelson P (2007) Genetic background influences murine prostate gene expression: implications for cancer phenotypes. Genome Biol 8:117.

Boukhtouche F, Janmaat S, Vodjdani G, Gautheron V, Mallet J, Dusart I, Mariani J (2006) Retinoid-Related Orphan Receptor {alpha} Controls the Early Steps of Purkinje Cell Dendritic Differentiation. J Neurosci 26:1531-1538.

Brady ME, Ozanne DM, Gaughan L, Waite I, Cook S, Neal DE, Robson CN (1999) Tip60 Is a Nuclear Hormone Receptor Coactivator. J Biol Chem 274:17599-17604.

Bruserud Ã, Stapnes C, ErsvÃ¦r E, Gjertsen BT, Ryningen A (2007) Histone Deacetylase Inhibitors in Cancer Treatment: A Review of the Clinical Toxicity and the Modulation of Gene Expression in Cancer Cells. In: Current Pharmaceutical Biotechnology, pp 388-400: Bentham Science Publishers Ltd.

Burright EN, Clark HB, Servadio A, Matilla T, Feddersen RM, Yunis WS, Duvick LA, Zoghbi HY, Orr HT (1995) SCA1 transgenic mice: a model for neurodegeneration caused by an expanded CAG trinucleotide repeat. Cell 82:937-948.

Caplen NJ, Taylor JP, Statham VS, Tanaka F, Fire A, Morgan RA (2002) Rescue of polyglutamine-mediated cytotoxicity by double-stranded RNA-mediated RNA interference. Hum Mol Genet 11:175-184.

Carlberg C, Hooft van Huijsduijnen R, Staple J, DeLamarter J, Becker- Andre M (1994) RZRs, a new family of retinoid-related orphan receptors that function as both monomers and homodimers. Mol Endocrinol 8:757-770.

Carlson K, Andresen J (2009) Emerging pathways in the spinocerebellar ataxias. Curr Opin Genet Dev 19:1-7.

Carlson M, Kish P, Ueda T (1989) Characterization of the solubilized and reconstituted ATP-dependent vesicular glutamate uptake system. J Biol Chem 264:7369-7376.

Casey J, John P., Blidner RA, Monroe WT (2009) Caged siRNAs for Spatiotemporal Control of Gene Silencing. Molecular Pharmaceutics 6:669-685.

Chan-Palay SPaV (1974) Cerebellar Cortex. New York: Springer-Verlag.

Chen HK, Fernandez-Funez P, Acevedo SF, Lam YC, Kaytor MD, Fernandez MH, Aitken A, Skoulakis EM, Orr HT, Botas J, Zoghbi HY (2003) Interaction of Akt-phosphorylated ataxin-1 with 14-3-3 mediates neurodegeneration in spinocerebellar ataxia type 1. Cell 113:457-468.

Chen L, Williams S, Mu Y, Nakano H, Duerr J, Buckbinder L, Greene W (2005) NF-kappaB RelA phosphorylation regulates RelA acetylation. Mol Cell Biol 25:7966-7975.

Chen YW, Allen MD, Veprintsev DB, Lowe J, Bycroft M (2004) The Structure of the AXH Domain of Spinocerebellar Ataxin-1. J Biol Chem 279:3758-3765.

Christopher S. Gondi JSR (2009) Concepts in in vivo siRNA delivery for cancer therapy. Journal of Cellular Physiology 9999:n/a.

Chung MY, Ranum LP, Duvick LA, Servadio A, Zoghbi HY, Orr HT (1993) Evidence for a mechanism predisposing to intergenerational CAG repeat instability in spinocerebellar ataxia type I. Nat Genet 5:254-258.

Clark HB, Orr HT (2000) Spinocerebellar ataxia type 1--modeling the pathogenesis of a polyglutamine neurodegenerative disorder in transgenic mice. J Neuropathol Exp Neurol 59:265-270.

Clark HB, Burright EN, Yunis WS, Larson S, Wilcox C, Hartman B, Matilla A, Zoghbi HY, Orr HT (1997) Purkinje cell expression of a mutant allele of SCA1 in transgenic mice leads to disparate effects on motor behaviors, followed by a progressive cerebellar dysfunction and histological alterations. J Neurosci 17:7385-7395.

Crawley JN (1996) Unusual behavioral phenotypes of inbred mouse strains. Trends in Neurosciences 19:181-182.

Crawley JN, Belknap JK, Collins A, Crabbe JC, Frankel W, Henderson N, Hitzemann RJ, Maxson SC, Miner LL, Silva AJ, Wehner JM, Wynshaw-Boris A, Paylor R (1997) Behavioral phenotypes of inbred mouse strains: implications and recommendations for molecular studies. Psychopharmacology 132:107-124.

Crepel F (1982) Regression of functional synapses in the immature mammalian cerebellum. Trends in Neurosciences 5:266-269.

Crepel F, Delhaye-Bouchaud N, Guastavino JM, Sampaio I (1980) Multiple innervation of cerebellar Purkinje cells by climbing fibres in staggerer mutant mouse. Nature 283:483-484.

Crusio WE (1996) Gene-targeting studies: new methods, old problems. Trends in Neurosciences 19:186-187.

Cummings CJ, Mancini MA, Antalffy B, DeFranco DB, Orr HT, Zoghbi HY (1998) Chaperone suppression of aggregation and altered subcellular proteasome localization imply protein misfolding in SCA1. Nat Genet 19:148-154.

Davidson BL, Paulson HL (2004) Molecular medicine for the brain: silencing of disease genes with RNA interference. The Lancet Neurology 3:145-149.

de Chiara C, Giannini C, Adinolfi S, de Boer J, Guida S, Ramos A, Jodice C, Kioussis D, Pastore A (2003) The AXH module: an independently folded domain common to ataxin-1 and HBP1. FEBS Letters 551:107-112.

Dingledine R, Borges K, Bowie D, Traynelis SF (1999) The Glutamate Receptor Ion Channels. Pharmacol Rev 51:7-62.

Dokmanovic M, Marks P (2005) Prospects: Histone deacetylase inhibitors. Journal of Cellular Biochemistry 96:293-304.

Drummond DC, Noble CO, Kirpotin DB, Guo Z, Scott GK, Benz CC (2005) Clinical Development of Histone Deacetylase Inhibitors as Anticancer Agents. Annual Review of Pharmacology and Toxicology 45:495-528.

Dunah AW, Jeong H, Griffin A, Kim Y-M, Standaert DG, Hersch SM, Mouradian MM, Young AB, Tanese N, Krainc D (2002) Sp1 and TAFII130 Transcriptional Activity Disrupted in Early Huntington's Disease. Science 296:2238-2243.

Dynan W, Tjian R (1983) The promoter-specific transcription factor Sp1 binds to upstream sequences in the SV40 early promoter. Cell 35:79-87.

Fernandez-Funez P, Nino-Rosales ML, de Gouyon B, She WC, Luchak JM, Martinez P, Turiegano E, Benito J, Capovilla M, Skinner PJ, McCall A, Canal I, Orr HT, Zoghbi HY, Botas J (2000) Identification of genes that modify ataxin-1-induced neurodegeneration. Nature 408:101-106.

Ferrante RJ, Ryu H, Kubilus JK, D'Mello S, Sugars KL, Lee J, Lu P, Smith K, Browne S, Beal MF, Kristal BS, Stavrovskaya IG, Hewett S, Rubinsztein DC, Langley B, Ratan RR (2004) Chemotherapy for the Brain: The Antitumor Antibiotic Mithramycin Prolongs Survival in a Mouse Model of Huntington's Disease. J Neurosci 24:10335-10342.

Fire A, Xu S, Montgomery MK, Kostas SA, Driver SE, Mello CC (1998) Potent and specific genetic interference by double-stranded RNA in Caenorhabditis elegans. Nature 391:806.

Fordyce D, Wehner J (1993) Effects of aging on spatial learning and hippocampal protein kinase C in mice. Neurobiol Aging 14:309-317.

Freiman RN, Tjian R (2002) NEURODEGENERATION: A Glutamine-Rich Trail Leads to Transcription Factors. Science 296:2149-2150.

Fremeau RT, Troyer MD, Pahner I, Nygaard GO, Tran CH, Reimer RJ, Bellocchio EE, Fortin D, Storm-Mathisen J, Edwards RH (2001) The Expression of Vesicular Glutamate Transporters Defines Two Classes of Excitatory Synapse. Neuron 31:247-260.

Fremeau RT, Jr., Kam K, Qureshi T, Johnson J, Copenhagen DR, Storm-Mathisen J, Chaudhry FA, Nicoll RA, Edwards RH (2004) Vesicular

Glutamate Transporters 1 and 2 Target to Functionally Distinct Synaptic Release Sites. Science 304:1815-1819.

Fu M, Wang C, Zhang X, Pestell RG (2004) Acetylation of nuclear receptors in cellular growth and apoptosis. Biochem Pharmacol 68:1199-1208.

Fu Y, Kuhl D, Pizzuti A, Pieretti M, Sutcliffe J, Richards S, Verkerk A, Holden J, Jr RF, Warren S (1991) Variation of the CGG repeat at the fragile X site results in genetic instability: resolution of the Sherman paradox. Cell 67:1047-1058.

Gaughan L, Brady ME, Cook S, Neal DE, Robson CN (2001) Tip60 Is a Co-activator Specific for Class I Nuclear Hormone Receptors. J Biol Chem 276:46841-46848.

Gaughan L, Logan IR, Cook S, Neal DE, Robson CN (2002) Tip60 and histone deacetylase 1 regulate androgen receptor activity through changes to the acetylation status of the receptor. J Biol Chem 277:25904-25913.

Gavaravarapu S, Kamine J (2000) Tip60 inhibits activation of CREB protein by protein kinase A. Biochem Biophys Res Commun 269:758-766.

Gerlai R (1996) Gene-targeting studies of mammalian behavior: is it the mutation or the background genotype? Trends in Neurosciences 19:177-181.

Giguere V, Tini M, Flock G, Ong E, Evans RM, Otulakowski G (1994) Isoform-specific amino-terminal domains dictate DNA-binding properties of ROR alpha, a novel family of orphan hormone nuclear receptors. Genes Dev 8:538-553.

Glaser KB, Staver MJ, Waring JF, Stender J, Ulrich RG, Davidsen SK (2003) Gene Expression Profiling of Multiple Histone Deacetylase (HDAC) Inhibitors: Defining a Common Gene Set Produced by HDAC Inhibition in T24 and MDA Carcinoma Cell Lines. Molecular Cancer Therapeutics 2:151-163.

Gold DA, Baek SH, Schork NJ, Rose DW, Larsen DD, Sachs BD, Rosenfeld MG, Hamilton BA (2003) RORalpha coordinates reciprocal signaling in cerebellar development through sonic hedgehog and calcium-dependent pathways. Neuron 40:1119-1131.

Goold R, Hubank M, Hunt A, Holton J, Menon RP, Revesz T, Pandolfo M, Matilla-Duenas A (2007) Down-regulation of the dopamine receptor D2 in mice lacking ataxin 1. Hum Mol Genet 16:2122-2134.

Gorrini C et al. (2007) Tip60 is a haplo-insufficient tumour suppressor required for an oncogene-induced DNA damage response. 448:1063-1067.

Gras C, Herzog E, Bellenchi GC, Bernard V, Ravassard P, Pohl M, Gasnier B, Giros B, El Mestikawy S (2002) A Third Vesicular Glutamate Transporter Expressed by Cholinergic and Serotoninergic Neurons. J Neurosci 22:5442-5451.

Hadj-Sahraoui N, Frederic F, Zanjani H, Delhaye-Bouchaud N, Herrup K, Mariani J (2001) Progressive atrophy of cerebellar Purkinje cell dendrites during aging of the heterozygous staggerer mouse (Rora+/sg). Developmental Brain Research 126:201-209.

Hamilton BA, Frankel WN, Kerrebrock AW, Hawkins TL, FitzHugh W, Kusumi K, Russell LB, Mueller KL, van Berkel V, Birren BW, Kruglyak L, Lander ES (1996) Disruption of the nuclear hormone receptor RORalpha in staggerer mice. Nature 379:736-739.

Hampton T, Stasko M, Kale A, Amende I, Costa A (2004) Gait dynamics in trisomic mice: quantitative neurological traits of Down syndrome. Physiol Behav 82:381 - 389.

Hatten ME, Messer A (1978) Postnatal cerebellar cells from staggerer mutant mice express embryonic cell surface characteristic. Nature 276:504-506.

He Y-W, Deftos ML, Ojala EW, Bevan MJ (1998) ROR[gamma]t, a Novel Isoform of an Orphan Receptor, Negatively Regulates Fas Ligand Expression and IL-2 Production in T Cells. Immunity 9:797-806.

Herman D, Jenssen K, Burnett R, Soragni E, Perlman SL, Gottesfeld JM (2006) Histone deacetylase inhibitors reverse gene silencing in Friedreich's ataxia. Nat Chem Biol 2:551-558.

Hirose T, Smith RJ, Jetten AM (1994) ROR-[gamma]: The Third Member of ROR/RZR Orphan Receptor Subfamily That Is Highly Expressed in Skeletal Muscle. Biochemical and Biophysical Research Communications 205:1976-1983.

Hlubek F, Lohberg C, Meiler J, Jung A, Kirchner T, Brabletz T (2001) Tip60 is a cell-type-specific transcriptional regulator. J Biochem (Tokyo) 129:635-641.

Ichise T, Kano M, Hashimoto K, Yanagihara D, Nakao K, Shigemoto R, Katsuki M, Aiba A (2000) mGluR1 in Cerebellar Purkinje Cells Essential for Long-Term Depression, Synapse Elimination, and Motor Coordination. Science 288:1832-1835.

Ingram DK, Jucker M (1999) Developing mouse models of aging: a consideration of strain differences in age-related behavioral and neural parameters[small star, filled]. Neurobiology of Aging 20:137-145.

Ino H (2004) Immunohistochemical characterization of the orphan nuclear receptor ROR alpha in the mouse nervous system. J Histochem Cytochem 52:311-323.

Ito M (1989) Long-Term Depression. Annual Review of Neuroscience 12:85-102.

J. Takács JH (1994) Developmental dynamics of Purkinje cells and dendritic spines in rat cerebellar cortex. Journal of Neuroscience Research 38:515-530.

Jarvis CI, Staels B, Brugg B, Lemaigre-Dubreuil Y, Tedgui A, Mariani J (2002) Age-related phenotypes in the staggerer mouse expand the ROR[alpha] nuclear receptor's role beyond the cerebellum. Molecular and Cellular Endocrinology 186:1-5.

Jean Mariani (1982) Extent of multiple innervation of purkinje cells by climbing fibers in the olivocerebellar system of weaver, reeler, and staggerer mutant mice. Journal of Neurobiology 13:119-126.

Jetten A, Kurebayashi S, Ueda E (2001) The ROR nuclear orphan receptor subfamily: critical regulators of multiple biological processes. Prog Nucleic Acid Res Mol Biol 69:205-247.

Jetten AM (2004) Recent Advances in the Mechanisms of Action and Physiological Functions of the Retinoid-Related Orphan Receptors (RORs). In: Current Drug Targets - Inflammation & Allergy, pp 395-412: Bentham Science Publishers Ltd.

Jimenez G, Guichet A, Ephrussi A, Casanova J (2000) Relief of gene repression by Torso RTK signaling: role of capicua in Drosophila terminal and dorsoventral patterning. Genes & Development 14:224-231.

Jones B, Roberts D (1968) The quantiative measurement of motor inco-ordination in naive mice using an acelerating rotarod. J Pharm Pharmacol 20:302-304.

Kale A, Amende I, Meyer G, Crabbe J, Hampton T (2004) Ethanol's effects on gait dynamics in mice investigated by ventral plane videography. Alcohol Clin Exp Res 28:1839 - 1848.

Kallen J, Schlaeppi J-M, Bitsch F, Delhon I, Fournier B (2004) Crystal Structure of the Human ROR{alpha} Ligand Binding Domain in Complex with Cholesterol Sulfate at 2.2 A. J Biol Chem 279:14033-14038.

Kamine J, Elangovan B, Subramanian T, Coleman D, Chinnadurai G (1996a) Identification of a cellular protein that specifically interacts with the essential cysteine region of the HIV-1 Tat transactivator. Virology 216:357-366.

Kamine J, Elangovan B, Subramanian T, Coleman D, Chinnadurai G (1996b) Identification of a Cellular Protein That Specifically Interacts with the Essential Cysteine Region of the HIV-1 Tat Transactivator. Virology 216:357-366.

Karsunky H, Mende I, Schmidt T, Moroy T (2002) High levels of the onco-protein Gfi-1 accelerate T-cell proliferation and inhibit activation induced T-cell death in Jurkat T-cells. Oncogene 21:1571.

Kawasaki H, Taira K (2003) Short hairpin type of dsRNAs that are controlled by tRNAVal promoter significantly induce RNAi-mediated gene silencing in the cytoplasm of human cells. Nucl Acids Res 31:700-707.

Kelly MA, Rubinstein M, Phillips TJ, Lessov CN, Burkhart-Kasch S, Zhang G, Bunzow JR, Fang Y, Gerhardt GA, Grandy DK, Low MJ (1998) Locomotor Activity in D2 Dopamine Receptor-Deficient Mice Is Determined by Gene Dosage, Genetic Background, and Developmental Adaptations. J Neurosci 18:3470-3479.

Kelly WK, O'Connor OA, Marks PA (2002) Histone deacetylase inhibitors: from target to clinical trials. Expert Opinion on Investigational Drugs 11:1695-1713.

Kim M-Y, Ann E-J, Kim J-Y, Mo J-S, Park J-H, Kim S-Y, Seo M-S, Park H-S (2007) Tip60 Histone Acetyltransferase Acts as a Negative Regulator of Notch1 Signaling by Means of Acetylation. Mol Cell Biol 27:6506-6519.

Kioussi C, Briata P, Baek SH, Rose DW, Hamblet NS, Herman T, Ohgi KA, Lin C, Gleiberman A, Wang J, Brault V, Ruiz-Lozano P, Nguyen HD, Kemler

R, Glass CK, Wynshaw-Boris A, Rosenfeld MG (2002) Identification of a Wnt/Dvl/[beta]-Catenin --> Pitx2 Pathway Mediating Cell-Type-Specific Proliferation during Development. Cell 111:673-685.

Klement IA, Skinner PJ, Kaytor MD, Yi H, Hersch SM, Clark HB, Zoghbi HY, Orr HT (1998) Ataxin-1 nuclear localization and aggregation: role in polyglutamine-induced disease in SCA1 transgenic mice. Cell 95:41-53.

Kouzarides T (2000) Acetylation: a regulatory modification to rival phosphorylation? The EMBO Journal 19:1176-1179.

Lam YC, Bowman AB, Jafar-Nejad P, Lim J, Richman R, Fryer JD, Hyun ED, Duvick LA, Orr HT, Botas J, Zoghbi HY (2006) ATAXIN-1 interacts with the repressor Capicua in its native complex to cause SCA1 neuropathology. Cell 127:1335-1347.

Landis DM, Sidman RL (1978) Electron microscopic analysis of postnatal histogenesis in the cerebellar cortex of staggerer mutant mice. J Comp Neurol 179:831-863.

LaSpada A, Wilson E, Lubahn D, Harding A, Fischbeck K (1991) Androgen receptor gene mutations in X-linked spinal and bulbar muscular atrophy. Nature 352:77-79.

Lassalle J, Halley H, Daumas S, Verret L, Frances B (2008) Effects of the genetic background on cognitive performances of TG2576 mice. Behavioral Brain Research 191:104-110.

Lathe R (1996) Mice, gene targeting and behaviour: more than just genetic background. Trends in Neurosciences 19:183-186.

Lathe R, Morris R (1994) Analysing brain function and dysfunction in trangenic animals. Neuropath Appl Neurobiol 20:350-358.

Legube G, Linares LK, Tyteca S, Caron C, Scheffner M, Chevillard-Briet M, Trouche D (2004) Role of the histone acetyl transferase Tip60 in the p53 pathway. J Biol Chem 279:44825-44833.

Li H, Zheng X, Zhang W, Bian Y, Wang D, Zhao J, Xia H (2007) Construction of an expression vector for high expression of siRNA. 23:1117-1118.

Li S-H, Cheng AL, Zhou H, Lam S, Rao M, Li H, Li X-J (2002) Interaction of Huntington Disease Protein with Transcriptional Activator Sp1. Mol Cell Biol 22:1277-1287.

Lim J, Crespo-Barreto J, Jafar-Nejad P, Bowman AB, Richman R, Hill DE, Orr HT, Zoghbi HY (2008) Opposing effects of polyglutamine expansion on native protein complexes contribute to SCA1. Nature 452:713-718.

Lin X, Antalffy B, Kang D, Orr HT, Zoghbi HY (2000) Polyglutamine expansion down-regulates specific neuronal genes before pathologic changes in SCA1. Nat Neurosci 3:157-163.

Linden DJ, Connor JA (1995) Long-Term Synaptic Depression. Annual Review of Neuroscience 18:319-357.

Lipp H, Stagliar-Bozizevic M, Wolfer D (1995) Analysis of behavior in large numbers of knockout mice: results, caveats and perspectives. Behav Genet 25:275.

Luthi-Carter R, Strand A, Peters NL, Solano SM, Hollingsworth ZR, Menon AS, Frey AS, Spektor BS, Penney EB, Schilling G, Ross CA, Borchelt DR,

Tapscott SJ, Young AB, Cha J-HJ, Olson JM (2000) Decreased expression of striatal signaling genes in a mouse model of Huntington's disease. Hum Mol Genet 9:1259-1271.

Machuca-Tzili L, Brook D, Hilton-Jones D (2005) Clinical and molecular aspects of the myotonic dystrophies: A review. Muscle & Nerve 32:1-18.

Mamontova A, Seguret-Mace S, Esposito B, Chaniale C, Bouly M, Delhaye-Bouchaud N, Luc G, Staels B, Duverger N, Mariani J, Tedgui A (1998) Severe Atherosclerosis and Hypoalphalipoproteinemia in the Staggerer Mouse, a Mutant of the Nuclear Receptor ROR{alpha}. Circulation 98:2738-2743.

Mariadason JM, Corner GA, Augenlicht LH (2000) Genetic Reprogramming in Pathways of Colonic Cell Maturation Induced by Short Chain Fatty Acids: Comparison with Trichostatin A, Sulindac, and Curcumin and Implications for Chemoprevention of Colon Cancer. Cancer Res 60:4561-4572.

Martinez M (2009) Progress in the therapeutic applications of siRNAs against HIV-1. Methods Mol Biol 487:343-368.

Matilla A, Roberson ED, Banfi S, Morales J, Armstrong DL, Burright EN, Orr HT, Sweatt JD, Zoghbi HY, Matzuk MM (1998) Mice lacking ataxin-1 display learning deficits and decreased hippocampal paired-pulse facilitation. J Neurosci 18:5508-5516.

Matsui T, Sashihara S, Oh Y, Waxman SG (1995) An orphan nuclear receptor, mROR [alpha], and its spatial expression in adult mouse brain. Molecular Brain Research 33:217-226.

Matsumoto M, Nakagawa T, Inoue T, Nagata E, Tanaka K, Takano H, Kuno J, Sakakibara S, Yamada M, Yoneshima H, Miyawaki A, Furuichi Y, Okano H, Mikoshiba SK, Noda T (1996) Ataxia and epileptic seizures in mice lacking type 1 inositol 1,4,5-trisphosphate receptor. Nature 379:168-171.

Matsuzaki H, Daitoku H, Hatta M, Aoyama H, Yoshimochi K, Fukamizu A (2005) Acetylation of Foxo1 alters its DNA-binding ability and sensitivity to phosphorylation. Proceedings of the National Academy of Sciences of the United States of America 102:11278-11283.

Matysiak-Scholze U, Nehls M (1997) The structural integrity of ROR alpha isoforms is mutated in staggerer mice: cerebellar coexpression of ROR alpha1 and ROR alpha4. Genomics 43:78-84.

Maycox P, Deckwerth T, Hell J, Jahn R (1988) Glutamate uptake by brain synaptic vesicles. Energy dependence of transport and functional reconstitution in proteoliposomes. J Biol Chem 263:15423-15428.

McAllister D, Merlo X, Lough J (2002) Characterization and expression of the mouse tat interactive protein 60 kD (TIP60) gene. Gene 289:169-176.

Meyer T, Kneissel M, Mariani J, Fournier B (2000) In vitro and in vivo evidence for orphan nuclear receptor ROR-gamma function in bone metabolism. Proceedings of the National Academy of Sciences of the United States of America 97:9197-9202.

Miller VM, Xia H, Marrs GL, Gouvion CM, Lee G, Davidson BL, Paulson HL (2003) Allele-specific silencing of dominant disease genes. Proceedings of

the National Academy of Sciences of the United States of America 100:7195-7200.

Minucci S, Pelicci PG (2006) Histone deacetylase inhibitors and the promise of epigenetic (and more) treatments for cancer. In: Nature Reviews Cancer, pp 38-51: Nature Publishing Group.

Miyazaki T, Fukaya M, Shimizu H, Watanabe M (2003) Subtype switching of vesicular glutamate transporters at parallel fibre/Purkinje cell synapses in developing mouse cerebellum. European Journal of Neuroscience 17:2563-2572.

Mizutani A, Wang L, Rajan H, Vig P, Alaynick W, Thaler J, Tsai C-C (2005) Boat, an AXH domain protein, suppresses the cytotoxicity of mutant ataxin-1. EMBO J 24:3339-3351.

Morris R (1984) Development of a water-maze for studying spatial learning in the rat. J Neurosci Methods 11:47-60.

Mottet D, Castronovo V (2008) Histone deacetylases: target enzymes for cancer therapy. Clinical and Experimental Metastasis 25:183-189.

Muller S, Ledl A, Schmidt D (2004) SUMO: a regulator of gene expression and genome integrity. In: Oncogene, pp 1998-2008: Nature Publishing Group.

Nance M (1997) Clinical Aspects of CAG Repeat Diseases. Brain Pathology 7:881-900.

Netravathi M, Pal PK, Purushottam M, Thennarasu K, Mukherjee M, Jain S (2009) Spinocerebellar ataxias types 1, 2 and 3: Age adjusted clinical

severity of disease at presentation correlates with size of CAG repeat lengths. Journal of the Neurological Sciences 277:83-86.

Ni B, Rosteck PR, Nadi NS, Paul SM (1994) Cloning and expression of a cDNA encoding a brain-specific Na(+)-dependent inorganic phosphate cotransporter. Proceedings of the National Academy of Sciences of the United States of America 91:5607-5611.

Okazawa H (2003) Polyglutamine diseases: a transcription disorder? Cellular and Molecular Life Sciences (CMLS) 60:1427-1439.

Okazawa H, Rich T, Chang A, Lin X, Waragai M, Kajikawa M, Enokido Y, Komuro A, Kato S, Shibata M, Hatanaka H, Mouradian MM, Sudol M, Kanazawa I (2002) Interaction between mutant ataxin-1 and PQBP-1 affects transcription and cell death. Neuron 34:701-713.

Orr HT, Zoghbi HY (2007) Trinucleotide Repeat Disorders. Annual Review of Neuroscience 30:575-621.

Orr HT, Chung MY, Banfi S, Kwiatkowski TJ, Jr., Servadio A, Beaudet AL, McCall AE, Duvick LA, Ranum LP, Zoghbi HY (1993) Expansion of an unstable trinucleotide CAG repeat in spinocerebellar ataxia type 1. Nat Genet 4:221-226.

Peart MJ, Smyth GK, van Laar RK, Bowtell DD, Richon VM, Marks PA, Holloway AJ, Johnstone RW (2005) Identification and functional significance of genes regulated by structurally different histone deacetylase inhibitors. Proceedings of the National Academy of Sciences of the United States of America 102:3697-3702.

Pfister EL, Kennington L, Straubhaar J, Wagh S, Liu W, Difiglia M, Landwehrmeyer B, Vonsattel JP, Zamore PD, Aronin N (2009) Five siRNAs Targeting Three SNPs May Provide Therapy for Three-Quarters of Huntington's Disease Patients. In, pp 774-778.

Phillips TJ, Hen R, Crabbe JC (1999) Complications associated with genetic background effects in research using knockout mice. Psychopharmacology 147:5.

Postigo A, Dean D (1997) ZEB, a vertebrate homolog of *Drosophila* Zfh-1, is a negative regulator of muscle differentiation. The EMBO Journal 16:3935-3943.

Rai M, Soragni E, Jenssen K, Burnett R, Herman D, Coppola G, Geschwind DH, Gottesfeld JM, Pandolfo M (2008) HDAC Inhibitors Correct Frataxin Deficiency in a Friedreich Ataxia Mouse Model. PLoS ONE 3:1958.

Ran Q, Pereira-Smith OM (2000) Identification of an alternatively spliced form of the Tat interactive protein (Tip60), Tip60(beta). Gene 258:141-146.

Riley BE, Zoghbi HY, Orr HT (2005) SUMOylation of the polyglutamine repeat protein, ataxin-1, is dependent on a functional nuclear localization signal. J Biol Chem 280:21942-21948.

Ryu H, Lee J, Hagerty SW, Soh BY, McAlpin SE, Cormier KA, Smith KM, Ferrante RJ (2006) ESET/SETDB1 gene expression and histone H3 (K9) trimethylation in Huntington's disease. Proceedings of the National Academy of Sciences 103:19176-19181.

Sandberg R, Yasuda R, Pankratz DG, Carter TA, Del Rio JA, Wodicka L, Mayford M, Lockhart DJ, Barlow C (2000) Regional and strain-specific gene expression mapping in the adult mouse brain. Proceedings of the National Academy of Sciences of the United States of America 97:11038-11043.

Sato Y, Seo N, Kobayashi E (2006) Genetic background differences between FVB and C57BL/6 mice affect hypnotic susceptibility to pentobarbital, ketamine and nitrous oxide, but not isoflurane. In: Acta Anaesthesiologica Scandinavica, pp 553-556: Blackwell Publishing Limited.

Serra HG, Byam CE, Lande JD, Tousey SK, Zoghbi HY, Orr HT (2004) Gene profiling links SCA1 pathophysiology to glutamate signaling in Purkinje cells of transgenic mice. Hum Mol Genet 13:2535-2543.

Serra HG, Duvick L, Zu T, Carlson K, Stevens S, Jorgensen N, Lysholm A, Burright E, Zoghbi HY, Clark HB, Andresen JM, Orr HT (2006) RORalpha-mediated Purkinje cell development determines disease severity in adult SCA1 mice. Cell 127:697-708.

Servadio A, Koshy B, Armstrong D, Antalffy B, Orr HT, Zoghbi HY (1995) Expression analysis of the ataxin-1 protein in tissues from normal and spinocerebellar ataxia type 1 individuals. Nat Genet 10:94-98.

Shahbazian MD, Orr HT, Zoghbi HY (2001) Reduction of Purkinje cell pathology in SCA1 transgenic mice by p53 deletion. Neurobiol Dis 8:974-981.

Shankar S, Srivastava R (2008) Histone deacetylase inhibitors: mechanisms and clinical significance in cancer: HDAC inhibitor-induced apoptosis. Adv Exp Med Biol 615:261-298.

Sidman RL, Lane PW, Dickie MM (1962) Staggerer, a new mutation in the mouse affecting the cerebellum. Science 137:610-612.

Skinner PJ, Vierra-Green CA, Clark HB, Zoghbi HY, Orr HT (2001) Altered trafficking of membrane proteins in purkinje cells of SCA1 transgenic mice. Am J Pathol 159:905-913.

Sonja Janmaat FF, Klaas Sjollema, Paul Luiten, Jean Mariani, Johannes van der Want, (2009) Formation and maturation of parallel fiber-purkinje cell synapses in the staggerer cerebellum ex vivo. The Journal of Comparative Neurology 512:467-477.

Spada AL, Wilson E, Lubahn D, Harding A, Fischbeck K (1991) Androgen receptor gene mutations in X-linked spinal and bulbar muscular atrophy. Nature 352:77-79.

Stack EC, Del Signore SJ, Luthi-Carter R, Soh BY, Goldstein DR, Matson S, Goodrich S, Markey AL, Cormier K, Hagerty SW, Smith K, Ryu H, Ferrante RJ (2007) Modulation of nucleosome dynamics in Huntington's disease. Hum Mol Genet 16:1164-1175.

Steffan JS, Bodai L, Pallos J, Poelman M, McCampbell A, Apostol BL, Kazantsev A, Schmidt E, Zhu Y-Z, Greenwald M, Kurokawa R, Housman DE, Jackson GR, Marsh JL, Thompson LM (2001) Histone deacetylase

inhibitors arrest polyglutamine-dependent neurodegeneration in Drosophila. Nature 413:739-743.

Sugars KL, Rubinsztein DC (2003) Transcriptional abnormalities in Huntington disease. Trends in Genetics 19:233-238.

Sun Y, Jiang X, Chen S, Fernandes N, Price BD (2005) A role for the Tip60 histone acetyltransferase in the acetylation and activation of ATM. Proc Natl Acad Sci U S A 102:13182-13187.

Takahashi JS, Pinto LH, Vitaterna MH (1994) Forward and Reverse Genetic Approaches to Behavior in the Mouse. Science 264:1724-1733.

Takamori S, Rhee JS, Rosenmund C, Jahn R (2000) Identification of a vesicular glutamate transporter that defines a glutamatergic phenotype in neurons. Nature 407:189-194.

Tang Y, Luo J, Zhang W, Gu W (2006) Tip60-Dependent Acetylation of p53 Modulates the Decision between Cell-Cycle Arrest and Apoptosis. Molecular Cell 24:827-839.

Taylor JP, Hardy J, Fischbeck KH (2002) Toxic proteins in neurodegenerative disease. Science 296:1991-1995.

Thomas E (2006) Striatal specificity of gene expression dysregulation in Huntington's disease. Journal of Neuroscience Research 84:1151-1164.

Thomas EA, Coppola G, Desplats PA, Tang B, Soragni E, Burnett R, Gao F, Fitzgerald KM, Borok JF, Herman D, Geschwind DH, Gottesfeld JM (2008) The HDAC inhibitor 4b ameliorates the disease phenotype and

transcriptional abnormalities in Huntington's disease transgenic mice. Proceedings of the National Academy of Sciences 105:15564-15569.

Tsai CC, Kao HY, Mitzutani A, Banayo E, Rajan H, McKeown M, Evans RM (2004) Ataxin 1, a SCA1 neurodegenerative disorder protein, is functionally linked to the silencing mediator of retinoid and thyroid hormone receptors. Proc Natl Acad Sci U S A 101:4047-4052.

Tsuda H, Jafar-Nejad H, Patel AJ, Sun Y, Chen HK, Rose MF, Venken KJ, Botas J, Orr HT, Bellen HJ, Zoghbi HY (2005) The AXH domain of Ataxin-1 mediates neurodegeneration through its interaction with Gfi-1/Senseless proteins. Cell 122:633-644.

Upchurch M, Wehner J (1989) Inheritance of spatial learning ability in inbred mice: a classical genetic analysis. Behav Neurosci 103:1251-1258.

Upchurch M, Pounder J, Wehner J (1988) Heterosis and resistance to DFP effects on spatial learning in C57BL X DBA hybrids. Brain Res Bull 21:499-503.

Varoqui H, Schafer MK-H, Zhu H, Weihe E, Erickson JD (2002) Identification of the Differentiation-Associated Na+/PI Transporter as a Novel Vesicular Glutamate Transporter Expressed in a Distinct Set of Glutamatergic Synapses. J Neurosci 22:142-155.

Voogd J, Glickstein M (1998) The anatomy of the cerebellum. Trends in Neurosciences 21:370-375.

Wolfer D, Bozicevic-Stagliar M, Lipp H (1995) The role of genetic background in assessing the behavior of transgenic mice. Soc Neurosci Abstr 21:1227.

Wu R, Wang H, Xia X, Zhou H, Liu C, Castro M, Xu Z (2009) Nerve injection of viral vectors efficiently transfers transgenes into motor neurons and delivers RNAi therapy against ALS. Antioxid Redox Signal.

Xia H, Mao Q, Paulson HL, Davidson BL (2002) siRNA-mediated gene silencing in vitro and in vivo. Nat Biotech 20:1006-1010.

Xia H, Mao Q, Eliason SL, Harper SQ, Martins IH, Orr HT, Paulson HL, Yang L, Kotin RM, Davidson BL (2004) RNAi suppresses polyglutamine-induced neurodegeneration in a model of spinocerebellar ataxia. Nat Med 10:816-820.

Xu WS, Parmigiani RB, Marks PA (2007) Histone deacetylase inhibitors: molecular mechanisms of action. Oncogene 26:5541-5552.

Yamamoto T, Horikoshi M (1997) Novel Substrate Specificity of the Histone Acetyltransferase Activity of HIV-1-Tat Interactive Protein Tip60.

J Biol Chem 272:30595-30598.

Yang Z, Cool BH, Martin GM, Hu Q (2006) A Dominant Role for FE65 (APBB1) in Nuclear Signaling. J Biol Chem 281:4207-4214.

Yasuo Aihara HM, Hideaki Onda, Setsuji Hisano, Hidetoshi Kasuya, Tomokatsu Hori, Shirou Yamada, Hideaki Tomura, Yuichiro Yamada, Ituro Inoue, Itaru Kojima, Jun Takeda, (2000) Molecular Cloning of a Novel Brain-Type Na+-Dependent Inorganic Phosphate Cotransporter. Journal of Neurochemistry 74:2622-2625.

Yuan Z, Guan Y, Chatterjee D, Chin Y (2005) Stat3 dimerization regulated by reversible acetylation of a single lysine residue. Science 307:269-273.

Yue S, Serra HG, Zoghbi HY, Orr HT (2001) The spinocerebellar ataxia type 1 protein, ataxin-1, has RNA-binding activity that is inversely affected by the length of its polyglutamine tract. Hum Mol Genet 10:25-30.

Zanjani H, Mariani J, Delhay-Bouchard N, Herrup K (1992) Neuronal cell loss in heterozygous staggerer mutant mice: a model for genetic contributions to the aging process. Brain Res Dev Brain Res 67:153-160.

Zhai W, Jeong H, Cui L, Krainc D, Tjian R (2005) In Vitro Analysis of Huntingtin-Mediated Transcriptional Repression Reveals Multiple Transcription Factor Targets. Cell 123:1241-1253.

Zoghbi HY (1995) Spinocerebellar ataxia type 1. Clin Neurosci 3:5-11.

Zoghbi HY, Orr HT (2000) Glutamine repeats and neurodegeneration. Annu Rev Neurosci 23:217-247.

Zu T, Duvick LA, Kaytor MD, Berlinger MS, Zoghbi HY, Clark HB, Orr HT (2004) Recovery from polyglutamine-induced neurodegeneration in conditional SCA1 transgenic mice. J Neurosci 24:8853-8861.